BEHAVIOR OF STABILIZING PILES UNDER STATIC AND DYNAMIC LOADING BASED ON PLASTIC DEFORMATION THEORY

何, 毅

https://doi.org/10.15017/1543978

BEHAVIOR OF STABILIZING PILES UNDER STATIC AND DYNAMIC LOADING BASED ON PLASTIC DEFORMATION THEORY

Yi He

To My Parents

BEHAVIOR OF STABILIZING PILES UNDER STATIC AND DYNAMIC LOADING BASED ON PLASTIC DEFORMATION THEORY

A Thesis Submitted
In Partial Fulfillment of the Requirements
For the Degree of
Doctor of Engineering

By
Yi He

to the
DEPARTMENT OF CIVIL AND STRUCTURAL ENGINEERING
GRADUATE SCHOOL OF ENGINEERING
KYUSHU UNIVERSITY
Fukuoka, Japan
August, 2015

DEPARTMENT OF CIVIL AND STRUCTURAL ENGINEERING
GRADUATE SCHOOL OF ENGINEERING
KYUSHU UNIVERSITY
Fukuoka, Japan

CERTIFICATE

The undersigned hereby certify that they have read and recommended to the Graduate School of Engineering for the acceptance of this thesis entitled, "***Behavior of stabilizing piles under static and dynamic loading based on plastic deformation theory***" by **Yi He** in partial fulfillment of the requirements for the degree of **Doctor of Engineering**.

Dated: August, 2015

Thesis Supervisor:

Prof. Hemanta Hazarika, Dr. Eng.

Examining Committee:

Prof. Haruyuki Hashimoto, Dr. Eng.

Prof. Yasuhiro Mitani, Dr. Eng.

Prof. Hemanta Hazarika, Dr. Eng.

ABSTRACT

Landslides occurring in both natural and cut slopes often result in serious damage to both lives and properties. Generally speaking, there are two categorized triggering factor for landslide: (1) static factor (e.g. raining, hurricane), (2) dynamic factor (e.g. earthquake). Recent years, the catastrophic earthquake occurs frequently, which results in many fatal landslides. For instance, more than 3000 landslides have been reported in Nepal after the Gorkha earthquake, in 2015. Therefore, considering the landslide risk reduction, it is very important to improve the stability of slopes. Especially, more focus should be put on the seismic performance of the earthquake induced landslide.

Stabilizing piles, as one of the most widely used application in reinforcement of slopes, has been proved to be an efficient solution against landslides. For dynamic analysis of pile reinforced slopes, the two-dimensional (2D) analytical method based on pseudo-static approach is usually used. However, it is commonly acknowledged that 2D plane-strain solutions are conservative to analyze slope stability comparing with three-dimensional (3D) solutions. Seeking a more accurate prediction of seismic stability in 3D cases could benefit the construction of slope. In this sense, it is necessary to provide a comprehensive accurate solution for reinforced slope subjected to seismic loading in 3D condition.

3D dynamic analysis of the pile reinforced slope stability involves two main aspects: (i) estimating of resistance force provided by the piles, (ii) 3D limit analysis of the reinforced slope subjected to specific seismic load. However, on one hand, in the previous literatures, the analytical solution of the soil-pile pressure (lateral force) of the pile is limited because of the different distribution between the predictions and field test results, which results in the misestimation of the slope stability. On the other hand, literature on the 3D seismic analysis of reinforced slope is scarce, which results in the miscalculation of the slope constructions.

Consequently, this study aims to present a comprehensive method to analyze the seismic performance of the pile-reinforced slope in 3D condition, incorporating the

static analysis of stabilizing piles. Furthermore, this study also focuses on clarifying the soil-pile interaction and the failure mechanism of the pile-reinforced slope in dynamic condition. Specifically, two major approaches for the analysis of slope reinforced with piles have been studied. One is to propose a new method to provide an accurate prediction of the lateral force. The other is to calculate the permanent displacement of reinforced slope subjected to seismic load in 3D condition.

In the first approach, the theory of plastic deformation is modified by considering soil arching effects. A new analytical method is presented for estimating the ultimate lateral force due to soil movement, which provides a more accurate prediction than previous studies. Furthermore, the effect of the inclination of the moveable soil layer on lateral force is also analyzed.

In the second approach, earthquake induced sliding displacements are commonly used to assess the seismic performance of slopes. Therefore, an analytical method is proposed to evaluate the cumulative displacement of reinforced slope induced by specific earthquake load. The lateral forces provided by the piles are evaluated by the presented approach mentioned above. In the presented dynamic analysis, the 2D analytical procedure for displacement assessment is extrapolated to 3D condition.

The thesis comprises the following chapters.

Chapter 1 introduces (1) background of this study, (2) two main issues in current study, namely lateral force and the earthquake-induced permanent displacement, (3) the scope and objectives of this study, and (4) the organization of the thesis.

Chapter 2 reviews two aspects of existing studies on the subject of slope reinforced with piles: analyses of slope stabilized with a row of piles and landslide movement calculation. The merits and demerits of each method are stated.

Chapter 3 analyses the lateral force acting on piles due to soil movement. Combining with the ‘plastic deformation theory’, soil arching effects along the depth of the moveable soil between two neighboring piles are considered to estimate lateral force.

Comparisons of the in situ observed results (from literatures) and the calculate results show that the proposed method yields satisfactory predictions.

Chapter 4 develops a limit equilibrium method to analyze the slope angle effect on the lateral force distribution of stabilizing piles. The soil arching zone is determined by Mohr's circle, which is a function of slope inclination. In addition, the lateral force in sandy slopes is obtained by considering the soil arching effects and the 'squeezing effect' between two neighboring piles proposed by Ito and Matsui. The numerical simulation results obtained by FLAC3D and the experimental data from the published literature are used to evaluate the proposed approach. It is shown that the proposed model could reasonably predict the distribution shape of the soil-pile pressure acting on the stabilizing piles. Parametric analysis is carried out to investigate the influence of the slope angle on the distribution of the soil-pile pressure. It is shown that the slope angle affects the distribution of the lateral force, rather than the magnitude.

Chapter 5 presents 3D limit analysis of seismic stability of slopes reinforced with one row of piles. The lateral forces provided by the piles are evaluated by the presented approach mentioned above. Based on the kinematic theory within the frame of the pseudo-static approach, a 3D model is proposed for evaluating the yield (or critical) acceleration. Furthermore, Newmark's analytical procedure is employed to estimate the cumulative displacement induced by the given earthquake loads. A simple example is studied, and the findings are: the yield accelerations of 2D mechanism are less than that in 3D mechanism with the same soil properties; the displacements in 2D mechanism are much larger than that in 3D conditions; it is possible to reduce the seismic displacement of the soil slopes using stabilizing piles both in 2D and 3D conditions.

Chapter 6 concludes the results and achievements of the study, and states the problems to be solved in future studies.

ACKNOWLEDGEMENT

This thesis would not be complete unless cooperation from many individuals.

I would like to thank my supervisor, Prof. Hemanta Hazarika, for giving me an opportunity of doing this interesting research topic and for his valuable advice and assistance throughout my doctor study. I have been given many great opportunities by Prof. Hemanta Hazarika, in doing exciting research projects as well as in teaching (He provided me an opportunity to be a teaching assistant in his class). His willingness to share his experience and thoughts on all projects that we had worked together makes my study even more meaningful. I would like to take this opportunity to express my sincere appreciation to my supervising professor, Prof. Hemanta Hazarika, for his patient to share his valuable experience, thoughts, supports, and advice.

It has been a great pleasure for me to have the opportunity to pursue my graduate study in Kyushu University. Three years ago, Prof. Yasufuku Noriyuki provided me the opportunity to study in Kyushu University. I would like to thank Prof. Yasufuku Noriyuki for his valuable suggestions on my research and advices during the three years in Japan. I also deeply appreciate Assistant Prof. Ishikura Ryohei, who is so kindly and easy to going that more like a friend. Also, great thanks to Staff Nakashima Michio and Ito Aki for their enthusiastic and help.

I would like to express my sincerely gratitude to members of my dissertation committee, Prof. Dr. Hemanta Hazarika, Prof. Dr. Haruyuki Hashimoto and Prof. Dr. Yasuhiro Mitani for their comments and contribution on the research.

I am deeply indebted to Prof. Dr. Junjie Yang, my former supervisors in China Ocean University, for recommending me to my further study in Japan.

I would like to thank all the students whom I have been studying with in Geotechnical Group where I really enjoy my studying life in Japan.

I would like to thank Prof. Sloan (Chief Editor of *Computers & Geotechnics*), and Prof. Erdik (Chief Editor of *Soil Dynamics and Earthquake Engineering*). Without their

strict and helpful comments my research will not be published in the international journals.

I would like to extend my grateful acknowledgement to China Scholarship Council (CSC) for providing me the opportunity and scholarship to pursue my PhD at Kyushu University.

Most importantly, I would like to thank my parents, for their love and encouragement and support to complete my studies in Japan. I had good and bad times during this journey but my parents always stand by me. My industrious honest and kind parents, strictly speaking, who never attended a formal school but they were good educators and they sent me school envisioning a better life for me.

TABLE OF CONTENT

LIST OF FIGURES

LIST OF TABLES

NOMENCLATURE

M_w	Moment magnitude scale
M_s	surface-wave magnitude
L_e	pile embedment length
K_p	Rankine passive pressure coefficient
σ'_{vo}	the effective overburden pressure
P_y	ultimate soil-pile pressure
α_B	coefficient ranging between 3 and 5
c_u	undrained shear strength
φ	internal friction angle of the soil
c	cohesion of the soil
D_1	the center-to-center pile spacing in a row
D_2	the clear spacing between the piles
γ	the unit weight of the soil
z	arbitrary depth from the ground surface.
F_s	safety factor
k_{ac}	anisotropic coefficient
F_{lr}	the required lateral resisting force per unit length of the slope
k	coefficient of seismic acceleration
g	gravitational acceleration
a	assumed seismic acceleration
W	potential sliding mass of weight
a_h	horizontal pseudo-static accelerations
a_v	vertical pseudo-static accelerations
k_h	horizontal pseudo-static coefficients
k_v	vertical pseudo-static coefficients
FOS	the factor of safety
t_r	resisting force
t_d	driving force
a_c	in terms of the gravity acceleration g

FOS	static factor of safety
α_{an}	angle from the horizontal of the sliding surface
r_0	radius of the log spiral with respect to angle θ_0
ω	angular velocity of failing soil mass
H	height of the slope
α	angles of the slope at the top
β	inclination of slope
F_t	total lateral force acting on a pile
F_p	stabilizing force per unit width of soil
μ	coefficient of friction
K	lateral stress ratio
K_a	Rankine ratio with a level ground surface
σ_1	major principal stress
σ_3	minor principal stress
θ_{de}	declination angle of stress
σ_h	active lateral stress
τ	shear stress
β_1	angle between sliding plane and the horizontal
ψ	angle between the normal of the arch and the horizontal
σ_{av}	vertical stress at an arbitrary point on the stress circle
$\bar{\sigma}_v$	average vertical stress
V	total vertical stress across the differential element
S	width of the differential element.
dV	differential vertical force at arbitrary point
dA	width of the differential element at arbitrary point
K_{an}	lateral stress ratio at the vertical failure surface
dz	thickness of the differential element
H	thickness of the sliding soil layer
z	depth below the surface of the soil
γ	unit weight of the soil

C_1	an integration constant
q	overloading exerted on the surface of the ground
p	lateral force acting on a pile per unit thickness of the layer
θ_s	angle between the slip plane and slope surface
σ_z	geostatic weight
N_1	$N_1=\tan^2(45^o+\varphi/2)$
σ_v'	component of the vertical stress in the direction of perpendicular the inclination of slope
σ_f.	component of the vertical stress in the direction of parallel the inclination of slope
σ_v	vertical stress
$\overline{\sigma}_v'$	average value of σ_v'
ξ	angle between the normal line and the vertical in the stress circle
R	radius of the circle
m	function of β, defined by equation (4.26)
σ_{3v}	vertical component of σ_3
E	elastic modulus
μ	Poisson's ratio
$[v_n]$	normal components of the velocity jump vector
$[v_t]$	Tangential components of the velocity jump vector
$\dot{\varepsilon}_1$	major principal strain
$\dot{\varepsilon}_3$	minor principal strain
$\dot{\varepsilon}_2$	medial principal strain
W	rate of work of externally forces
D	rate of work
γ_i	unit weight vector
v_i	velocity vector
S_t	velocity discontinuity surface
D_t	velocity discontinuity surface
D_v	dissipation within volume

W_γ	work rate of the weight
c_d	developed cohesion required for the slope to become unstable
φ_d	developed friction angle required for the slope to become unstable
r_0	Initial values of the radius of the spiral (lower contour of the horn)
r_0'	Initial values of the radius of the spiral (upper contour of the horn)
r	Radius of spiral related to angle θ (lower contour of the horn)
r'	Radius of spiral related to angle θ (upper contour of the horn)
θ	Angle of spiral
θ_0	Initial value of the angle of spiral
θ_h	Final value of the angle of spiral
b	width of 'insert plane'
W_s	rate of the inertial force
f_i	Non-dimensional function related to horizontal direction
D_p	dissipation rate induced by the reinforcement
D_c	rate of work dissipation caused by soil cohesion
D^{3D}	3D term of dissipation rate
D^{2D}	plain-strain term of dissipation rate
F_p	total lateral force exerted on a stabilizing
θ_p	specifies the position of the stabilizing piles
r_p	radius of F_p about the rotation center
n	number of the piles
k_c	critical acceleration coefficient
k'	function of the independent variable parameters
O	rotational center
G	weight of block
l	distance from gravity center to rotational center

CHAPTER 1

INTRODUCTION

1.1 BACKGROUND

1.1.1 LANDSLIDE

A landslide, also known as a landslip, is a geological phenomenon that includes a wide range of downward and outward ground movements, such as rockfall, deep failure of slopes and shallow debris flows (Cruden, 1991). The term "landslides" encompasses five basic types of movement: flows, slides, topples, falls and spreads. In addition, the actual movements of the landslides usually combine two or more basic types of movements according to Glossary of Geology (Jackson, 1997) and other references (Varnes, 1974; Hutchinson, 1988; WP/WLI, 1990; Cruden and Varnes, 1996; Highland and Bobrowsky, 2008; Gokceoglu and Sezer, 2009). Landslides can occur in offshore, coastal and onshore environments. Although the action of gravity is the primary reason for a landslide to occur, there are other contributing factors affecting the original slope stability.

Actually, almost every landslide has multiple causes. Slope movement occurs when forces acting down-slope (mainly due to gravity) exceed the strength of the soil materials that compose the slope. Causes include factors that increase the effects of down-slope forces and factors that contribute to low or reduced strength. Landslides can be initiated in slopes already on the verge of movement by rainfall, snowmelt, changes in water level, stream erosion, changes in ground water, earthquakes, volcanic activity, disturbance by human activities, or any combination of these factors (Guzzetti, 2006).

Each year, landslides cause thousands of casualties and billions of dollars in damages across the world (UNEP, 1997; EM-DAT, 2003). For example, (1) in Japan,

disasters from single landslide events include a large scale failure of Ontake San, Nagano Prefecture in 1984 (volume:$3.4\times10^7 m^3$, 15 deaths), Tamanoki Landslide of Ohmi-Cho, Niigata Prefecture in 1985 (10 deaths), Jizuki Yama Landslide, Nagano City in 1985 (26 deaths), and others. More than 300 landslides and slope failures have been reported since the Southern Hyogo Earthquake of January 17, 1995; (2) it is estimated that in the United States, they cause in excess of $1 billion in damages and from about 25 to 50 deaths each year (Highland, 2006); (3) it is reported that at least 10 million people in China are exposed to landslide risk, and landslides result in more than 500 deaths and missing each year. Since 2001, more than 400 fatal landslide events have been reported. These fatal landslides caused at least 3000 people dead and missing, and more than $ 100 billion in property damage (Wen et al., 2005). Especially in 2008, more than 150,000 landslides induced by Wenchuan earthquake caused about 20,000 fatalities; (4) in the period 1968-2006, a total of 517 fatal landslides have been recorded in Nepal, causing a total of 2931 deaths, representing an average of about 75 fatalities occurring in just 13 fatal landslides per annum. The average number of fatalities per fatal landslide is 5.7 deaths (Petley et al., 2007). In addition, the recent Gorkha earthquake in Nepal caused countless landslides. The details of the earthquake induced landslides can be seen in following section. **Table 1.1** lists the worldwide most catastrophic landslides of 20th century. It is modified from Schuster (1996). Actually, more than 30 catastrophic landslides have been reported in 20th century, just a few of them are listed herein.

Globally, landslides cause hundreds of billions of dollars in damages and hundreds of thousands of deaths and injuries each year. Therefore, it's very important to study the landslide so as to mitigate the potential disaster from landslide.

1.1.2 EARTHQUAKE-INDUCED LANDSLIDES

The destructive impact of earthquakes, in many parts of the world, is greatly enhanced by the triggering of landslides during or after the shaking. There can be little doubt that after the direct effect of structural damage due to the strong ground-motion caused by earthquake, landslides are the most important consequence of earthquake

shaking. As well as causing disruption to communications, earthquake induced landslides can, in some cases, contribute significantly to the death toll. Indeed, the vast majority of the more than 1000 victims of the EI Salvador earthquake of 13 January (Mw = 7.7) and 13 February 2001 (Mw = 6.7) were directly caused by landslides (Bommer and Rodriguez, 2002). Moreover, many serious damages caused by the earthquake induced landslides have been reported for the last few decades, especially after a series of disastrous earthquake events occurred in recent years. For example, in 1999, Chi-Chi earthquake (Ms = 7.6) induced 9272 landslides, which caused 2400 deaths, more than 8000 casualties and over 10 billion US$ of economic loss in Taiwan (Chang et al., 2005). Less than three years later, the 2008 Wenchuan earthquake shocked the Sichuan province and induced as many as 60,104 landslides (Gorum et al., 2011), which directly caused more than 20000 deaths (Yin et al, 2009). A quarter of the total deaths, and over one third of the total lost was caused by the earthquake induced landslides. Recently, the landslide situation in the aftermath of the Gorkha earthquake in Nepal is steadily becoming more clear due to the efforts of the National Aerospace and Space Administration (NASA)-U.S. Geological Survey-Interagency Volunteer Earthquake Response Team. To date, the response teams have identified over 3000 landslides, and assembled a database of over 250 identified landslides and other large mass movements. The Google Earth map of the 250 landslides is shown in **Figure 1.1**. The landslides are concentrated in the northern area of the earthquake affected region, and many are along highways. **Figure 1.2** shows one of the landslides occurred in Langtang region after the Gorkha earthquake in Nepal. It is reported more than 8200 people dead in the earthquake and the aftershock. The casualties caused by the earthquake induced landslides are not clear so far. As seen, a strong earthquake can induce a large amount of landslides and cause very serious property damage and human casualties. **Table 1.2** shows earthquakes responsible for triggering landslides.

A number of studies on slopes subjected to seismic load have been carried out and a series of countermeasures have been developed to mitigate the landslide disasters. However, these studies are usually carried out based on the two-dimensional (2D) slope

Table 1.1 The most Catastrophic Landslides of the 20th Century - Worldwide

Year	Country (State/Province)	Name & type(s)	Triggering process	Impact
1911	Tadzhik Rep. (Formerly USSR)	Usoy rock slide	Usoy earthquake	Destroyed Usoy village; 54 killed
1919	Indonesia (Java)	Kalut lahars	Eruption of Kalut volcano	5,110 killed; 104 villages destroyed or damaged
1920	China (Ningxia)	Haiyuan landslides	Haiyuan earthquake	100,000 killed; many villages destroyed
1949	Tadzhik Rep. (formerly USSR)	Khait rock slide	Khait earthquake	12,000 - 20,000 killed or missing; 33 villages destroyed
1958	Japan (Shizuoka)	Kanogawa slides and mud/debris flows	Heavy rain	1,094 dead/missing; 19,754 homes destroyed or badly damaged
1967	Brazil (Serra das Araras)	Serra das Araras slides, avalanches, debris/mud flows	Heavy rain	1,700 dead from landslides and floods
1980	United States (Washington)	Mount St. Helens rock slide-debris avalanche	Eruption of Mount St. Helens	World 1s largest historic landslide; only 5-10 killed, but major destruction of homes, highways, etc.; major debris flow; deaths low because of evacuation
1987	Ecuador (Napo)	Reventador landslides	Reventador earthquakes	1,000 killed; total losses: US$ 1 billion
1998	Honduras, Guatemala, Nicaragua, El Salvador	Hurricane Mitch flooding Landslides debris-flows	Hurricane Mitch	Approximately 10,000 people killed in the flooding and landslides

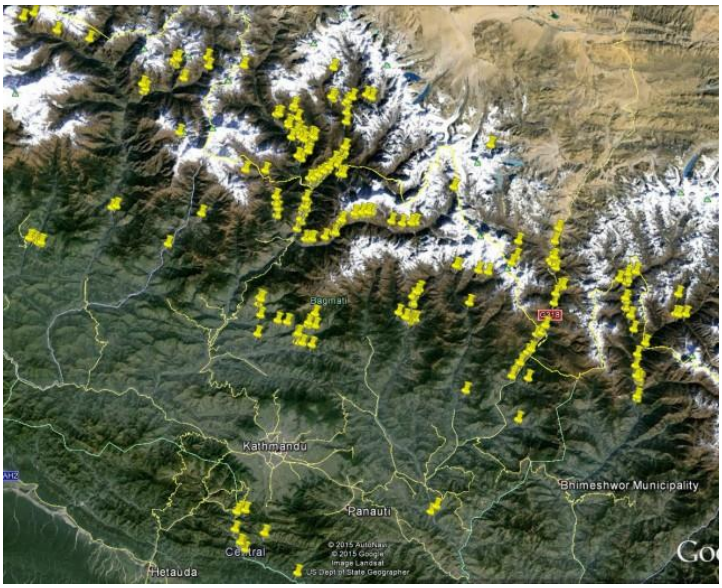

Figure 1.1 250 identified landslides surveyed by NASA-U.S. Geological Survey-Interagency Volunteer Earthquake Response Team (Photo from the landslide blog of American Geophysical Union).

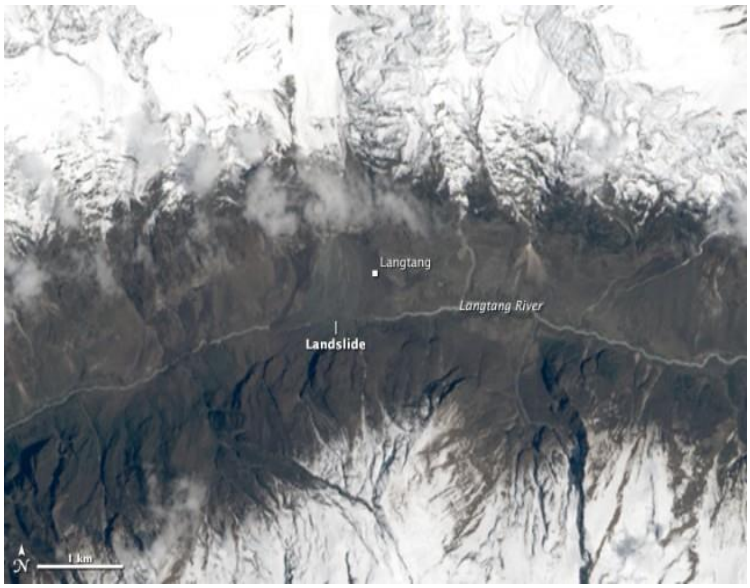

Figure 1.2 Landslide in Langtang region in Nepal (Photo from NASA Landsat8).

models. It is commonly acknowledged that 2D plane strain solutions are conservative to analyze slope stability when compared with three-dimensional (3D) solutions (Cavounidis, 1987). It is necessary to analyze the seismic loaded slopes using 3D

models. The failure mechanisms of the 3D slopes and the displacement of slopes due to the seismic load should be analyzed because it is quite different from that of the 2D conditions. Furthermore, the influence of the countermeasures utilized to mitigate the landslide disasters under dynamic loading condition should be evaluated as well.

1.2 PREVENTIVE COUNTERMEASURES

In landslide mitigation engineering, there are two principles, active and passive countermeasures. The passive measures are mainly land-use planning keeping the endangered areas free of settlements and infrastructure to prevent economic damages. Active countermeasures, which may be used as single or in combination, are: drainage; modification of the slope profile by excavation and/or filling; restraining and other structures, including anchors, piles, and so on; erosion control, both local to the particular site and catchment-wide. They are reviewed in detail by Hutchinson (1977). The following discussion in this section concentrates on the first three of the above methods, which are those most generally used at present.

1.2.1 DRAINAGE

The first task is always to deal with surface water and to lead it away from the landslide area. Concerning sub-surface drainage, two approaches exist. One is to attempt to intercept the ground-water, by cut-off trenches and the like, before it reaches the slide area: this may be practicable for small landslides but is difficult to accomplish reliably in the case of large ones. Furthermore, in some cases the precipitation falling on the slope itself may be important.

The alternative approach is to aim to reduce the ground-water pressures directly at the locations which matter, that is, on the slip surfaces (Hazarika, 2007a, 2007b). It should be borne in mind that, in clays, drainage measures may take a year or more to become fully effective and additional measures may thus have to be taken to secure stability in the short-term.

Table 1.2 Earthquakes responsible for triggering landslides

Earthquake	Country	Date	Magnitude		Focal depth	Maximum intensity	Area affected by landslides	Number of slides
		Day/month/year	Ms	Mw	km	MMI	km^2	
Coalinga	USA	02 05 1983	6.7	6.2	7	VIII	650	>10,000*
San Salvador	El Salvador	10 10 1986	5.4	5.7	12	VIII	380	1,000-10,000*
Spitak	Armenia	07 12 1988	6.8	6.7	5	IV	2200	1,000-10,000*
Loma Prieta	USA	17 10 1989	7.1	6.9	8	VIII	14000	1,000-10,000*
Manjil	Iran	20 06 1990	7.3	7.4	19	X	1000	100-1,000*
Luzon	Philippines	16 07 1990	7.8	7.7	25	VIII	3000	100-1,000*
Valle de la Estrella	Costa Rica	22 04 1991	7.6	7.5	21.5	IX	2000	1,000-10,000*
Northridge	USA	17 01 1994	6.8	6.7	18	IX	10000	>10,000*
Paez	Colombia	06 06 1994	6.6	6.8	12	X	250	1,000-10,000
Hyogu-Ken Nanbu	Japan	17 01 1995	6.8	6.9	22	X	910	100-1,000
Chi-chi	Taiwan, China	21 09 1999	7.3	7.6	8	XI	10000	≈10000
Wenchuan	China	12 05 2008	8.0	7.9	19	XII	>50000	>60,000

Note: * data from **Rodríguez et al., 1999.**

1.2.2 Profile Changes by Cutting and Filling

It is instructive to study the effects of cuts and fills on a landslide by applying the influence line concept, familiar from structural engineering. A fill may be simulated by a downward influence load, a cut by an upward one.

Vertical cut slopes should not be used unless the cut is in rock or very well cemented soil. Long-term stable cut slopes in most soils and geographic areas are typically made with about a 1:1 or ¾:1 (horizontal: vertical) slope.

Slope failures, or landslides, typically occur where a slope is over-steep, where fill material is not compacted, or where cuts in natural soils encounter groundwater or zones of weak material. To prevent failures, the slide area should be stabilized by removing the slide material, flattening the slope, adding drainage, or using structures.

1.2.3 Piles, anchors, restraining structures

A vast variety of methods can be used to either internally or externally stabilize the unstable slope. Internally stabilized systems, such as the soil nailing slopes or micro piles (or anchors) stabilized slopes, are in-situ reinforcement methods. On the other hand, the method of using retaining walls or sheet piles can be classified as an externally stabilized system.

In this thesis, we focus on the internally stabilized systems. Using a row of piles can be categorized as an internally stabilized system. There are some advantages of using a row of piles to stabilize the slope include: i) the availability of the construction equipment for piles; ii) the piles are structurally capable of resisting long-term environmental effects and iii) the economic benefits of using piles in comparison to other slope stabilization methods.

1.3 Scope and objectives

In the planning and design of stabilizing piles, it is necessary to analyze the soil-pile pressure acting on the piles. In addition, since the earthquake-induced landslides

occur frequently in recent years, it is important to analyze the seismic performance of a potential landslide under seismic loadings. And commonly, earthquake induced sliding displacements are used to assess the seismic performance of slopes. Therefore, the current study focuses on analysis of (1) soil-pile pressure acting on the piles (lateral force), and (2) the permanent landslide movement due to seismic load.

Two major approaches for the analysis of slope reinforced with piles have been studied so far. One is to estimate the soil-pile pressure per unit length of the pile in static condition. The other is to calculate earthquake-induced permanent displacement of the three-dimensional (3D) slope with/without reinforcement.

For the soil-pile pressure analysis, the most widely used method is proposed by Ito and Matsui (1975). In their model, the squeezing effect between two neighboring piles is analyzed by the theory of plastic deformation. However, the predictions by Ito and Matsui's method show the linear distribution of the soil-pile pressure, which is different from the field observed data. Moreover, many researchers analyze the behavior of the stabilizing piles in slopes without considering the effects of slope angle, while the natural slopes always have inclination with different angles.

For the landslide movement analysis, there are four general categories methods: (1) experimental methods, (2) empirical methods, (3) analytical methods and (4) numerical simulation methods. According to the results of these methods, some laws or codes have been proposed to guide the engineering practice. For example, based on statistical results, the distance of twice of maximum slope height is taken as the danger slopes zone in Japan (refer to **Figure 1.3**) (Chand et al. 2011). However, the 3D analytical analysis for the slopes reinforced with piles is scarce. Especially, considering the seismic load, the failure mechanism of the slope with or without the reinforcement should be studied in depth.

The objectives of this study are to solve the problems mentioned above, namely:

(1) To evaluate the soil-pile pressure acting on the piles due to the lateral soil movement based on the modified plastic deformation theory

(2) To present a new method for evaluating the effects of slope angle on the soil-pile pressure of the piles.

(3) To evaluate the effects of seismic loading on earthquake-induced permanent displacement of 3D slopes based on Newmark's method (1965).

(4) To develop numerical tool for evaluating the failure mechanisms of the 3D slopes reinforced with one row of stabilizing piles subjected to seismic load.

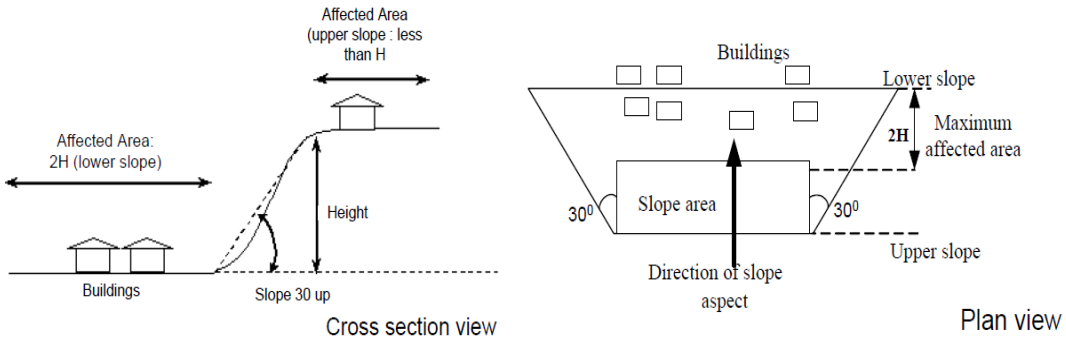

Figure 1.3 Abstracting the Japanese method to measure the dangerous slopes in the vicinity of building.

1.4 THESIS ORGANIZATION

The thesis comprises the following chapters.

Chapter 1 introduces (1) background of this study, (2) two main issues in current study, namely soil-pile pressure per unit length of the pile in static condition and the earthquake-induced permanent displacement, (3) the scope and objectives of this study, and (4) the organization of the thesis.

Chapter 2 reviews two aspects of existing studies on the subject of slope reinforced with piles: analyses of slope stabilized with a row of piles and landslide movement calculation. The merits and demerits of each method are stated.

Chapter 3 analyses the soil-pile pressure per unit length of the pile under static loading. The theory of plastic deformation is adopted, and the model proposed by Ito and

Matsui is modified by considering the soil arching effects along the depth of the moveable soil between two neighbouring piles. In addition, the parametric analysis is carried out to investigate the influence of the governing factors, which includes the geometric and mechanical parameters. The results shows that the all the parameters impart significant influence on the lateral force. In situ observed tests from the literatures are employed to validate the proposed approach. The comparison charts illustrate that the prediction due to the proposed approach shows greater agreement with the test results comparing with Ito and Matsui's solution (1975).

Chapter 4 presents a limit equilibrium method to analyse the lateral force (soil-pile pressure per unit thickness) on stabilizing piles embedded in semi-infinite slopes. In addition, the soil arching effects between two neighbouring stabilizing piles are analysed, and the lateral active stress in the rear of the piles is obtained. Furthermore, the squeezing effect between two piles proposed by Ito and Matsui is combined with the lateral active stress in the slope to evaluate the distribution of the soil-pile pressure per unit length of the stabilizing piles in sandy slopes. A numerical simulation using FLAC^{3D} is used to evaluate the proposed approach. The simulation shows that the proposed model could reasonably predict the shape of the distribution of the soil-pile pressure acting on the stabilizing piles, while some discrepancy exists between the numerical results and predicted values. Furthermore, the prediction of the proposed model is also evaluated through comparison to the experimental data from the published literature. Parametric analysis is carried out to investigate the influence of the slope angle on the distribution of the soil-pile pressure. The shape of the distribution of the soil-pile pressure acting on the piles varies with the angle of the slope, while the magnitude of the soil-pile pressure remains in the same order.

Chapter 5 presents three-dimensional (3D) limit analysis of seismic stability of slopes reinforced with one row of piles. A 3D rotational mechanism for earth slope is adopted. The lateral forces provided by the piles are evaluated by the theory of plastic deformation. Expressions for calculating the yield acceleration coefficient are derived. A random iteration method is employed to find the critical acceleration coefficient for the 3D slopes

with or without reinforcement. Based on the kinematic theory within the frame of the pseudo-static approach, a 3D model is proposed for evaluating the critical state and the subsequent displacement response. Furthermore, the Newmark's analytical procedure is employed to estimate the cumulative displacement induced by given earthquake loads. An example is shown to illustrate the influence of the piles on the seismic displacement of the 3D slopes.

Chapter 6 concludes the results and achievements of the study, and states the problems to be solved in future studies.

The organization of this thesis is shown in **Figure 1.4**.

REFERENCES

Chang, K.-J., Taboada, A., Lin, M.-L., and Chen, R.-F. 2005. Analysis of landsliding by earthquake shaking using a block-on-slope thermo-mechanical model: Example of Jiufengershan landslide, central Taiwan. Engineering Geology, 80(1-2): 151-163.

Cruden, D.M. 1991. A Simple Definition of a Landslide. Bulletin of the International Association of Engineering Geology, 43(1): 27-29.

Cruden, D.M. and Varnes, D.J. 1996. Landslide types and processes. In Landslides, Investigation and Mitigation. Special Report 247, Transportation Research Board, Washington D.C. 36-75.

EM-DAT 2003. The OFDA/CRED International Disaster Database - www.em-dat.net - Universit´e Catholique de Louvain - Brussels - Belgium.

Gokceoglu, C., and Sezer, E. 2009. A statistical assessment on international landslide literature (1945–2008). Landslides, 6(4): 345-351.

Gorum, T., Fan, X., van Westen, C.J., Huang, R.Q., Xu, Q., Tang, C., and Wang, G. 2011. Distribution pattern of earthquake-induced landslides triggered by the 12 May 2008 Wenchuan earthquake. Geomorphology, 133(3-4): 152-167.

Guzzetti, F. 2006. Landslide hazard and risk assement, University Bonn, Perugia.

Hazarika, H. 2007. Earthquake Hazard Mitigation Measures using Tire Derived

Geomaterials. Earthquake Hazards and Mitigations (Ayothiraman & Hazarika Eds.), 453-462.

Hazarika, H. 2007. Structural Stability and Flexibility during Earthquakes using Tyres (SAFETY) - A Novel Application for Seismic Disaster Mitigation -Scrap Tire Derived Geomaterials – Opportunities and Challenges- (Hazarika and Yasuhara Eds.), 115-126.

Highland, M. (2006): Estimating landslide losses—preliminary results of a seven-state pilot project. Open-File Report 2006-1032, USGS.

Highland, L.M., Bobrowsky, Peter 2008. The landslide handbook—A guide to understanding landslides. Geological Survey Circular, Reston, Virginia, U.S.

Wen, B.P., Han, Z.Y., Wang S.J., Wang, E.Z. & Zhang, J.M. 2005. Recent landslide disasters in china and lessons learned from landslide risk management. Landslide Risk Management. (Eds: Hungr, O., Fell, R., Couture, R. & Eberhardt, E.), 427-434. London: Taylor & Francis Group.

Petley, D.N., Hearn, G.J., Hart, A., Rosser, N.J., Dunning, S.A., Oven, K. & Mitchell, W.A. 2007. Trends in landslide occurrence in Nepal. Natural Hazards, 43(1): 23-44.

Schuster, R.L. 1996. The 25 most catastrophic landslides of the 20th century, in Chacon, Irigaray and Fernandez (eds.), Landslides, Proc. Of the 8th International Conf. & Field Trip on Landslides, Granada, Spain, 27-28 Sept. Rotterdam: Balkema.

Bommer, Julian J., Rodriguez, Carlos E. 2002. Earthquake-induced landslides in Central America. Engineering Geology, 63(3-4): 189-220.

Cavounidis, S. 1987. On the ratio of factors of safety in slope stability analyses. Geotachnique, 37(2): 207-210.

Hutchinson, J.N. 1988. General report: Morphological and geotechnical parameters of landslides in relation to geology and hydrology. In 5th International Symposium on Landslides, Lausanne, pp. 3-35.

HUTCHINSON, J. N. 1977. Assessment of the effectiveness of corrective measures in relation to geological conditions and types of slope movement. Symposium on Landslides and other Mass Movements, Prague, Bull. International Association of

Engineering Geology, No. 16, 131-155.

Ito, T., and Matsui, T., 1975. Methods to estimate lateral force acting on stabilizing piles. Soils and Foundations, 15(4): 43–59.

Jackson, J.A. 1997. Glossary of Geology. In Glossary of Geology. American Geological Institute, Alexandria, Virginia.

Newmark, N. W. 1965. Effects of Earthquakes on Dams and Embankments. The Fifth Rankine Lecture of the British Geotechnical Society, Geotechnique, England, Vol. XV, No. 2, 137-160.

UNEP 1997. World Atlas of Desertification, London: Arnold.

Varnes, D.J. 1974. The logic of geological maps, with reference to their interpretation and use for engineering purposes. U.S. Geological Survey Professional Paper, 837: 48.

WP/WLI, 1990. A suggested method for reporting a landslide. International Association Engineering Geology Bulletin, 41(1): 5-12.

Yin, Y., Wang, F., and Sun, P. 2009. Landslide hazards triggered by the 2008 Wenchuan earthquake, Sichuan, China. Landslides, 6(2): 139-152.

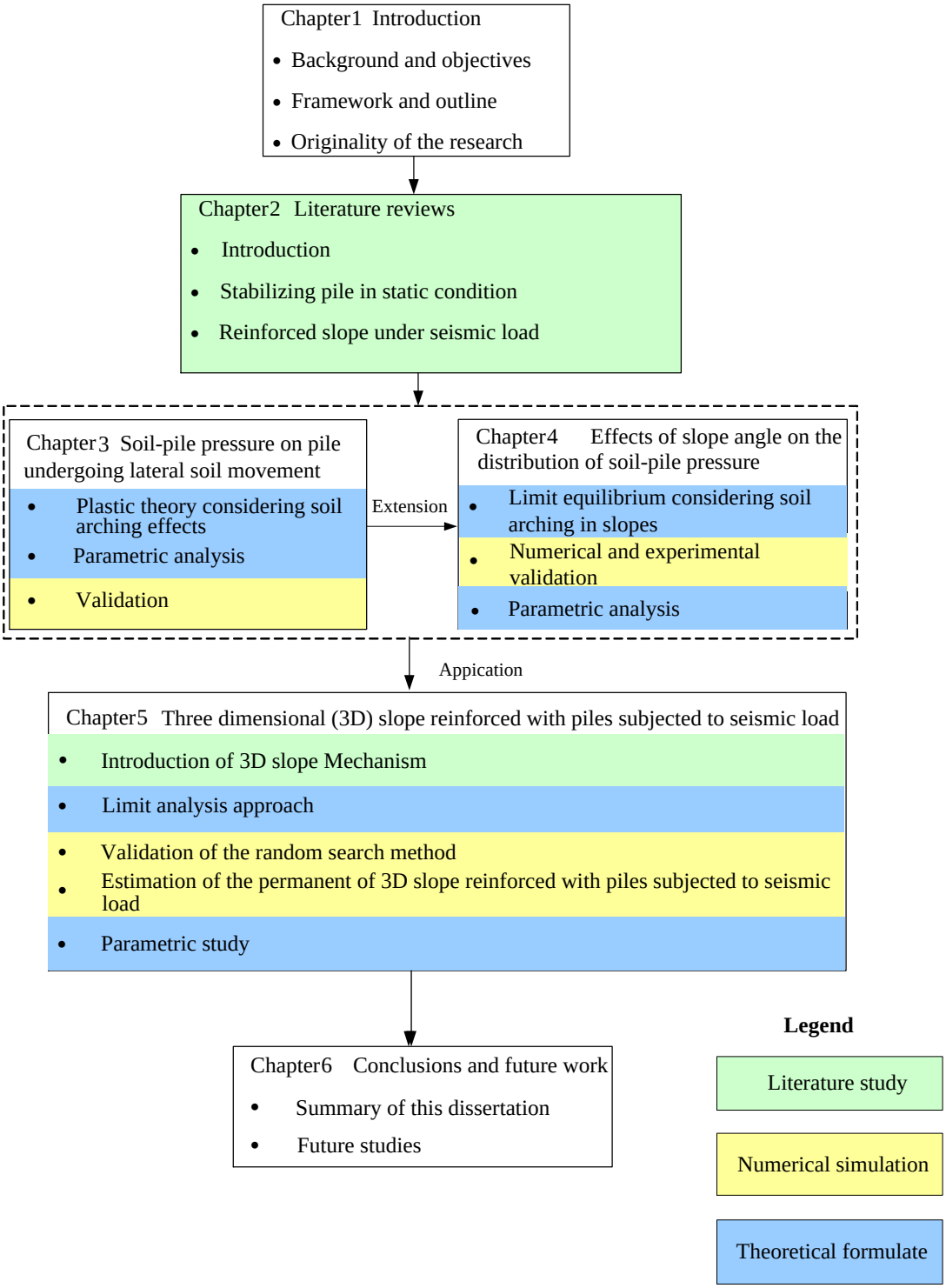

Figure 1.4 **The organization of this thesis.**

CHAPTER 2

LITERATURE REVIEW

2.1 INTRODUCTION

When piles are subjected to soil movement, these piles are known as passive piles. Soil movement is encountered in practice when piles are placed in an unstable slope, landslides, adjacent to deep excavation, tunnel operation, marginally stable riverbank with high fluctuating water level and also in piles supporting bridge abutment adjacent to approach embankments. The design of such piles may be based on the assumptions that forces from moving soil will act against the piles and 'squeeze' past the piles. On the other hand, active piles referred to a pile subjected to an external horizontal force.

As mentioned above, the stabilizing piles used to enhance the stability of the slopes are considered as the passive piles. The characterization of the problem of landslides and the use of piles to improve the stability of slopes requires better understanding of the integrated effect of laterally loaded pile behavior and soil-pile interaction above the sliding surface. Therefore, a representative model for the soil-pile interaction above the failure surface is required to reflect and describe the actual distribution of the soil driving force along that particular portion of the pile.

In this chapter, limit equilibrium analyses of slopes reinforced with piles are briefly discussed. In addition, different uncoupled analysis methods proposed in the literature for piled-slopes are reviewed followed by discussions of the available methods found in the literature to predict the limit soil pressure provided by stabilizing piles. Besides the analytical methods, the experimental methods and numerical methods are also discussed herein.

2.2 STABILIZING PILES UNDER STATIC LOAD CONDITION

2.2.1 EXPERIMENTAL METHODS

Poulos et al. (1995) described a series of laboratory tests on single instrumented model piles embedded in calcareous sand undergoing lateral movement. The experimental apparatus consisted of a testing vessel made from steel sheet of 3.2 mm thickness, and having internal dimensions of 450 mm wide by 565 mm long and by 700 mm in height, as shown in **Figure 2.1**. Key parameters influencing the maximum bending moment in the pile for a constant soil density have been identified to be pile head fixity condition, the ratio of the depth of moving soil to the pile embedded length, and pile diameter and stiffness. Normalized expressions for maximum bending moment are also presented in their research. A boundary element analysis was used to predict the experimental results, and the theoretical predictions were generally in good agreement with the measured values. The predicted maximum bending moments were generally within ± 20% of those measured, and the position of the maximum bending moment was very well predicted in all cases, even for the cases where the agreement between the predicted and the measured magnitude was not as satisfactory.

After that, Chen et al. (1997) investigated the pile-soil-pile interaction using the same apparatus, but the setup of the piles is different from the former tests. The findings of the test are: (1) for piles in a single row, the maximum bending moment decreased with decreasing pile spacing and, in general, was not significantly affected by either the number of piles or the pile head condition; (2) for piles in a line, each pile generally behaved differently; (3) the extent of the group effect on the lateral response of a pile in a group was dependent on a number of factors, including the position of the pile in the group, the pile spacing, the number of piles and head fixity.

Guo and his group (Guo and Ghee, 2004; Guo and Qin, 2005; Ghee and Guo, 2005) investigated the response of a pile due to lateral soil movement and axial load. Typical results deduced from single pile tests in sand were presented previously in terms of effect of pile diameter, soil movement profile, sliding depth and magnitude of axial

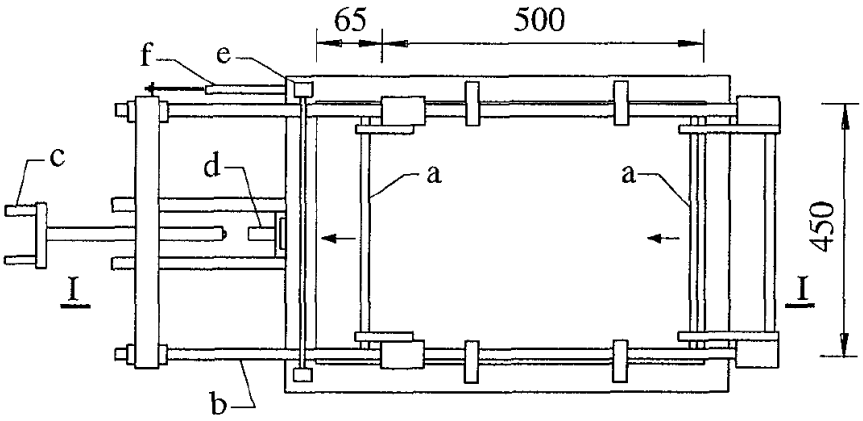

a. Steel plate b. Loading system c. Winching wheel
d. Load cell e. Transducer fixing frame f. Transducer

(a) Plan view

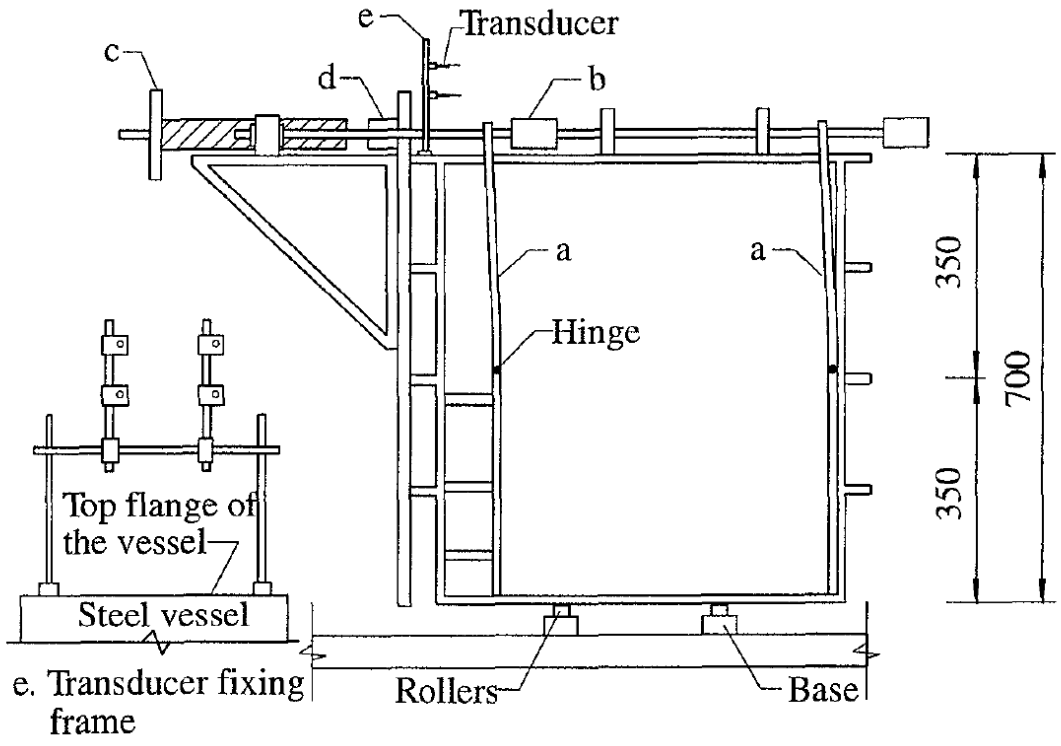

(b) Elevation view

Figure 2.1 Experimental apparatus used in the researches of Polous et al.(1995) and Chen et al.(1997).

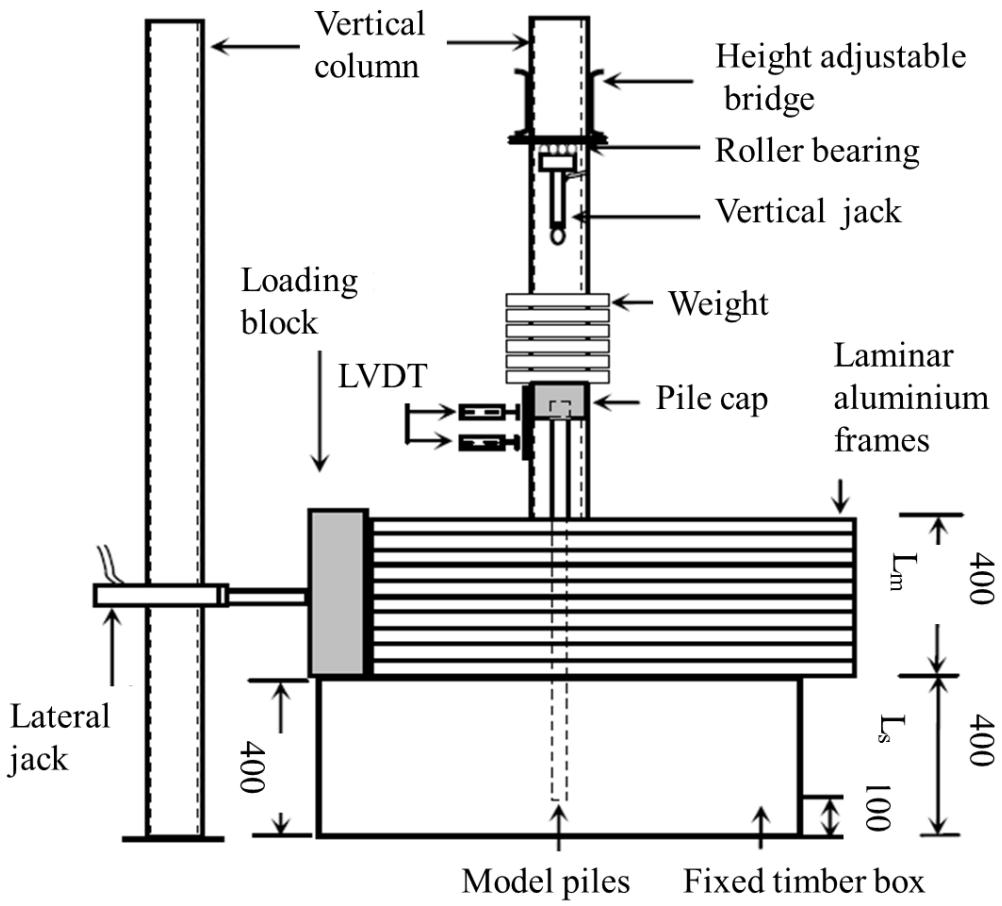

Figure 2.2 Experimental apparatus used in the researches of Guo and Ghee (2006).

load. After that, a laboratory experiment on the behavior of axially loaded pile groups was conducted by Guo and Ghee (2006). The experimental apparatus is shown in **Figure 2.2**. Results from the tests were reported, which were conducted on two instrumented pile groups embedded in sand subjected to a uniform lateral soil movement at a sliding depth of $0.57L_e$ (L_e = pile embedment length). Analysis revealed the effect of the direction and depth of soil movement, together with the magnitude of axial load, which are illustrated via profiles of bending moment, shear force, soil reaction, and pile deflection along instrumented piles in groups at various stages.

There are many other experiments on the behavior of piles subjected to lateral soil movement. For example, (1) performance of piles has been investigated through

centrifuge modelling (Springman, 1989; Stewart et al., 1994; Bransby and Springman, 1997; Ellis and Springman, 2001; Leung et al., 2000, 2003, 2006; Ong et al., 2006,2009; Abdoum et al., 2003; Dobry et al., 2003; Dobry, 2007; Finn, 2005; Bhattacharya et al., 2004; Brandenberg et al., 2007); (2) Performance of piles has been investigated through laboratory model tests for piles subjected to lateral soil movements (Fukuoka, 1977; Chen, 1994; Pan et al., 2000, 2002a; Tsuchiya et al., 2001; White et al., 2008).

2.2.2 ANALYTICAL METHODS

The analytical methods used to analyze the responses of stabilizing piles can generally be classified into two categories. The first is stress-based methods as proposed by Broms (1964), De Beer and Wallays (1972), Viggiani (1981), Randolph and Houlsby (1984), Ito and Matsui (1975). The second is displacement-based methods as proposed by Hull et al. (1992), Poulos (1995b), Lee et al. (1995), and Jeong et al. (2003). In the stress-based approach, some researchers make use of the ultimate soil pressure to be applied to the shafts in order to estimate the pile response utilizing several procedures. Reversely, in the displacement-based approach, the relative displacement between the soil and pile is considered. The response of the pile is derived based on the deformation of the pile subjected to a lateral soil movement.

2.2.2.1 Stress-based method

Broms (1964) used the Rankine passive pressure coefficient K_p, and the effective overburden pressure σ'_{vo} to estimate the ultimate soil-pile pressure (P_y) in sand for single pile. The equation is expressed as following:

$$P_y = \alpha_B K_p \sigma'_{vo} \tag{2.1}$$

in which, α_B is a coefficient ranging between 3 and 5.

A similar method was utilized by Randolph and Houlsby (1984) to derive exact solutions for limiting lateral resistance of a circular pile in cohesive soil. Their analyses were based on a perfectly plastic soil response. They reported that the limiting pressures that can develop were 9.14 c_u and 11.94 c_u for perfectly smooth and perfectly rough piles

respectively.

De Beer & Wallays (1972) proposed a semi-empirical method to estimate the maximum bending moment for piles subjected to asymmetrical surcharges. An assumption is made that a constant lateral pressure distribution acted on the pile in the soft layer. The magnitude of this lateral pressure was a function of the total vertical overburden pressure. They suggested that the lateral loading was caused by horizontal consolidation and creep, implying that their method was primarily intended to design piles in the long term (Kok, et al., 2009). The method cannot be used to calculate the variation of bending moment with depth along the pile.

Viggiani (1981) categorized the failure mechanisms of piles subjected to moving ground by considering different factors. First of all, the real pile-soil interaction problem was simplified by making the following assumptions:

1) The ground has two layers of soil, with the top layer sliding uniformly over a layer of underlying soil.

2) Both the ground surface and the slip surface are horizontal.

3) Both soil layers are saturated clays in undrained conditions.

4) The undrained shear strength (c_u) is constant in each layer.

Based on these assumptions, Viggiani identified six different failure mechanisms for piles embedded into a two layered purely cohesive soil, which depend on the yield moment of the pile section, the strength parameters of the stable and sliding soil layers, the thickness of the sliding soil mass and the length and diameter of the pile. His proposed approach was based on the concepts developed by Broms (1964) to evaluate the ultimate load of a vertical pile subjected to a horizontal point load.

Viggiani's solutions are idealized, but enable the potential failure mechanisms of piles subjected to lateral soil movement to be categorized and understood. However, many aspects of real landslides, such as an inclined ground surface and slip plane, and long-term drained strength parameters, are not considered.

Ito and Matsui (1975) proposed a theoretical method to analyze the growth mechanism of lateral forces acting on stabilizing piles when the soil flowed to squeeze between piles. The method was developed to specifically estimate pressures acting on passive piles in a row. The force that the failing mass exerts on a row of piles can be expressed as a function of the soil strength, the pile diameter, spacing, and location. Assuming that a portion of that force is counteracting the driving forces of the slope, the safety factor of the slope after the placement of piles can be calculated as a function of pile size and position.

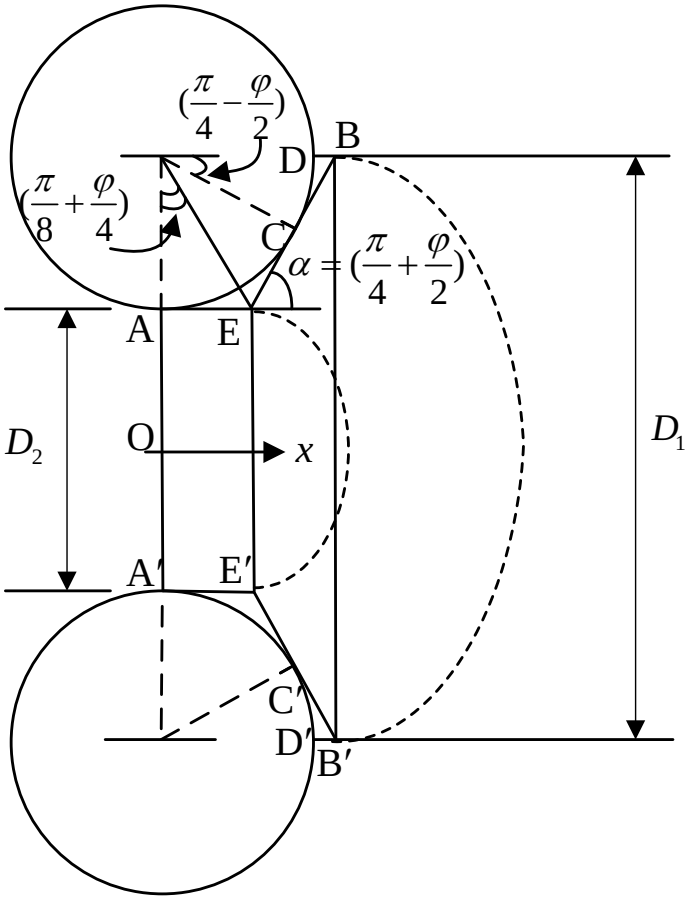

Figure 2.3 State of plastic deformation in the ground just around piles (after Ito and Matsui, 1975).

It is assumed that piles placed in plastically deforming ground can prevent further plastic deformations. In order to design the piles, the lateral forces need to be estimated

as accurately as possible. These forces, however, are a function of the movement of the sliding mass. They may vary from zero in case of no movement, to an ultimate value, in case of large movements (Hassiotis, et al., 1997). The theory developed by Ito and Matsui (1975) estimates an ultimate value for the lateral force, assuming that no reduction in the shear resistance along the sliding surface has taken place due to strains-softening caused by the movement of the landslide. For that reason, only the soil around the piles is assumed to be in a state of plastic equilibrium, satisfying the Mohr-Coulomb yield criterion. Then, the lateral load acting on the piles can be estimated regardless of the state of equilibrium of the slope. Inherent in this approach is the assumption that the soil is soft and able to plastically deform around the piles. The theory of plastic deformation is based on the following additional assumptions:

1. When the soil layer deforms, two sliding surfaces, AEB and A'E'B', occur making an angle of ($\varphi/4 + \pi/2$) with the x-axis (**Figure 2.3**).

2. The soil is in a state of plastic equilibrium only in the area AEBB'E'A' where the Mohr-Coulomb yield criterion applies.

3. The active earth pressure acts on lane AA'.

4. Plane strain conditions exist with respect to depth.

5. The piles are rigid.

6. The frictional forces on surfaces AEB and A'E' B' are neglected when the stress distribution in the soil AEBB'E'A' is considered.

In this method, the lateral force per unit length of the pile (P_D) at each depth is given as follows:

$$p_D = A\times c[\frac{1}{N_\varphi \tan\varphi}(B-2N_\varphi^{1/2}\tan\varphi-1)+\frac{2\tan\varphi+2N_\varphi^{1/2}+N_\varphi^{-1/2}}{N_\varphi^{1/2}\tan\varphi+N_\varphi-1}]-c[D_1\frac{2\tan\varphi+2N_\varphi^{1/2}+N_\varphi^{-1/2}}{N_\varphi^{1/2}\tan\varphi+N_\varphi-1}$$
$$-2D_2N_\varphi^{-1/2}]+\frac{\gamma z}{N_\varphi}(A\times\exp(\frac{D_1-D_2}{D_2}N_\varphi\tan(\frac{\pi}{8}+\frac{\varphi}{4}))-D_2) \quad (2.2)$$

in which, $N_\varphi = \tan^2(\frac{\varphi}{2} + \frac{\pi}{4})$, $A = D_1(\frac{D_1}{D_2})^{N_\varphi^{1/2}\tan\varphi + N_\varphi - 1}$, c is the cohesion of the soil, D_1 is the center-to-center pile spacing in a row, D_2 is the clear spacing between the piles (referring to Figure 2.3), φ is the internal friction angle, γ is the unit weight of the soil, z is an arbitrary depth from the ground surface.

Ito and Matsui's method (1975) is still widely referred by other researchers (Hassiotis, et al., 1997; Cai and Ugai, 2000; Won et al., 2005; Defae and Knappett, 2015; Hajiazizi and Azaheri, 2015). However, the differences exist between the linear predictions of the lateral force by this method and the non-linear observed data. The author finds that a more accurate prediction can be obtained if the soil arching effects is taken into account, which is developed between two neighboring pile along the depth of the moveable soil. The modified method will be discussed in the following chapter.

2.2.2.2 Displacement-based method

As mentioned previously, this method estimate the pile response based on using relative lateral displacements between the pile and the soil. Displacement-based approaches are considered more complicated than the stress-based approaches because the relationship between the movements of the pile and the soil are interrelated.

Poulos (1973) developed a computer program PALLAS to simulate the pile response by a given soil movement, using the simplified boundary element method. Hull et al. (1992) developed a program with the ability to model the pile head and tip loading by using a modified nonlinear boundary element approach. Poulos (1995) and Lee et al. (1995) carried out numerical analyses using a computer program, ERCAP (CPI, 1992), to present an approach for the design of slope stabilizing piles by assessing their response to lateral ground movement. The pile was modelled as a simple elastic beam, and the soil as an elastic continuum. To impose the lateral load on the pile, the unstable soil was moved downslope along the drag zone (or slip surface) as a rigid body (refer to **Figure 2.4**).

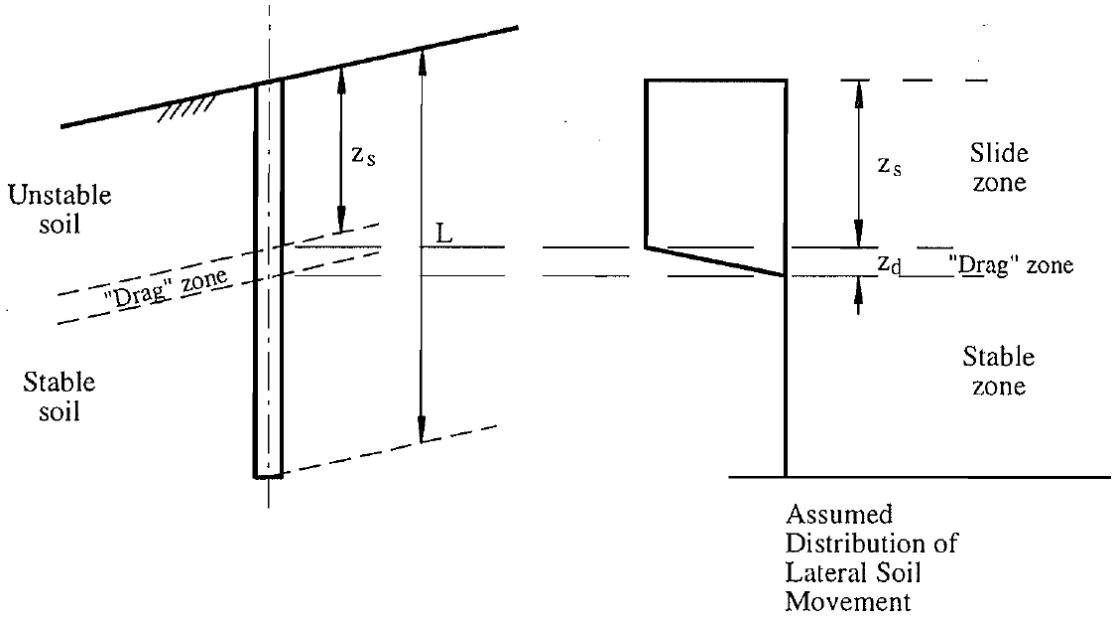

Figure 2.4 **Basic problem of a pile in unstable slope (Poulos, 1995).**

Poulos (1995) highlighted three different failure modes via the analysis of ERCAP:

(i) Flow mode: when the depth of the slip plane is shallow, the unstable soil becomes plastic and flows around the stationary pile (see **Figure 2.5**). The pile deflection is considerably less than the soil movement under "flow mode". For practical uses, Poulos endorsed the flow mode that creates the least damage from soil movement on the pile.

(ii) Short pile mode: when the slip plane is relatively deep and the length of the pile in the stable soil is relatively shallow, the unstable sliding soil carries the pile through the stable soil layer (**Figure. 2.6**).

(iii) Intermediate mode: when the depth of the failure surface is relatively deep and the soil strength along the pile length in both unstable and stable layers is fully mobilized (**Figure 2.7**). In this mode, the pile deflection at the upper portion exceeds the soil movement and a resisting force is applied from downslope to this upper portion of the pile.

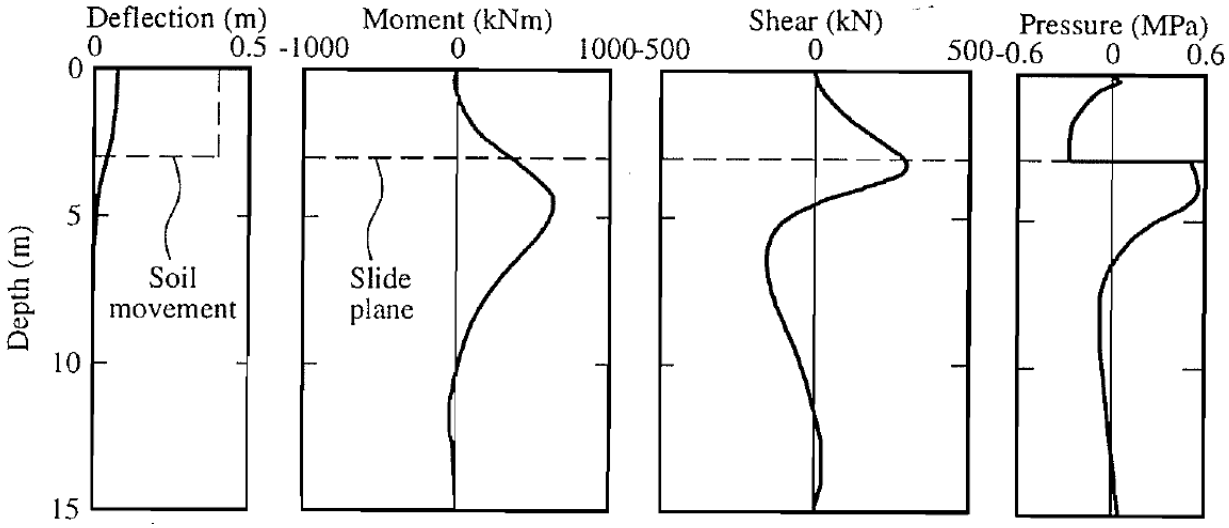

Figure 2.5 Flow mode of failure (Poulos, 1995).

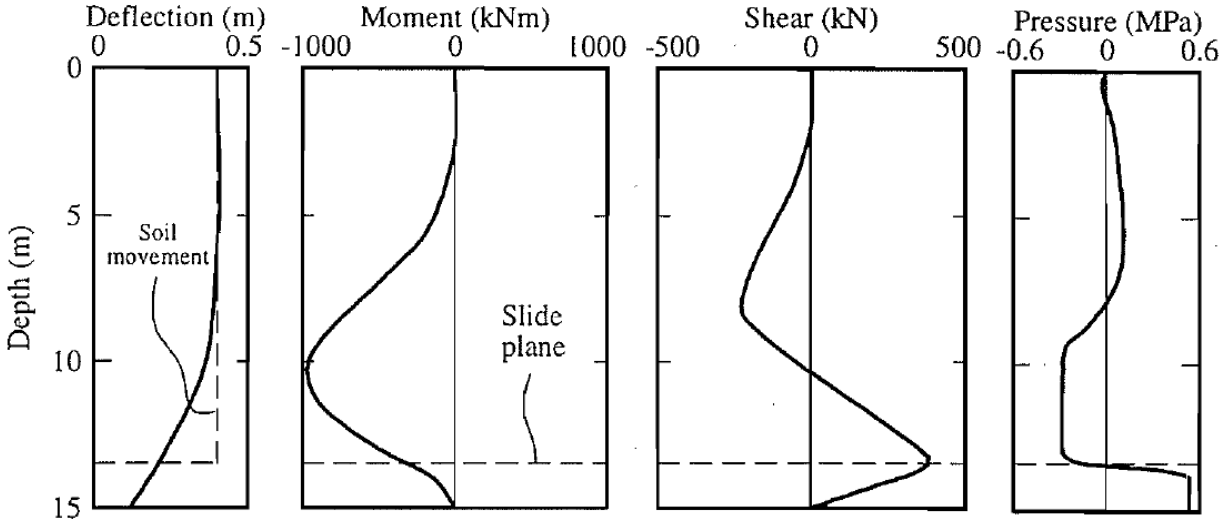

Figure 2.6 Short pile mode of failure (Poulos, 1995).

The following observations were made by Poulos (1995): (1) the maximum shear force in the pile is developed at the level of the slide plane; (2) for the flow mode, the maximum moment occurs below the slide plane, in the stable soil, and the pile movement is considerably less than the soil movement; (3) for the short-pile mode, the maximum moment occurs well above the slide plane in the unstable soil, and the soil and pile movements are similar; and (4) for the intermediate mode, large moments are developed both above and below the slide zone, and the pile head movement can exceed

the soil movement.

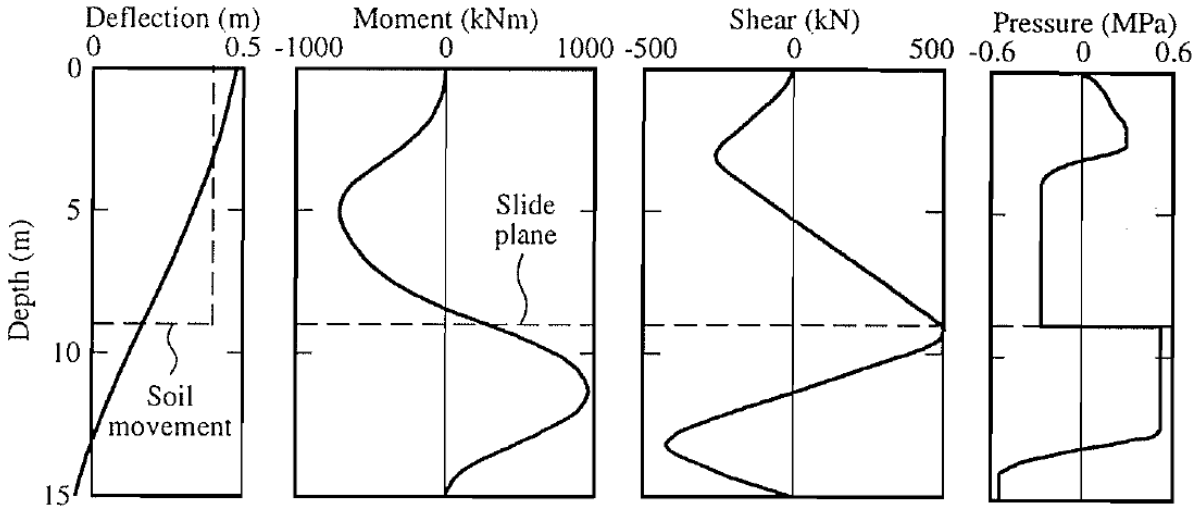

Figure 2.7 Intermediate mode of failure (Poulos, 1995).

2.2.2.3 Limit analysis method

Ausilio et al. (2001) used the kinematic approach of limit analysis to analyze the stability of earth slopes reinforced with piles. In their research, the analysis involved two steps: (1) the case of slope without piles was considered and a procedure was developed to calculate the safety factor for the slope, which was defined as a reduction coefficient for the strength parameters of the soil; (2) the stability of slopes reinforced with piles was analyzed. To account for the presence of the piles, a lateral force and a moment were assumed and applied at the depth of the potential sliding surface. Expressions were derived allowing the assumed force to increase the safety factor to a desired value and the most suitable location of piles within the slope to be evaluated.

Based on the limit analysis, Ausilio et al. (2001) found that: (1) installing a row of piles was an effective remedy to improve slope stability especially when the sliding surface for the unreinforced slope was relatively shallow; (2) the optimal location of the piles within the slope was near the toe of the slope where the stabilizing force needed to increase the safety factor to the desired value takes a minimum value.

Nian et al. (2008) developed a similar approach to analyzing the stability of a slope

with stabilizing piles in nonhomogeneous and anisotropic soils. The research indicated that the optimal location of a row of piles within the slope was near the toe of the slope. This conclusion was in line with the results of Ausilio et al. (2001). Furthermore, Nian et al. (2008) pointed out that Piles also appeared to be very effective when they were installed in the region from the middle to the toe of the slope in the case of lower design safety factor F_s, anisotropic coefficient k_{ac}, and gentle slope. The study also showed that both the anisotropy and non-homogeneity of the soil strength strongly affected the required lateral stabilizing force provided by piles, especially the effect of anisotropy.

2.2.3 NUMERICAL METHODS

In recent decades, numerical methods have been used by several researchers (Chow, 1996; Jeong et al., 2003; Zeng and Liang, 2002; Yamin and Liang, 2010; Kourkoulis et al., 2012) to investigate the soil-pile interaction in pile reinforced slopes. These methods are becoming increasingly popular because they offer the ability to model complex geometries, 3D soil-structure phenomena (such as pile group effects), and soil and pile non-linearity. However, numerical methods are computationally intensive and time-consuming.

More recently, Kourkoulis et al. (2012) introduced a "Hybrid" method for analysis and design of slope stabilizing piles, combining the accuracy of rigorous three-dimensional (3D) finite element (FE) simulation with the simplicity of widely accepted analytical techniques. This approach consists of two steps: (1) evaluating the required lateral resisting force per unit length of the slope (F_{lr}) required to increase the safety factor of the slope to the desired value; and (2) estimation of the optimum pile configuration that offers the required F_{lr} for a prescribed deformation level. The first step utilizes the results of conventional slope-stability analysis. A novel approach is proposed for the second step, which involves decoupling the slope geometry from the computation of the piles' lateral capacity, which allows for the numeric simulation of only a limited region of soil around the piles. In modeling only a representative region of the soil around the pile, the ultimate resistance is computed by imposing a uniform displacement

profile onto the model boundary.

2.3 SLOPES WITH/ WITHOUT REINFORCEMENT UNDER SEISMIC LOAD

2.3.1 TWO DIMENSIONAL SLOPES UNDER SEISMIC LOAD

Three types of methods have been developed to date to assess the stability of slopes subjected to earthquakes: (1) pseudo-static methods, (2) dynamic sliding block methods, and (3) stress-strain methods. Each method has strengths and weaknesses, and each can be appropriately applied in different situations (Jibson, 2011).

This section reviews these three categories methods and discusses their advantages and limitations.

2.3.1.1 Pseudo-static method

The pseudo-static method was first presented by Terzaghi (1950). It is a simple method can be applied to natural or artificial slopes for evaluating of seismic stability of a slope. It is assumed that the effect of the earthquake force acting on the whole or an element of the slope is represented by a horizontal force and/or a vertical force equal to the product of the gravitation force and a coefficient k. The schematic of the pseudo-static method applied in a slope is shown in **Figure 2.8**.

Thus the assumed seismic acceleration a is k times the gravitational acceleration g, i.e. $a_s=kg$. In the direction of horizontal and vertical, the assumed pseudo-static forces acting on a potential sliding mass of weight W can be expressed respectively as

$$f_h = \frac{a_h}{g} W = k_h W$$
$$f_v = \frac{a_v}{g} W = k_v W \tag{2.3}$$

where a_h and a_v are horizontal and vertical pseudo-static accelerations, respectively, k_h and k_v are horizontal and vertical pseudo-static coefficients, respectively. The factor of safety (FOS) is expressed as the ratio of the resisting force to the driving force,

$$FOS=\frac{\tau_r}{\tau_d} \quad (2.4)$$

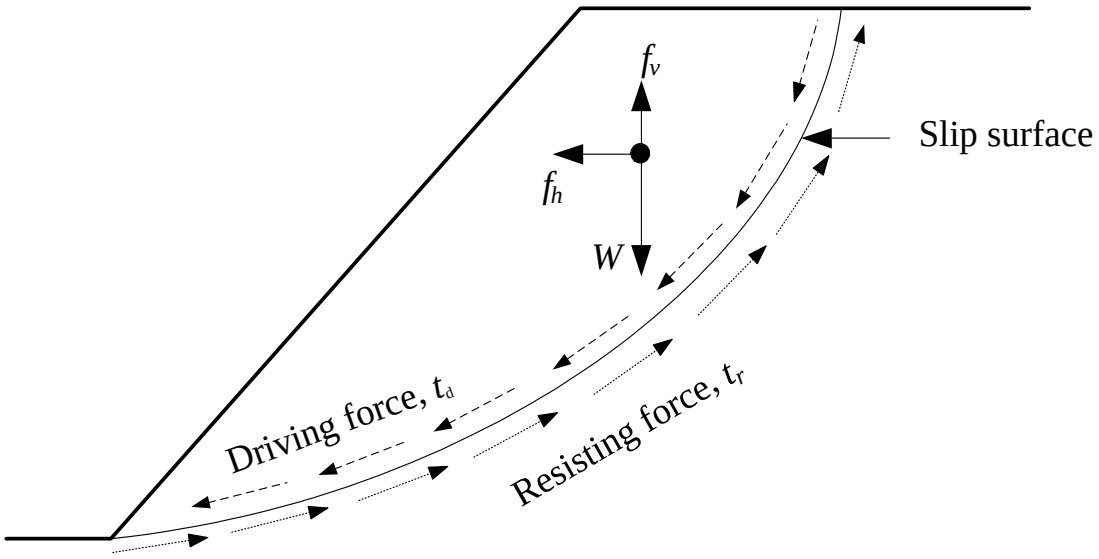

Figure 2.8 Earthquake Forces acting on a slope in pseudo-static slope stability analysis.

There are three points for the pseudo-static seismic force mentioned: (1) magnitude, (2) direction and (3) point of application, which should be determined in the application of the pseudo-static methods.

(a) **Magnitude**

According to Eq. 2.3, the magnitude of the assumed pseudo-static force is determined by the seismic coefficient. The key problem for the pseudo-static procedure is how to select an appropriate seismic coefficient under an acceptable FOS. There have been studies for determining the most appropriate pseudo-static coefficient by a matter of experience and judgment.

Terzaghi (1950)'s classical paper, probably the earliest recommendations on the values of the seismic coefficient published by a renowned geotechnical engineering or engineering geologist, made the original suggestion to use of k_h=0.1 for severe earthquakes, k_h=0.2 for violent and/or destructive earthquakes, and of k_h=0.5 for catastrophic earthquakes.

There are many other researches on the study of seismic coefficients (Makdisi and Seed, 1977; Seed, 1979; Marcuson and Franklin, 1983; Hynes-Griffin and Franklin, 1984; Bray and Rathje, 1998; Kramer, 1996; Pyke, 1991; Krinitzsky, 1993; Kavazanjian et al., 1997; Stewart et al., 2003). The recommendations for selecting the seismic coefficients proposed by these researchers are listed in **Table. 2.1**. All of these recommended pseudo-static coefficients can fall into two categories: (1) magnitude-based coefficients and (2) peak ground acceleration (PGA)-based coefficients (Zhang, 2013).

(b) **Direction**

In most of the research mentioned above, only the horizontal acceleration is taken into account for evaluating the stability and deformation of a slope. It is because that, as shown in **Figure 2.8**, the horizontal force clearly increases the driving force and decreases the FOS. Conversely, the vertical pseudo-static force typically has less influence on the FOS than the horizontal pseudo-static force does because the vertical pseudo-static reduces both the driving force and resisting force. As a result, the effects of vertical accelerations are frequently omitted in pseudo-static analysis (Kramer, 1996).

Analyses performed by several investigators with an inclined seismic force (i.e. coupled with vertical component of the earthquake force) have shown that the inclination can have a significant influence on the seismic slope stability analysis (Chopra, 1966; Ling, 1998).

(c) **Point of application**

The pseudo-static force in an analysis, which presents the earthquake effects in horizontal direction, requires a decision as to its point of application. Usually, it is applied at the centre of gravity of a potential sliding mass or of a typical vertical slice in any method of slices. Alternatively, the force also can be applied at the level of the base of a slice. Different points of application of pseudo-static force induce a significant difference in the result. Seed (1979) provided a well-known example, the analysis of Sheffield Dam. In his study the seismic forces were applied at the base and the center of

gravity of each slice, respectively, and the results of factor of safety were 1.21 and 1.32, respectively (Chowdhury et al., 2010).

Table 2.1 Pseudo-static coefficient from several studies (Zhang, 2013)

Recommended pseudo-static coefficient (k/g)	FOS	Permanent displacement (D/m)	Original application	References
0.1 (R-F=IX) 0.2 (R-F=X) 0.5 (R-F=XI)	>1.0	-	Nature or artificial slope	Terzaghi, 1950
0.1 (M=6.5) 0.15 (M=8.25)	>1.5	<1	Earth dams	Makdisi and Seed, 1977
0.1 (M=6.5) 0.15 (M=8.25)	>1.15	<1	Earth dams	Seed, 1979
(1/3~1/2)PGA	>1.0	-	-	Marcuson, 1981
1/2 PGA	>1.0	<1	Earth dams	Hyness-Griffin and Franklin, 1984
1/2 PGA (M=8.25) 1/3 PGA (M=7.5) 1/4 PGA (M=7.0) 1/5 PGA (M=6.5)	>1.0	-	-	Pyke, 1991
0.15	>1.1	-	Dams	CDCDMG, 1997
(0.6~0.75) PGA_{rock}	>1.0	<0.15~0.3	Soild-waste landslides	Bray and Rathje, 1998
(0.25~0.75) PGA_{rock}	>1.0	<0.05~0.15	Urbanized slopes	Stewart, 2003

Note: R-F is Rossi-Forel earthquake intensity scale, IX: severe earthquake, X destructive earthquake, XI catastrophic earthquake; M is earthquake magnitude; PGA is peak ground acceleration, in terms of acceleration of gravity.

Generally speaking, it is recommended that pseudo-static analysis, which provides only a very rough approximation of slope behavior during earthquake shaking, should be used only for preliminary assessments and screening procedures, then followed by more sophisticated analysis (Stewart et al., 2003; Wasowski et al., 2011; Jibson et al., 2011)

2.3.1.2 Dynamic sliding block methods

Displacement-based dynamic sliding block method is another widely used approach to evaluate the seismic slope stability in earthquake geotechnical engineering. This method regards the permanent displacement as the index of slope performance.

Newmark (1965) first proposed the basic elements of a procedure for evaluating the potential displacements of an embankment due to earthquake shaking. Newmark envisaged that sliding would be imminent once the inertia forces on a potential failure block were large enough to overcome the yield resistance and that movement would stop when the inertia forces were reversed.

In his analysis, a soil mass moving downward along a failure surface under inertia force due to earthquake shaking is considered to be analogous to a rigid block with weight and an external force sliding on an inclined plane as shown in **Figure 2.9**. Thus, the movement of slope would begin to occur if the inertia force induced by earthquake on a potential slide mass exceeds the yield acceleration. The failure mechanism and corresponding yield acceleration must be determined first so that the analogous inclined plane and external force can be simulated. Subsequently, the overall displacements of a failure slope under earthquake loads can be assessed (Chen et al., 1978; Chen, 1980). This can be achieved in the following step (Chang et al., 1984):

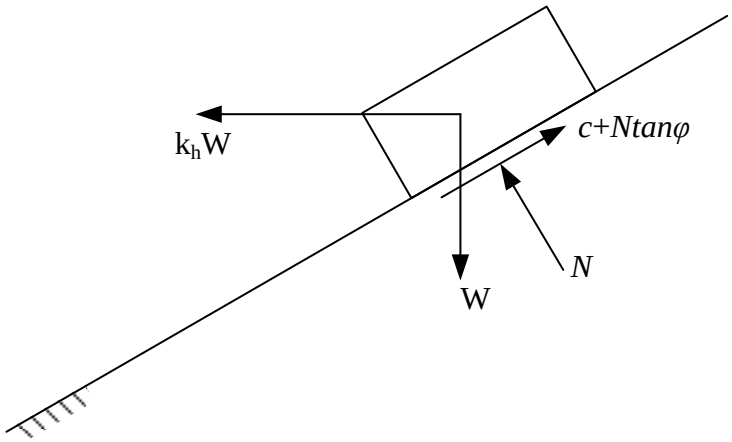

Figure 2.9 Rigid block on an inclined slope.

1. Calculate the yield acceleration at which slippage will just begin to occur.
2. Apply various values of the pseudo-static force to the slope. These values are obtained from a discretized accelerogram of an actual or simulated earthquake.
3. According to the yield acceleration and accelerogram of an earthquake, the time history of velocity of the sliding soil mass of a slope can be calculated. The

magnitude of displacements can be evaluated by integrating all the positive velocity.

4. Determine the "stability" of the slope on the basis of this estimated total displacement by rigid body sliding.

In summary, a pseudo-static analysis is first used to calculate a critical or yield acceleration value a_c. The permanent displacement for a sliding mass is then calculated by double integration of the earthquake acceleration time history data above the critical acceleration. Newmark showed that the critical or yield acceleration, parallel to the slope, of a potential landslide block is a simple function of the static factor of safety and landslide geometry, expressed as:

$$a_c = (\mathrm{FOS} - 1) g \sin \alpha_{an} \tag{2.5}$$

where a_c is in terms of the gravity acceleration g; FOS is the static factor of safety; and α_{an} is the angle from the horizontal of the sliding surface.

It should be noted that Newmark's concept implied that movements would stop when the inertia forces were reversed. Actually, the velocity could remain positive even if the inertia forces were reversed or the inertia forces were not reversed but less than the yield resistance on the potential failure surface. Positive velocity thereby causes sliding on the surface. On the other hand, the velocity could be negative even though the inertia forces were greater than yield resistance. It all depends on the magnitude and direction of both velocity and inertia force, while not either one alone. Besides, as also indicated by Newmark, the uphill resistance without serious error in the calculations, may be taken as infinitely large. In this situation, ground motions in the direction of the downward slope tend to move the mass downhill, but ground motions in the upward direction along the slope leave the mass without relative additional motion except where these are extremely large in magnitude. Thus, the negative velocity or velocity heading uphill is not allowed in this analysis.

Since the rigid-block method was published in 1965 by Newmark, it has seen numerous applications. As reviewed by Garini et al., (2011), the applications in recent

years include (1) the seismic deformation analysis of earth dams and embankments (Yegian et al., 1991a; 1991b; Sawada et al., 1993; Kramer, 1996); (2) the displacements associated with landslides (Jibson, 1993; Del Gaudio et al., 2003); (3) the seismic deformation of landfills with geosynthetic liners (Bray and Rathje, 1998; Yegian et al., 1998); (4) the seismic settlement of surface foundations (Richards et al., 1993); and (5) the potential sliding of concrete gravity dams (Danay and Adeghe, 1993; Fenves and Chopra, 1986). The extension of the analogue by Richards and Elms (1979) to gravity retaining walls has met worldwide acceptance, and has found its way into seismic codes of practice. Several other generalised applications have also appeared (e.g. Stamatopoulos, 1996; Rathje and Bray, 2000; Ling, 2001; Fardis, 2009; Wartman et al., 2003).

2.3.1.3 Stress-strain methods

With the developments of computer technology and simulation approach in recent decades, the numerical simulation method is becoming increasingly used in engineering practice and more and more popular for the real dynamic analysis. These methods can be categorized into continuous methods, e.g. finite element method (FEM) (Clough, 1960), finite difference method (FDM) (Mitchell and Griffiths, 1980), boundary element method (BEM) (Brebbia and Wrobel, 1980), and discontinuous methods, e.g. rigid block spring method (RBSM) (Kawai, 1977; 1978), discrete element method (DEM) (Cundall, 1971) and discontinuous deformation analysis (DDA) (Shi and Goodman, 1985; 1989).

2.3.2 TWO DIMENSIONAL (2D) SLOPES REINFORCE WITH PILES UNDER SEISMIC LOAD

Li et al. (2010) used the kinematic theorem of limit analysis method to analyze the seismic stability of 2D slopes reinforce with a row of piles. In their method, a homogeneous and isotropic soil slope reinforced with a row of piles is considered. Based on the requirement of limit analysis, the soil is assumed to deform plastically according to the normality rule associated with the Mohr-Coulomb yield condition. It has been proved that of the various failure mechanisms of the slope, the rotational one has been found to be the most adverse for earth slopes (Chen and Liu, 1990). So the rotational

log-spiral collapse mechanism, which had been earlier examined by Chen (1975) and other researchers, was adopted in their approach. The geometry of the failure surface (**Figure 2.10**) is described by the log-spiral equation, which can be expressed as

$$r = r_0 e^{(\theta-\theta_0)\tan\varphi} \tag{2.6}$$

where φ is the internal friction angle of the soil, and r_0 is the radius of the log spiral with respect to angle θ_0. The failing soil mass rotates as a rigid body about the Point O with angular velocity ω. The slope geometry is defined by height H, and angles α and β, which are also indicated in **Figure 2.10**.

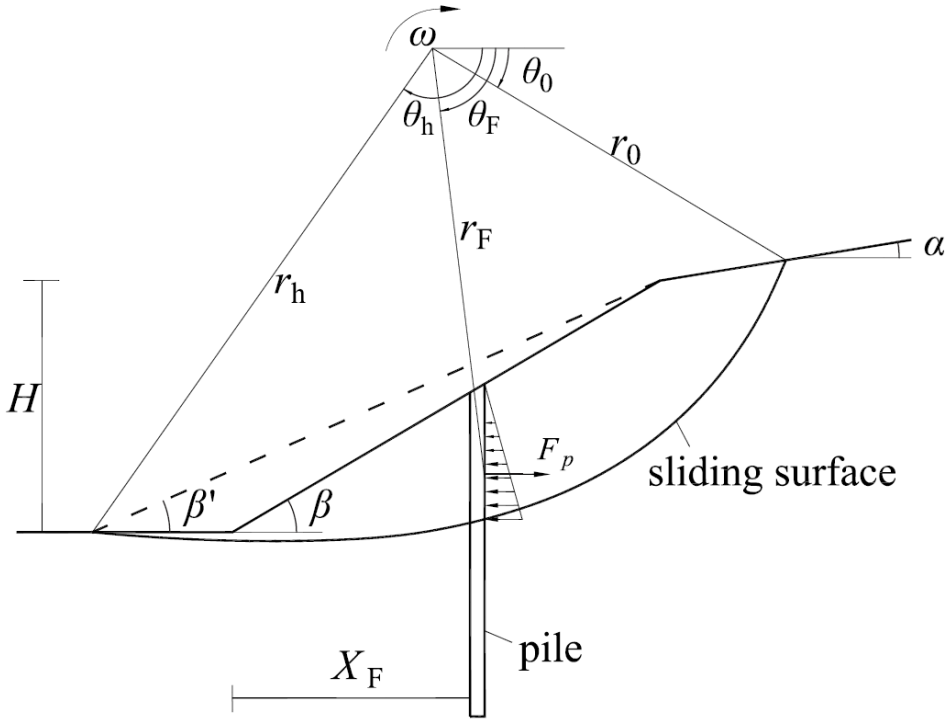

Figure 2.10 Rigid rotation collapse mechanism for a slope reinforced with piles.

In their method, the resistant forces provided by the installed piles were estimated by plastic deformation theory (Ito and Matsui, 1975). It is assumed that only the soil around the piles is to be in a state of plastic equilibrium satisfying the Mohr-Coulomb's yield criterion. Then, the lateral load acting on the piles can be calculated regardless of the state of equilibrium of the slope. Based on the assumptions used, the lateral force per

unit thickness of the layer acting on the piles was estimated by Eq. 2.2. The total lateral force acting on a pile due to the plastically deforming layer around the pile, F_t, can be obtained by integrating Eq. 2.2 along the depth of the pile in the failing wedge. Then, the stabilizing force per unit width of soil, F_p (**Figure. 2.10**), provided by the pile can be calculated by dividing F_t with the center-to-center distance between the piles.

In summary, Li et al. (2010) used the upper-bound theorem of limit analysis to determine the yield seismic coefficient and its corresponding failure mechanism. In addition, to account for the presence of the piles, a lateral force is assumed to be applied at the failure mass. For slopes without piles, the calculated results of the critical acceleration coefficient are fairly coincident with that obtained by Newmark's method. The seismic displacement investigation shows the efficiency of piles in limiting the deformation of the slope under earthquake loading.

2.4 SUMMARY AND CONCLUSIONS

Firstly, the studies in the field of the stabilizing piles under static load condition are reviewed, which include three parts of contents, i) experimental methods, ii) analytical methods, and iii) numerical methods. Secondly, the 2D slopes with or without reinforcement under seismic load are reviewed. Some conclusions can be drawn:

(a) Three kinds of methods can be used to analyse the responses of the piles subjected to lateral soil movement. In detail, experimental method can provide the qualitative and quantitative observations on the obtained results although this method is time-consuming, expensive and of limited utility. Especially, it is difficult to obtain an effective empirical formula from a laboratory experimental test to evaluate the realistic pile response accurately. Analytical method can be more directly used without the need of statistically-significant database of previous events. Numerical simulation method can be used to provide more information, and it is a very useful method to validate the analytical method.

(b) Three categories methods can be used to analyse the seismic stability of a slope. Each of these types of methods has strengths and weaknesses and each can be

appropriately applied in different situations. In detail, pseudo-static methods can simply and directly determine the FOS and the critical coefficient k_c of a slope, while the widely used Newmark's methods and its extensions can determine the co-seismic deformation of a slope. Furthermore, the permanent displacement of the slope, which is reinforced with piles, can be evaluated using the kinematic theorem of limit analysis within the framework of the pseudo static approach.

REFERENCES

Abdoum, T., Dobry, R., O'Rourke, T.D., and Goh, S.H. 2003. Pile response to lateral spreads: centrifuge modeling. Journal of Geotechnical and Geoenvironmental Engineering, ASCE, 129(10): 869-878.

Ausilio, E., Conte, E., and Dente, G. 2001. Stability analysis of slopes reinforced with piles. Computers and Geotechnics, 28(8): 591–611.

Danay, A. and Adeghe, L.N. 1993. Seismic induced slip of concrete gravity dams. Journal of structural Engineering, ASCE, 119(1): 108-129.

De Beer E.E., and Wallays, M. 1970. Stabilization of a slope in schist by means of bored piles reinforced with steel beams, Proceeding of the 2nd International Congress on Rock Mechanics, Beograd, 361-369.

Del Gaudio, V., Pierri, P., and Wasowski, J. 2003. An approach to time-probabilistic evaluation of seismically induced landslide hazard. Bulletin of the Seismological Society of America, 93(2): 557-569.

Bhattacharya, W. and Madabhushi, S.P.G. 2008. A critical review of methods for pile design in seismically liquefiable soils. Bulletin of Earthquake Engineering, 6, 407-446.

Brandenberg, S.J., Boulanger, R.W., Kutter, B.L., and Change, D. 2007. Static pushover analyses of piles groups in liquefied and lateral spreading ground in centrifuge tests. Journal of Geotechnical and Geoenvironmental Engineering, ASCE, 131(4): 529-531.

Bransby, M. F. and Springman, S. 1999. Centrifuge modeling of pile groups adjacent to

surcharge loads. Soils and Foundations, 37(2): 39-49.

Bray, J.D., and Rathje, E.M. 1998. Earthquake-induced displacements of solid-waste landfills. Journal of Geotechnical and Geoenvironmental Engineering, 124(3): 242-253.

Brebbia, C.A., and Wrobel, L. 1980. The boundary element method. Computer methods in fluids.(A 81-28303 11-34) London, Pentech Press, Ltd., 1980: 26-48.

Broms, B. B. 1964. Lateral resistance of piles in cohesive soils. Journal of Soil Mechanics and Foundations Division, ASCE, 90(2): 27-63.

Cai, F., and Ugai, K. 2000. Numerical analysis of the stability of a slope reinforced with piles. Soils and Foundations, 40(1): 73–84.

Clough, R.W. 1960. The finite element method in plane stress analysis. In 2nd Conference on Electronic Computation, Pittsburgh, PA.

CPI. 1992. Users Manual for Program ERCAP, Coffey Partners International Pty Ltd, North Ryde, Australia.

Chang, C.J., Chen, W.F. and Yao, J.T.P. 1984. Seismic displacement in slopes by limit analysis. Journal of Geotechnics Engineering, ASCE, 110(7): 860-874.

Chen, W. F. 1975. Limit analysis and soil plasticity, Elsevier, Amsterdam.

Chen, .W.F., and Liu, X.L. 1990. Limit Analysis in Soil Mechanics, Elsevier, Amsterdam.

Chen, L.T., Poulos, H. G., and Hull, T. S. 1997. Model tests on pile groups subjected to lateral soil movement. Soils and foundations, 37(1): 1-12.

Chen, W.F. 1980. Plasticity in soil mechanics and landslides. Journal of Mechanics Division, 106(3): 443-464.

Chen, W.F., Chang, C.J. and Yao, J.T.P. 1978. Limit analysis of earthquale-induced slope failure. In: R.L. Seirakowski (Editor), Proc. 15th Annual meeting of the society of engineering science. University of florida, Gainesville, FL, 533-538.

Chopra, A.K. 1966. The importance of the vertical component of earthquake motions. Bulletin of the Seismological Society of America, 56(5): 1163-1175.

Chow, Y.K. 1996. Analysis of piles used for slope stabilization. International Journal for

Numerical and Analytical Methods in Geomechanics, 20: 635-646.

Chowdhury, R., Flentje, P., and Bhattacharya, G. 2010. Geotechnical slope analysis. CRC Press, Taylor & Francis Group, LLC.

Cundall, P. 1971. A computer model for simulating progressive, large scale movements in blocky rock system. In Symposium of International Society of Rock Mechanics, Nancy, France, 11–18.

Defae, A., Knappett, J.A. 2015. Newmark sliding block model for pile-reinforced slopes under earthquake loading. Soil Dynamics and Earthquake Engineering, 75: 265–278.

Dobry, R., Abdoum, T., O'Rourke, T.D., and Goh, S.H. 2003. Single piles in lateral spreads: field bending moment evaluation. Journal of Geotechnical and Geoenvironmental Engineering, ASCE, 129(10): 879-889.

Dobry, R. 2007. Pile response to lateral spreads: field observations and current research. The fifteenth spencer J. Buchanan Lecture. Texas A&M University.

Ellis, E.A., Durrani, I. K., and Reddish, D.J. 2010. Numerical modelling of discrete pile rows for slope stability and generic guidance for design. Geotechnique, 60(3): 185-195.

Fardis, M.N. 2009. Seismic design, assessment and retrofitting of concrete buildings: based on EN-Eurocode 8. Springer.

Finn, W.D.L. 2005. A study of piles during earthquakes: issues of design and analysis. Bulletin of earthquake Engineering, 3: 141-234.

Fukuoka, M. 1977. The effects of horizontal loads on piles due to landslide. Proceeding of 9th international conference on soil mechanics and foundation engineering, Specialty Session 10, Tokyo, 77-80.

Fenves, G. Chopra, A.K. 1986. Simplified analysis for earthquake resistant design of concrete gravity dam, Earthquake Engineering Research Center, University of California Berkeley, California.

Garini, E., Gazetas, G., and Anastasopoulos, I. 2011. Asymmetric 'Newmark' sliding caused by motions containing severe 'directivity' and 'fling' pulses. Géotechnique, 61(9): 733-756.

Ghee, E. H. and Guo, W.D. 2005. Behaviour of axially laoded single piles in clay subjected to lateral soil movement. Gunmittted to Special issue if the Geotechnical Engineering, ICE.

Guo, W.D., & Ghee, E. H. 2004. Model tests on single piles in sand subject to lateral soil movement. Proceedings of the 18th Australasian Conference on the Mechanics of Structures and Materials, 2: 997-1003.

Guo, W. and Ghee, E. 2006. Behavior of axially loaded pile groups subjected to lateral soil movement. Foundation Analysis and Design, 174-181.

Guo W.D. and Qin, H.Y., 2005. Veritically loaded single piles in sand subjected to lateral soil movement. 6th Int. Conf. on Tall Buildings (ICTB-VI), 6-8 December, HongKong, in press.

Hajiazizi, M., and MAzaheri, A.R. 2015. Use of Line segment slip surface for optimized design of piles in stabilization of the earth slopes. International Journal of Civil Engineering, 13(1): 14-27.

Hassiotis, S., Chameau, J.L., and Gunaratne, M. 1997. Design Method for Stabilization of Slopes with Piles. Journal of Geotechnical and Geoenvironmental Engineering, 123(4): 314-323.

Hull, T.S., Lee, C.Y., and Poulos, H.G. 1992. Behavior of fixed and free head piles in a laterally sliding soil. New Zealand Geomechanics Society, Christchurch, New Zealand,151-156.

Hynes-Griffin, M.E., and Franklin, A.G. 1984. Rationalizing the seismic coefficient method. Defense Technical Information Center.

Ito, T., and Matsui, T. 1975. methods to estimate lateral force acting on stabilizing piles. Soils and Foundations, 15(4): 43-59.

Jeong, S., Kim, B., Won, J., and Lee, J. 2003. Uncoupled analysis of stabilizing piles in weathered slopes. Computers and Geotechnics, 30(8): 671-682.

Jibson, R.W. 1993. Predicting earthquake-induced landslide displacements using Newmark's sliding block analysis. Transportation Research Record: 9-9.

Jibson, R.W. 2011. Methods for assessing the stability of slopes during earthquakes—A retrospective. Engineering Geology, 122(1-2): 43-50

Kavazanjian, E., and Consultants, G. 1997. Design Guidance: Geotechnical Earthquake Engineering for Highways. Design Principles. Federal Highway Administration.

Kawai, T. 1977. A new discrete analysis of nonlinear solid mechanics problems involving stability, plasticity and crack. In the Symposium on Applications of Computer Methods in Engineering, Los Angeles, USA, pp. 1029-1038.

Kawai, T. 1978. New discrete models and their application to seismic response analysis of structures. Nuclear Engineering and Design, 48(1): 207-229.

Kourkoulis, R., Gelagoti, I F., Anastasopoulos, and Gazetas, G. 2012. Hybrid Method for Analysis and Design of Slope Stabilizing Piles. Journal of Geotechnical and Geoenvironmental Engineering, 138(1): 1-14.

Kramer, S.L. 1996. Geotechnical earthquake engineering. Prentice-Hall Civil Engineering and Engineering Mechanics Series, Upper Saddle River, NJ: Prentice Hall.

Krinitzsky, E.L. 1993. Fundamentals of earthquake-resistant construction. Wiley. com.

Lee, C.Y., Hull, T.S., and Poulos, H.G. 1995. Simplified pile-slope stability analysis. Computers and Geotechnics, 17(1):1-16.

Leung, C.F., Chow, Y.K., and Shen, R.F. 2000. Behavior of pile subject to excavation-induced soil movement. Journal of Geotechnical and Geoenvironmental Engineering, ASCE, 126(11): 947-954.

Leung, C.F., Lim, J.K., Shen, R.F., and Chow, Y.K. 2003. Behavior of pile groups subject to excavation-induced soil movement. Journal of Geotechnical and Geoenvironmental Engineering, ASCE, 129(1): 58-65.

Leung, C.F., Ong, D.E.L., and Chow, Y.K. 2006. Pile behavior due to excavation-induced soil movement in clay. Π: collape wall. Journal of Geotechnical and Geoenvironmental Engineering, ASCE, 132(1): 45-53.

Li, X., He, S., and Wu, Y. 2010. Seismic Displacement of Slopes Reinforced with Piles. J. Geotech. Geoenviron. Eng., 136(6): 880–884.

Ling, H.I. 2001. Recent applications of sliding block theory to geotechnical design. Soil Dynamics and Earthquake Engineering, 21: 189-197.

Makdisi, F.I., and Seed, H.B. 1977. Simplified procedure for estimating dam and embankment earthquake-induced deformations. In ASAE Publication No. 4-77.

Marcuson W.F., and Franklin, A.G. 1983. Seismic Design, Analysis, and Remedial Measures to Improve Stability of Existing Earth Dams, DTIC Document.

Mitchell, A.R., and Griffiths, D.F. 1980. The finite difference method in partial differential equations(Book). Chichester, Sussex, England and New York, Wiley-Interscience. Proceedings of the National Symposium on Soil Erosion and Sediment by Water, Chicago, Illinois, December 12-13, 1977.

Newmark, N.M. 1965. Effects of earthquakes on dams and embankments. Géotechnique, 15: 139-159.

Nian, T.K., Chen, G.Q., Luan, M. T., Yang, Q., and Zheng, D.F. 2008. Limit analysis of the stability of slopes reinforced with piles against landslide in nonhomogeneous and anisotropic soils. Canadian Geotechnical Journal, 45(8): 1092-1103.

Ong, D.E.L., Leung, C.F., and Chow, Y.K. 2006. Pile behavior due to excavation-induced soil movement in clay. I: stable wall. Journal of Geotechnical and Geoenvironmental Engineering, ASCE, 132(1): 36-44.

Ong, D.E.L., Leung, C.F., and Chow, Y.K. 2009. Pile behavior due to excavation-induced soil movement in very soft clay. Journal of Geotechnical and Geoenvironmental Engineering, ASCE, 135(10): 1462-1474.

Rathje, E.M., and Bray, J.D. 2000. Nonlinear coupled seismic sliding analysis of earth structures. Journal of Geotechnical and Geoenvironmental Engineering, 126(11): 1002-1014.

Richards, R., and Elms, D.G. 1979. Seismic behavior of gravity retaining walls. Journal of the Geotechnical Engineering Division, 105(4): 449-464.

Richards, J., Elms, D., and Budhu, M. 1993. Seismic bearing capacity and settlements of

foundations. Journal of Geotechnical Engineering, 119(4): 662-674.

Pan, J.L., Goh, A.T.C., Wong, K.S., and Teh, C.I. 2000. Model tests on single piles in soft clay. Canadian Geotechnical Journal, 37(4):890-897.

Pan, J.L., Goh, A.T.C., Wong, K.S., and The, C.I. 2002a. Ultimate soil pressures for piles subjected to lateral soil movements. Journal of Geotechnical and Geoenvironmental Engineering, ASCE, 128(6): 530-535.

Poulos, H.G. 1973. Analysis of piles in soil undergoing lateral movement. Journal of the Soil Mechanics and Foundations Division, ASCE; 99(5): 391-406.

Poulos, H.G. 1995. Design of reinforcing piles to increase slope stability. Canadian Geotechnical Journal, 32(5):808-818.

Poulos, H. G., Chen, L.T., and Hull, T. S. 1995. Model tests on single piles subjected to lateral soil movement. Soils and foundations, 35(4): 85-92.

Pyke, R. 1991. Selection of Seismic Coefficients for Use in Pseudo-Static Slope Stability Analyses. http://www.tagasoft.com/Discussion/article2_html.

Randolph, M.F. and Houlsby, G.T. 1984. The Limiting Pressure on a Circular Pile Loaded Laterally in Cohesive Soil. Geotechnique, 34(4): 613-623.

Sawada, T., Chen, W.F., and Nomachi, S.G. 1993. Assessment of seismic displacements of slopes. Soil Dynamics and Earthquake Engineering, 12: 357-362.

Seed, H.B. 1979. Considerations in the earthquake-resistant design of earth and rockfill dams. Geotechnique, 29(3): 13-41.

Shi, G.-H., and Goodman, R.E. 1985. Two dimensional discontinuous deformation analysis. International Journal for Numerical and Analytical Methods in Geomechanics, 9: 541-556.

Shi, G.-H., and Goodman, R.E. 1989. Generalization of two-dimensional discontinuous deformation analysis for forward modelling. International Journal for Numerical and Analyrucal Methods in Geomechanics, 13: 359-380.

Sousa, J., and Voight, B. 1991. Continuum simulation of flow failures. Geotechnique, 41(4): 515-538.

Springman, S. M. 1989. Lateral loading of piles due to simulated embankment

construction. Ph.D Thesis, University of Cambridge.

Stamatopoulos, C. 1996. Sliding system predicting large permanent co-seismic movements of slopes. Earthquake Engineering & Structural Dynamics, 25(10): 1075-1093.

Stewart, D.P., Jewell, R.J., and Randolph,M.F. 1994. Design of piles bridge abutment on soft clay for loading from lateral soil movement. Geotechnque, 44(2): 277-296.

Stewart, J.P., Blake, T.F., and Hollingsworth, R.A. 2003. A Screen Analysis Procedure for Seismic Slope Stability. Earthquake Spectra, 19(3): 697.

Terzaghi, K. 1950. Theoretical Soil Mechanics. John Wiley & Sons, Inc.

Tsuchiya, T., Kakurai, M., Yamashita, K., and Hamada, J. 2001. Large-scale laminar shear box for lateral pile load test with ground displacements. International Journal of Physical Modeling in Geotechnics, 2: 43-51.

Viggiani, C. 1981. Ultimate lateral load on piles used to stabilize landslides. Proceedings of 10th International Conference on Soil Mechanics and Foundation Engineering, Stockholm, Vol. 3: 555-560.

Wasowski, J., Keefer, D.K., and Lee, C.-T. 2011. Toward the next generation of research on earthquake-induced landslides: Current issues and future challenges. Engineering Geology, 122(1-2): 1-8.

Wartman, J., Asce, M., Bray, J.D., and Seed, R.B. 2003. Inclined Plane Studies of the Newmark Sliding Block Procedure. Journal of Geotechnical and Geoenvironmental Engineering, 129(8): 673-684.

White, D.J., Thompson, M.J., Suleiman, M.T., and Schaefer, V.R. 2008. Behavior of slender piles subject to free-field lateral soil movement. Journal of Geotechnical and Geoenvironmental Engineering, ASCE, 134(4): 428-436.

Won, J., You, K., Jeong, S. 2005. Coupled effects in stability analysis of pile–slope systems. Computers and Geotechnics, 32(4): 304-315.

Kok, S.T., Bujang K. H., Noorzaie, J., Jaafar, M.S., Gue, S.S. 2009. Modeling of passive piles−an overview. Electronic Journal of Geotechnical Engineering, 14 (Bundle P): 1-22.

Yamin, M., and Liang, R.Y. 2010. Limiting equilibrium method for slope/drilled shaft system. International Journal for Numerical and Analytical Methods in Geomechanics, 34(10): 1063-1075.

Yegian, M.K. and Marciano, E.A. 1991a. Seismic risk analysis for earth dams. Journal of Geotechnical and Geoenvironmental Engineering. ASCE, 117(1): 18-34.

Yegian, M.K., Marciano, E.A., and Ghahraman, V.G. 1991b. Earthquake-induced permanent deformations: probabilistic approach. Journal of Geotechnical Engineering, 117(1): 35-50.

Yegian, M., Harb, J., and Kadakal, U. 1998. Dynamic response analysis procedure for landfills with geosynthetic liners. Journal of Geotechnical and Geoenvironmental Engineering, 124(10): 1027-1033.

Zeng, S., and Liang, R. 2002. Stability analysis of drilled shafts reinforced slope. Soils and Foundations, 42(2): 93–102.

Zhang, Y.B. 2013. New analysis methods for earthquake induced landslides considering tension failure and the trampoline effect. Ph. D thesis, Kyushu University, Fukuoka, Japan.

CHAPTER 3

SOIL-PILE PRESSURE OF STABILIZING PILE UNDERGOING LATERAL SOIL MOVEMENT

3.1 INTRODUCTION

Landslide occurring in both natural and cut slopes often results in serious damage to both human lives and properties (Liu and Zhao, 2013; Cai and Ugai, 2004). Lots of research has been carried out to reduce the damage of landslide disasters. Stabilizing piles, as one of the most widely used countermeasure in reinforcement engineering of slopes, has been proved to be an efficient solution to landslides (Guo 2013). Stabilizing piles as passive piles are embedded into a stable base of slope to provide additional stability (see **Figure. 3.1**). The distributions of the soil-pile pressure acting on passive piles are dependent on soil movements. Due to the complex plastic deformation of soil, estimation of the lateral force on passive piles cannot be easily solved.

Several previous researchers have attempted to estimate the soil-pile pressure (lateral force) exerted on stabilizing piles by experimental approach and theoretical analysis approach. A number of instrumented field cases have been reported. For example, Franx and Boonstra (1948), Heyman and Boersma (1961), Heyman (1965), Leussink and Wenz (1969) and Nicu et al. (1971) (a summary of these and other cases was made by Marche and Lacroix, 1972). In most of the above mentioned cases, the piles have been in bridge abutments where the horizontal displacements of the soil arose from the construction of an embankment at the soil surface. Leussink and Wenz (1969) have described a test on a pile near an ore-storage large to cause structural failure of the pile. From an examination of case records, Marche and Lacroix (1972) attempted to

Figure 3.1 Stabilizing pile used in various reinforcement engineering: (a) remediation of embankment slope in San Diego; (b) Spanish Peaks Landslide Stabilization; (c) bank remediation along Harrods Creek using piles.

relate the ratio of the horizontal displacement of a pile to the embankment settlement with the relative flexibility of the pile, and found that this ratio increases with increasing pile-flexibility.

De Beer and Wallays (1972) have described a relatively simple method of determining bending moments and forces in a pile when an unsymmetrical surcharge is placed around the pile. Ito and Matsui (1975) proposed an analysis to evaluate the lateral force acting on a single row of piles due to soil movement. Their analysis was carried out in the light of the theory of plastic deformation, simultaneously the interaction between piles and soil was considered. It is convenient to estimate the ultimate soil pressure on pile segment embedded in the sliding soil layer using this method, because the pressure depends on only 4 parameters: the cohesion c, the internal friction angle φ, pile diameter, and spacing between piles. This method has been widely referred by other researchers (Hassiotis, 1997; Cai and Ugai, 2000, Hazarika et al, 2000).

As mentioned previously, Poulos (1995) presented a method in which a boundary element method was employed to analyze the response of a row of passive piles incorporated in limit equilibrium solutions of slope stability in which the pile is modeled as a simple elastic beam. The method evaluates the maximum shear force that each pile can provide based on an assumed input free field soil movement (Ashour and Ardalan, 2012). Poulos (1995) revealed the existence of three modes of failure: (*i*) the "flow mode", (*ii*) "intermediate mode", and (*iii*) the "short-pile mode". These three modes of failure highlighted by Polous definitely promote the application of analysis of stabilizing piles. This classification of failure modes was diffusely adopted by researchers (Chen and Poulos, 1997; Ashour et al. 2000, 2004; Won et al. 2005; Jeong et al. 2003; Nian et al. 2008; Suleiman et al. 2014). In this chapter a row of piles in the deforming ground with the "flow mode" mechanism is analyzed, here the soil movement is larger than the pile deflection. In addition, the soil arching effects along the height of the sliding layer between two neighboring piles are considered to provide the non-linear distribution of lateral force on each pile.

In this chapter, the lateral force on a row of piles under laterally movement of the sliding layer is analyzed. In **Section 3.2**, the soil arching theory is introduced and the analysis is carried out in deforming ground considering the arching effects in the rear of piles. The distribution of the soil stress exerted on the piles is non-linear based on the soil arching theory. In **Section 3.3**, from parametric analysis of the factors utilized in the proposed formulae, it reveals that all the factors including the internal friction angle, the cohesion, the pile diameter, the height of the unstable soil layer influenced the lateral stress enormously. What's more, In **Section 3.4**, the numerical simulation results together with field experiments from literatures are introduced to validate the proposed approach.

3.2 PLASTIC THEORY CONSIDERING SOIL ARCHING EFFECTS

3.3.1 INTRODUCTION OF SOIL ARCHING EFFECT

Soil arching was described by Terzaghi (1936, 1943) as one of the most universal phenomena in the field of soil mechanics. Transferring of soil pressure from a yielding support to an adjacent non-yielding support is the essence of the phenomena (Bosscher and Gray, 1985).

In silos and ditches, some equations have been set up by many researchers to estimate the soil pressure by considering the soil arching effects. However, the shape of the soil arching in their research was not defined (Janssen, 1895; Marston, 1913). It is considered that loosely added contents of silos and trenches are partially supported by friction from vertical walls (**Figure 3.2**). Unlike a free-standing structural arch, the arching that acts in partial support of granular contents cannot be represented by trajectory of the major stress because, instead of being a continuous curve, it rises to vertical at the center. The flat "arch" of **Figure 3.2** derives from supportive friction F (at the ends), which equals lateral force times a coefficient of friction μ, the lateral force being obtained from vertical stress times a lateral stress ratio, K, which was obtained experimentally by Janssen for grain (1895), but was later assumed by Marston and Anderson to be equal to the ratio of principal stresses, $K_a = \sigma_1/\sigma_3$, which is the Rankine

ratio with a level ground surface. This assumption was also advanced by Terzaghi (1943) and others, until corrected in 1945 by Krynine (1945).

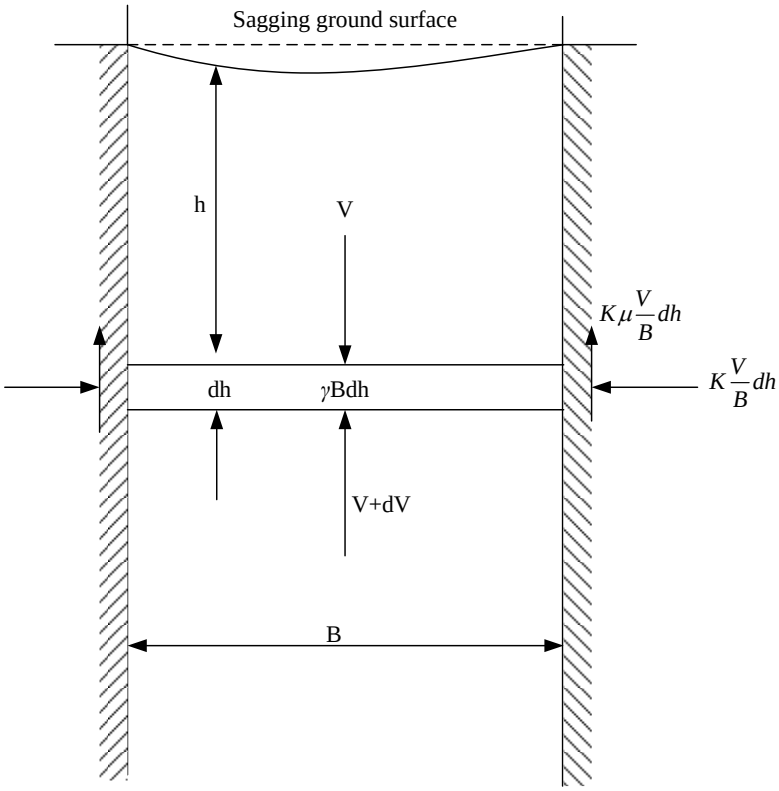

Figure 3.2 Differential element in classical representation of soil arching (after Handy, 1985).

Krynine (1945) considered that if friction at the ends of the flat "arch" is the product of $K_a\mu$, it must equal σ_1/σ_3, but σ_3 is a principal stress that, by definition, must act on a plane of zero friction. This is a paradox: It must be wrong to be right. Krynine resolved the problem by use of the Mohr circle, showing that rotation of the principal stresses gives wall pressure σ_h, instead of σ_3 in **Figure 3.3**, and the shearing stress is at P_A rather than M (Handy, 1985). Krynine derived an expression for the ratio of horizontal-to-vertical stress at a wall with fully mobilized friction:

$$K = \frac{\sigma_h}{\sigma_v} = \frac{1-\sin^2\varphi}{1+\sin^2\varphi} \tag{3.1}$$

However, the K of Eq. (3.1) is not appropriate either, since σ_v at the wall is less than the average σ_{av} across the continuum and in equilibrium with the fill depth and density.

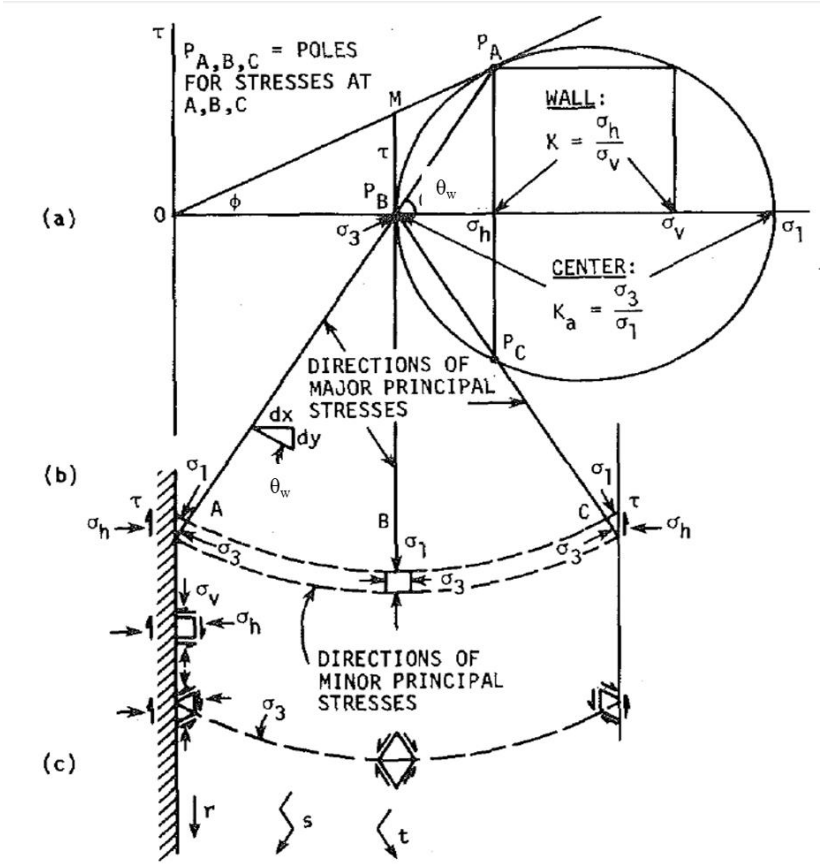

Figure 3.3 (a) Mohr Circle to show arching stresses at rough wall, enabling deviation of Eq. (3.1); (b) continuous inverted arch defined by trajectory of minor principal stresses; (c) shear line direction and randomized shears, r, s and t, to give net vertical movements (after Handy, 1985).

Handy (1985) used the Mohr Circle to analyze the arching effects between two retaining walls. It is assumed that two parallel, unyielding, vertical settling of the fill occurs that its weight becomes partially supported by fully developed friction on the walls. Minor principal planes drawn through the Mohr circle poles (**Figure 3.3(a)**) show radiating major principal stress directions, whereas the trajectory of the minor principal stress, σ_3, defines a continuous compression arch that dips downward instead of upward (**Figure 3.3(b)**). This "minor arch" may also be defined by intersections of shear lines

drawn by the numerical method of Sokolovskii (1965) that is also based on the Mohr diagram (**Figure 3.3(c)**). This argument requires that the soil be in a state of plastic equilibrium, which in turn requires that slip occur only along directions defined by the slip lines.

Furthermore, Handy (1985) noticed that the arching element of **Figure 3.3(b)** is bounded by surfaces representing principal planes of zero shearing stress. Thus, moment equilibrium requires that the stresses be constant throughout the arch. If the element is of uniform density and thickness and, thus, of uniform weight throughout, the shape will be a catenary, namely the shape taken by a chain held at ends. It must dip downward if the arch is supportive, or upward if the reverse is true, which may explain some of the difficulty in intuitively visualizing an internal, partially supported soil arch. Perhaps it is simplest to imagine a tensile analogue for the direction of least compression.

The equation for catenary is:

$$y = \frac{a_{ca}}{2}[\exp(\frac{x}{a_{ca}}) + \exp(-\frac{x}{a_{ca}})] \tag{3.2}$$

in which a_{ca} is a coefficient and x is a relative distance from the center line and has limits ± 1. Differential equation can be expressed:

$$\frac{dy}{dx} = \frac{1}{2}[\exp(\frac{x}{a_{ca}}) - \exp(-\frac{x}{a_{ca}})] = -\cot\theta \tag{3.3}$$

where θ_{de} is the angle showing in **Figure 3.3(a)**. For fully developed wall friction, $\theta_{de\max} = \pm(45^{o}+\varphi/2)$ when $x = \mp 1$ at the walls, enabling evaluation of a.

Based on the analysis using Mohr Circle, Handy (1985) found that: (1) soil arching initiated from a rough wall in two stages. The first stage was rotation of minor and major principal stresses at the wall. This produced wall pressures appreciably higher than those predicted from Rankine or Coulomb analyses, and is essentially hydrostatic or triangular in distribution; (2) as wall movement proceeded, arching action becomes continuous in soil between two walls, or forms a semi-arch between the wall and a boundary slip

surface separating mobile from immobile soil where the minor principal stress becomes horizontal. This second state of arching, or bin effect, reduced vertical and horizontal pressures, particularly near the base of the wall; (3) in its second stage, arching action reduced wall pressures significantly below those from the Coulomb analysis, but placed their center of action higher on the wall.

Other researchers have analyzed the soil arching effects assuming the arch shaped as elliptic and parabolic (Livingston, 1961; Walker, 1966; Stevic et al., 1979). Furthermore, the trajectory of the arch was examined theoretically by Kingsley (1989). It is shown that the minor principal stress arch can be approximated by a catenary or a circle. More recently, the soil arching theory has been developed to study on retaining wall based on the catenary and circle shaped arch respectively (Wang, 2000; Paik and Salgado, 2003). In the following section, a circle shaped arch proposed by Paik and Salgado (2003) is adopted and extended to *c*-φ soil, and the limit equilibrium of the differential element in the soil arching zone is analyzed to investigate the lateral active soil stress

3.3.2 SOIL ARCING EFFECTS BETWEEN TWO NEIGHBORING PILES

When the sliding layer moves laterally, the soil around the piles deforms. Between two neighboring piles, the soil arching occurs along the height of the sliding layer. In the rear of piles the direction of major and minor principal stress of the soil rotates in the soil arching zone. In this analysis, the soil arching zone in the rear of piles is shown as the dashed area in **Figure 3.4**. The plane view of soil deforming between two neighboring piles is depicted in **Figure 3.5**. In addition, a typical cross section, UU′, as shown in **Figure 3.6**, is employed to display the soil stress in the rear of the plane AA′ (**Figure 3.5**). In this section, the analysis is conducted in two stages. Firstly, the soil pressure acting on the plane AA′ is analyzed based on the soil arching theory. Secondly, considering the squeezing effect between the piles, the lateral force acting on the piles is calculated.

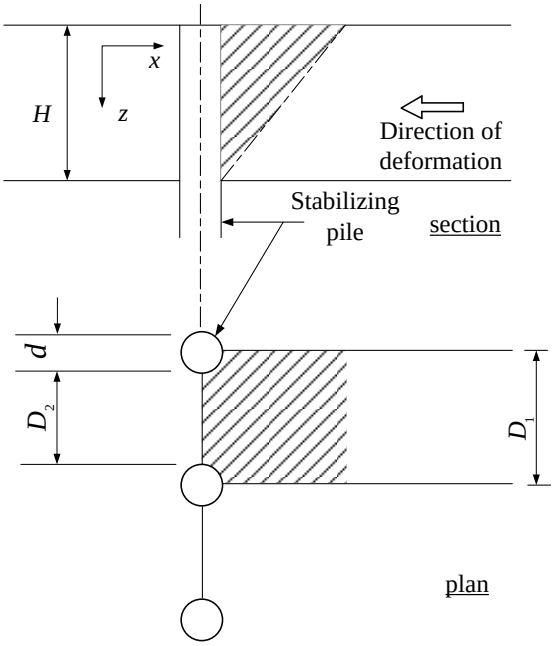

Figure 3.4 The soil arching zone in the rear of stabilizing piles.

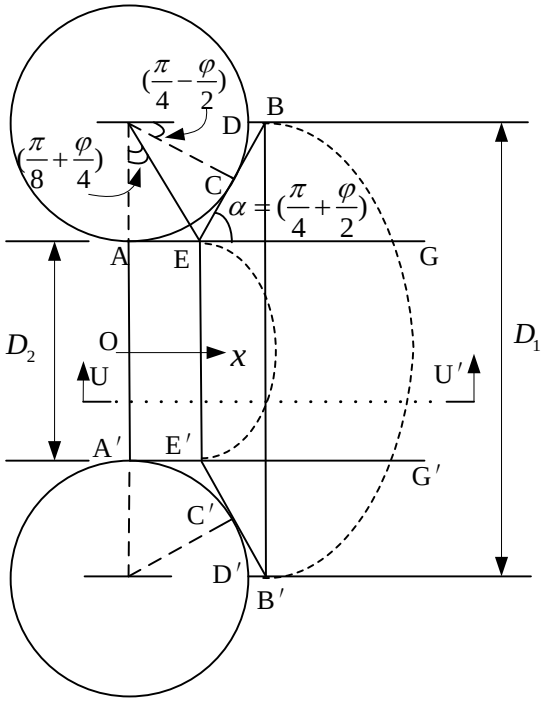

Figure 3.5 Plastic deformation of soil between neighboring piles (after Ito and Matsui, 1975).

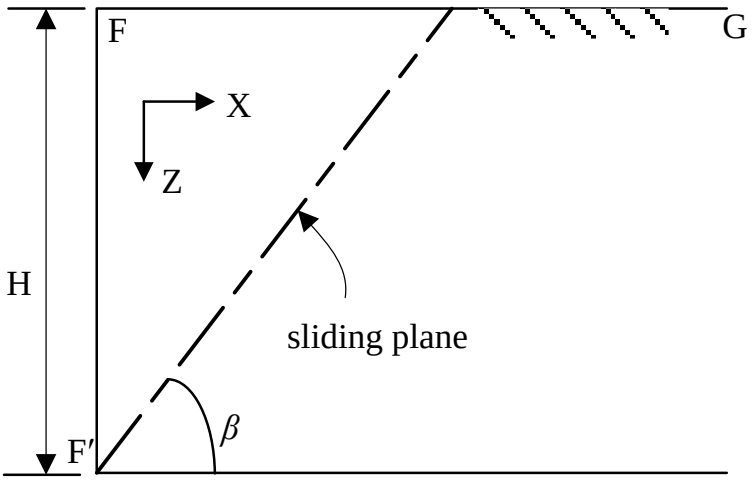

Figure 3.6 Cross section of the deformation in soil ground in the rear of piles.

As mentioned previously, the trajectory of soil arching is assumed to be an arc of a circle. In addition, in order to inquire into the state of soil stress in the rear of the plane AA′ (**Figure 3.5**), we assume that when soil layer deforms, the plane AA′ (**Figure 3.5**) is in active. Furthermore, when the active stress on the plane AA′ is analyzed, only the area between the two parallel lines AG and A′G′ (**Figure 3.5**) is considered. It is noted that assumption of the active stress is same to that of Ito and Matsui (1975). Moreover, they assumed that the Coulomb's active earth pressure was applied on the plane. However, some recent research indicates that the active earth pressure predicted by soil arching theory provides more accurate result than that by Coulomb's method. Based on soil arching theory proposed by Paik and Salgado (2003), the active stress on plane AA′ (**Figure 3.5**) in deforming ground are discussed.

When soil layer deforms, the actual soil arching zone would be complicated. In this study, assumption mentioned previously is utilized to simplify the analysis. The cross section UU′ is shown in **Figure 3.6**. The angle between sliding plane and the horizontal is β_1. In the deforming ground, the rotation of the principal stress on the line FF′ (**Figure 3.6**) is described as **Figure 3.7**. In the rear of the line FF′, the shape of the soil arching is an arc of a circle which dips downward instead of upward. The trajectory of minor

principal stress on the differential element is represented by the dotted lines, while the direction of major principal stress is the normal of the arch.

The active earth pressure acted on the line FF′ includes two components: the active lateral stress σ_h and the shear stress τ. A theoretical approach has been proposed by Paik and Salgado (2003) to estimate the active lateral stress σ_h behind a retaining wall for cohesionless soil. This approach is adopted herein and extended for c-φ soil.

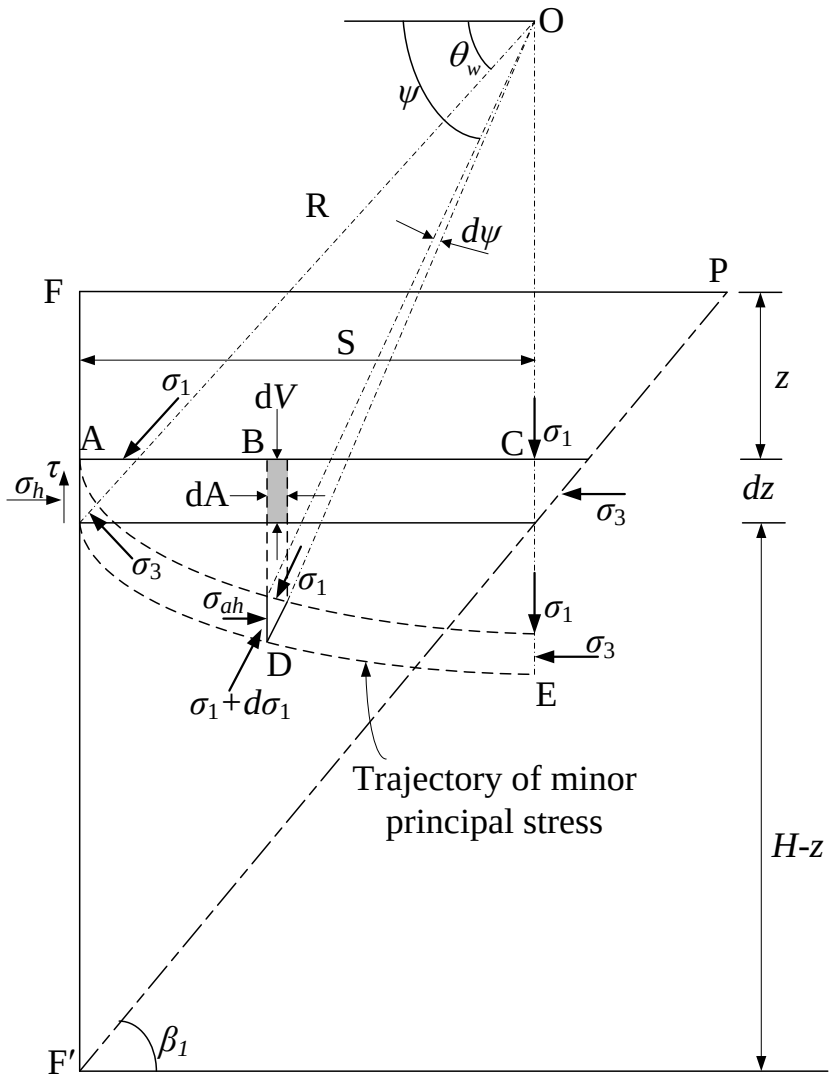

Figure 3.7 Stress on differential element in the soil arching zone (after Paik and Salgado, 2003).

Considering the force equilibrium in the triangular element at point A in **Figure 3.7**, the lateral stress is obtained as:

$$\sigma_h = \sigma_1 \cos^2 \theta_w + \sigma_3 \sin^2 \theta_w \tag{3.4}$$

At an arbitrary point D of the arch, whose original location is point B, a similar equation is given by

$$\sigma_{ah} = \sigma_1 \cos^2 \psi + \sigma_3 \sin^2 \psi \tag{3.5}$$

where ψ is the angle between the normal of the arch at point D and the horizontal, σ_{ah} the lateral stress at point D. Considering that the soil is in active state, the Mohr-Coulomb's yielding criterion is applied:

$$\sigma_3 = \sigma_1 N - 2cN^{1/2} \tag{3.6}$$

where, $N = \tan^2(\pi/4 - \varphi/2)$, c is the cohesion of soil. Substituting Eq. (3.6) into Eq. (3.4), the lateral stress at point D is obtained:

$$\sigma_{ah} = (\cos^2 \psi + N \sin^2 \psi)\sigma_1 - 2cN^{1/2} \sin^2 \psi \tag{3.7}$$

Since σ_{ah}-σ_3=σ_1-σ_{av}, substitution for σ_{ah} gives

$$\sigma_{av} = (\sin^2 \psi + N \cos^2 \psi)\sigma_1 - 2cN^{1/2} \cos^2 \psi \tag{3.8}$$

where σ_{av} is the vertical stress at an arbitrary point D. As depicted by Eq. (3.8), the vertical stress varies with angle ψ, which changes from θ_w to $\pi/2$. In this problem, it seems impossible to calculate the vertical stress at every point in the analyzing zone, so the average vertical stress $\bar{\sigma}_v$ is introduced, which can be expressed as:

$$\bar{\sigma}_v = \frac{V}{S} \tag{3.9}$$

in which V is the total vertical stress across the differential element and S the width of the differential element. The total vertical stress V of the differential element can be calculated by the following formula:

$$
\begin{aligned}
V &= \int_{\theta_w}^{\pi/2} dV \\
&= \int_{\theta_w}^{\pi/2} \sigma_{av} dA \\
&= \int_{\theta_w}^{\pi/2} [\sigma_1(\sin^2\psi + N\cos^2\psi) - 2cN^{1/2}\cos^2\psi](R\cdot d\psi\cdot\sin\psi)
\end{aligned}
\tag{3.10}
$$

where dV is the differential vertical force on the shaded portion at arbitrary point B , and dA the width of the shaded portion at point B.

Substituting Eq. (3.10) into Eq. (3.9), and considering $S=R\cdot\cos\theta$, the average vertical stress is obtained as follow:

$$
\bar{\sigma}_v = \int_{\theta_w}^{\pi/2} \sigma_1(\sin^2\psi + N\cos^2\psi)\frac{\sin\psi}{\cos\theta_w}\cdot d\psi - \int_{\theta_w}^{\pi/2} 2cN^{1/2}\cos^2\psi\frac{\sin\psi}{\cos\theta_w}\cdot d\psi \tag{3.11}
$$

Integrating of Eq. (3.11) yields

$$
\bar{\sigma}_v = \sigma_1(1-\frac{1-N}{3}\cos^2\theta_w) - \frac{2c}{3}N^{1/2}\cos^2\theta_w \tag{3.12}
$$

The Eq. (3.12) can be rewritten as:

$$
\sigma_1 = \frac{3\bar{\sigma}_v + 2cN^{1/2}\cos^2\theta_w}{3-(1-N)\cos^2\theta_w} \tag{3.13}
$$

Substituting Eqs. (3.6) and (3.13) into Eq. (3.4), the lateral stress is obtained

$$
\sigma_h = \frac{3(\cos^2\theta_w + N\sin^2\theta_w)}{3-(1-N)\cos^2\theta_w}(\bar{\sigma}_v + \frac{2c}{3}N^{1/2}\cos^2\theta_w) - 2cN^{1/2}\sin^2\theta_w \tag{3.14}
$$

in which θ_w=45º+φ/2 when the line FF′ is in the active condition. In order to simplify the expression of Eq. (3.14), let

$$
K_{an} = \frac{3(\cos^2\theta + N\sin^2\theta_w)}{3-(1-N)\cos^2\theta_w} \tag{3.15}
$$

and

$$T = \frac{3(\cos^2\theta_w + N\sin^2\theta_w)}{3-(1-N)\cos^2\theta_w}\cdot\frac{2c}{3}N^{1/2}\cos^2\theta_w - 2cN^{1/2}\sin^2\theta_w$$
$$= 2cN^{1/2}(\frac{1}{3}\cos^2\theta_w\cdot K_{an} - \sin^2\theta_w) \tag{3.16}$$

Then the Eq. (3.14) can be expressed as:

$$\sigma_h = K_{an}\bar{\sigma}_v + T \tag{3.17}$$

Eq. (3.17) shows that the active lateral stress consists of two components: the cohesion effect and non-cohesion effect. In cohesionless soil, the relation between active lateral stress and average vertical stress on the line FF′ is succinct, which can be written as $\sigma_h = K_{an}\bar{\sigma}_v$.

3.3.2 LIMIT EQUILIBRIUM EQUATION IN SOIL ARCHING ZONE

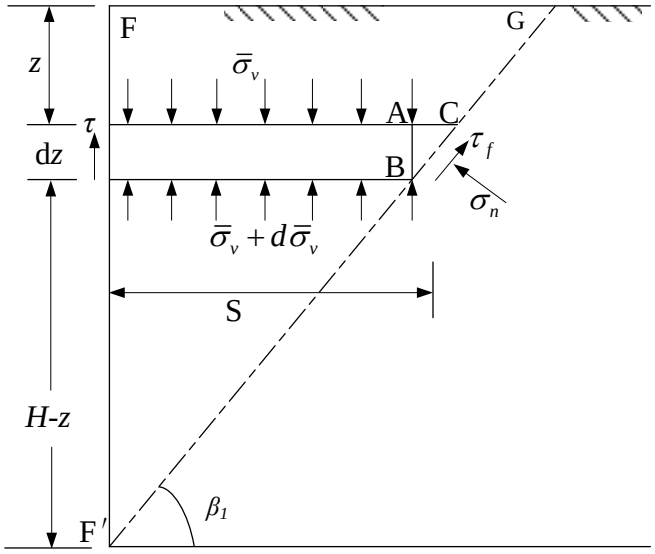

Figure 3.8 Soil stress on differential element

The stress on the differential element in the soil arching zone is shown as **Figure 3.8**. The angle β_1 is assumed to be 45°+φ/2. It has been proved that the right edge of the differential element, namely the triangular area ABC, is in the state of limit equilibrium, so that the stress in this area can be neglected when total stress on the differential

element is analyzed. At left edge of the differential element, the shear stress along the line FF′ should be taken into account, which can be expressed as:

$$\tau = \sigma_h \tan\varphi + c = (K_{an}\bar{\sigma}_v + T)\tan\varphi + c \tag{3.18}$$

In the vertical direction of **Figure 3.8**, considering the width of soil arching zone, all the vertical force must be in equilibrium. The equation is set up as follow:

$$\gamma S \cdot D_2 dz = (K_{an}\bar{\sigma}_v + T)\tan\varphi \cdot D_2 dz + cD_2 dz + S \cdot D_2 d\bar{\sigma}_v \tag{3.19}$$

in which $\bar{\sigma}_v$ is the average vertical stress, S is the width of the differential element, D_2 is the clear interval between two neighboring piles, dz is the thickness of the differential element. Diving by D_2 in both sides of Eq. (3.19), and considering $S = (H\text{-}z)/\tan\beta$ (**Figure 3.8**), the general solution of Eq. (3.19) is obtained:

$$\bar{\sigma}_v = (H-z)^{K_{an}\tan\varphi\tan\beta_1}\left[-\gamma\frac{(H-z)^{1-K_{an}\tan\varphi\tan\beta_1}}{1-K_{an}\tan\varphi\tan\beta_1} - \frac{(T\tan\varphi + c)\tan\beta_1}{K_{an}\tan\varphi\tan\beta_1}(H-z)^{-K_{an}\tan\varphi\tan\beta_1} + C_1\right] \tag{3.20}$$

where H is the thickness of the sliding soil layer, z the depth below the surface of the soil, γ the unit weight of the soil, C_1 an integration constant. Considering the condition of overload acting on the surface of the ground (**Figure 3.9**), Substituting the boundary condition that $\bar{\sigma}_v = q$ when $z = 0$, the constant C_1 is obtained

$$C_1 = qH^{-K_{an}\tan\varphi\tan\beta_1} + \gamma\frac{H^{1-K_{an}\tan\varphi\tan\beta_1}}{1-K_{an}\tan\varphi\tan\beta_1} + \frac{(T\tan\varphi + c)}{K_{an}\tan\varphi}H^{-K_{an}\tan\varphi\tan\beta_1} \tag{3.21}$$

in which q is the overloading exerted on the surface of the ground. The average vertical stress at an arbitrary depth is given by Eq. (3.22)

$$\bar{\sigma}_v = \frac{\gamma H[(1-\frac{z}{H})^{K_{an}\tan\varphi\tan\beta_1} - (1-\frac{z}{H})]}{1-K_{an}\tan\varphi\tan\beta_1} + \frac{(T\tan\varphi + c)}{K_{an}\tan\varphi}[(1-\frac{z}{H})^{K_{an}\tan\varphi\tan\beta_1} - 1] + q(1-\frac{z}{H})^{K_{an}\tan\varphi\tan\beta_1}$$

(3.22)

Combining Eq. (3.17) with Eq. (3.22), the active lateral stress is obtained

$$\sigma_h = \frac{K_{an}\gamma H[(1-\frac{z}{H})^{K_{an}\tan\varphi\tan\beta_1} - (1-\frac{z}{H})]}{1-K_{an}\tan\varphi\tan\beta_1} + \frac{(T\tan\varphi + c)}{\tan\varphi}\cdot \\ [(1-\frac{z}{H})^{K_{an}\tan\varphi\tan\beta_1} - 1] + K_{an}q(1-\frac{z}{H})^{K_{an}\tan\varphi\tan\beta_1} + T \tag{3.23}$$

It is noted that, when Eq. (3.23) is utilized to estimate the active lateral stress in pure cohesive soil whose internal friction angle equals to zero, the parameter φ should be substituted by a value close to 0, such as 0.01º.

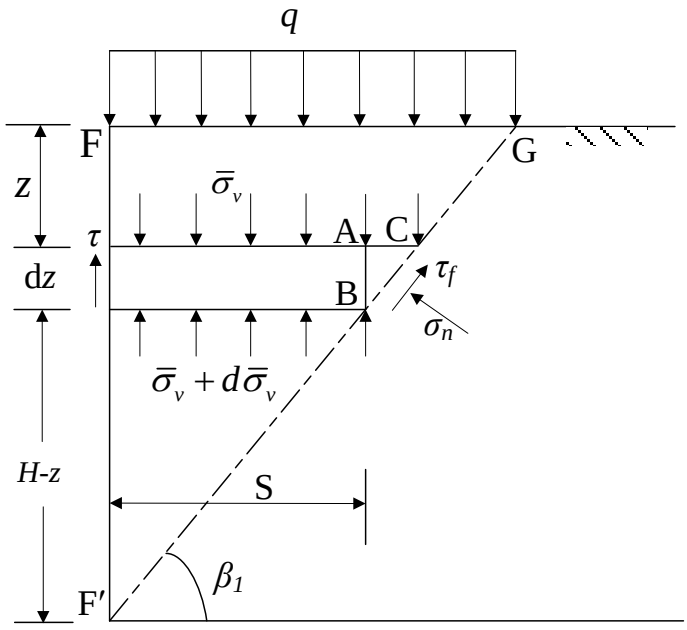

Figure 3.9 Soil stress on differential element with overloading on the surface of the ground.

3.3.3 THE SQUEEZING EFFECTS OF THE SOIL BETWEEN NEIGHBORING PILES

In order to analyze the lateral force acting on the piles, the squeezing effects of the soil between neighboring piles should be taken into account. Some assumptions have been made by Ito and Matsui (1975) to estimate the squeezing effects. In this analysis,

the assumptions of the deforming soil around the piles made by Ito and Matsui are adopted. Based on these assumptions and soil arching theory, the active stress on plane AA′ (**Figure 3.5**) in the theory of plastic deformation proposed by Ito and Matsui (1975) is replaced by Eq. (3.23). Then, the lateral force acting on a stabilizing pile p per unit thickness of the layer in the direction of x-axis can be estimated by new formula. As derived in Appendix, the equations for the squeezing effects between two neighboring piles can be expressed as Eq. (3.24) and (3.25) respectively for cohesionless soil and c-φ soil.

Cohesionless soil ($c=0$):

$$p = \{\frac{\gamma H K_{an}}{1-K_{an}\tan\varphi\tan\beta}\times[(1-\frac{z}{H})^{K_{an}\tan\varphi\tan\beta}-(1-\frac{z}{H})]+K_{an}q(1-\frac{z}{H})^{K_{an}\tan\varphi\tan\beta}\}$$
$$\times\{D_1(\frac{D_1}{D_2})^{N_1^{1/2}\tan\varphi+N_1-1}\times\exp[\frac{D_1-D_2}{D_2}N_1\tan\varphi\tan(\frac{\pi}{8}+\frac{\varphi}{4})]-D_2\} \tag{3.24}$$

c-φ soil:

$$p = cD_1(\frac{D_1}{D_2})^{N_1^{1/2}\tan\varphi+N_1-1}\{\frac{(2N_1^{1/2}\tan\varphi+1)}{N_1\tan\varphi}\times[\exp(\frac{D_1-D_2}{D_2}N_1\tan\varphi\tan(\frac{\pi}{8}+\frac{\varphi}{4}))-1]$$
$$+\frac{2\tan\varphi+2N_1^{1/2}+N_1^{-1/2}}{N_1^{1/2}\tan\varphi+N_1-1}\}-cD_1\frac{2\tan\varphi+2N_1^{1/2}+N_1^{-1/2}}{N_1^{1/2}\tan\varphi+N_1-1}$$
$$+\sigma_h\times[D_1(\frac{D_1}{D_2})^{N_1^{1/2}\tan\varphi+N_1-1}\times\exp(\frac{D_1-D_2}{D_2}N_1\tan\varphi\tan(\frac{\pi}{8}+\frac{\varphi}{4}))-D_2] \tag{3.25}$$

in which z is the arbitrary depth of the sliding soil layer, σ_h can be obtained by Eq. (20), $N_1 = \tan^2(45^o+\varphi/2)$.

3.3 PARAMETRIC ANALYSIS

Eqs. (3.24) and (3.25) show that the lateral forces exerted on the stabilizing piles vary with many parameters. In both cohesionless soil and c-φ soil, the common parameters are unit weight γ, the height of the unstable soil layer H, the depth of the analyzed soil z, pile diameter D_1-D_2, and the interval between two neighboring piles D_1. Besides, there are two mechanical parameters, the internal friction angle φ, and the

cohesion *c*. In the present paper, the effects of all the parameters are evaluated.

The height of the unstable soil layer

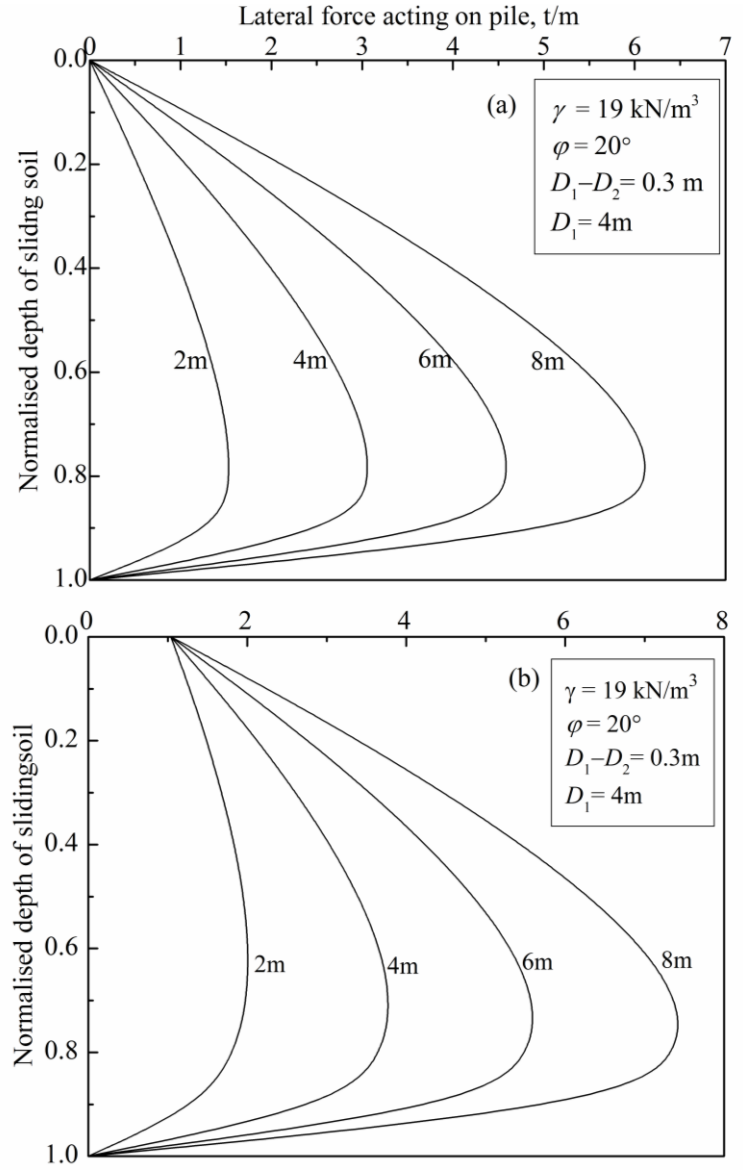

Figure 3.10 Lateral force distribution along the unstable soil layer with respect to different height of sliding layer: (a) cohesionless soil (c = 0 kN/m^2), (b) c-φ soil (c = 10 kN/m^2).

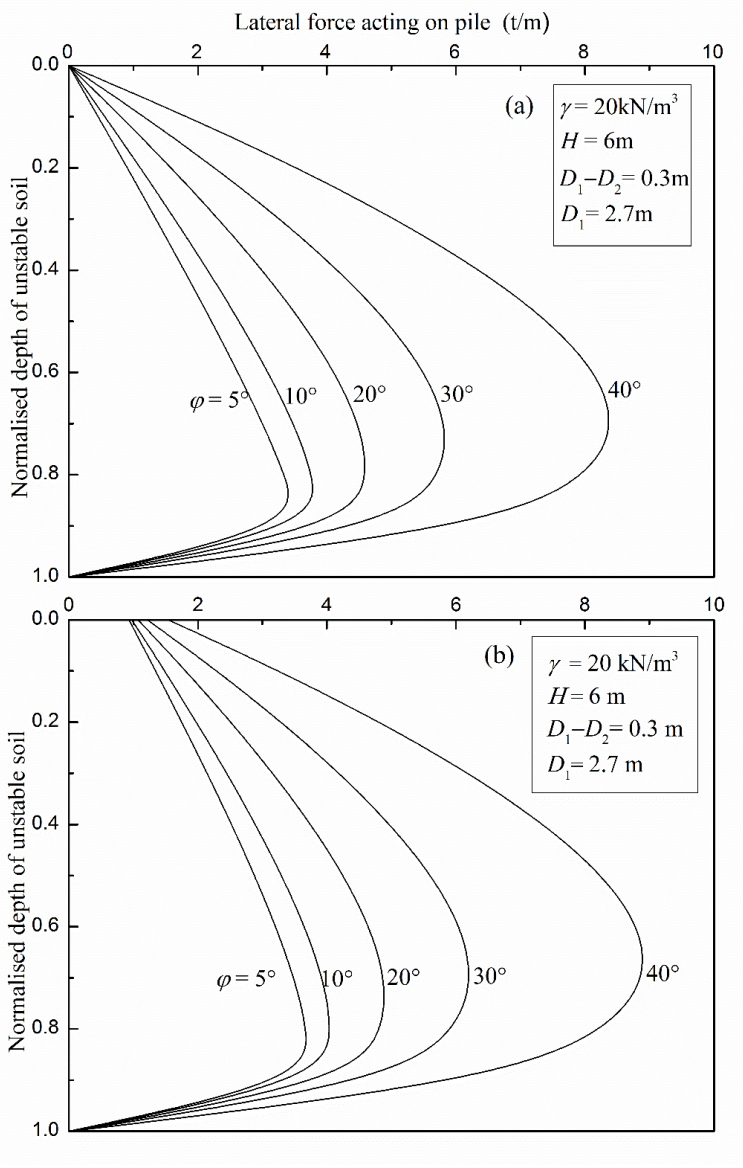

Figure 3.11 The distribution of lateral force versus the internal friction angle along the height of the sliding soil for (a) cohesionless soil (c = 0 kN/m^2) and (b) c-φ soil (c = 10 kN/m^2).

Figure 3.10 displays the distribution of the lateral force along the normalized depth of unstable soil with respect to different H. In both cohesionless soil and c-φ soil, the height of the sliding soil layer changes from 2 m to 8 m, but the shape of distribution of the lateral force does not change much with the variation of H. However, the magnitude

of the lateral force increases with the growth of the height H. It is found from Fig. 8 that the magnitude of the lateral force in c-φ soil is greater than that in cohesionless soil in the same depth with the same internal friction angle. In addition, peak value of the force is always in the range of $0.6H$~ $0.8H$.

Internal friction angle and cohesion

As the Mohr-Coulomb's criterion is utilized to estimate the lateral force, the internal friction angle and cohesion are the most affecting parameters for the lateral force. **Figure 3.11** displays the lateral force distribution on pile with the internal friction angle varying from 5º to 40º, and the depth of the sliding layer is 6 m. **Figures 3.11(a)** and **(b)** display the lateral forces on piles in cohesionless soil and c-φ soil, respectively.

Figure 3.11 reveals that for both cohesionless soil and c-φ soil as the internal friction angle increases, the lateral force acting on the stabilizing pile increases at every depth. The magnitude of the lateral force in both kinds of soils in the same depth is in the same order. The maximum value of the lateral force is in the range of $0.8H$ ~$0.85H$ when the internal friction angle is less than 20º. The height of the point of the peak value decreases while the internal friction angle increases. When φ = 40º the maximum value of the force is in the range of $0.6H$ ~$0.7H$.

As mentioned above, the peak value is in the range of $0.6H$~ $0.8H$, the lateral forces at depth $0.7H$ versus ratio D_2/D_1 is shown in **Figure 3.12**. The two figures show that when the ratio D_2/D_1 is less than 0.7, and the internal friction angle φ more than 20º, the lateral force calculated from Eqs. (3.24) and (3.25) may be a big value. The trend of the lateral force versus internal friction angle on basis of the proposed method is similar to that of Ito and Matsui's analysis (1975).

The effect of the cohesion is shown in **Figure 3.13**. It is found in the figure that the lateral force increases while the cohesion grows. However, the increment of the lateral force due to the effect of cohesion is less than that due to internal friction angle. Note that a value of φ closes to 0º that 0.01º is substituted to calculate the force, it is because the internal friction angle cannot be zero in Eq. (3.25).

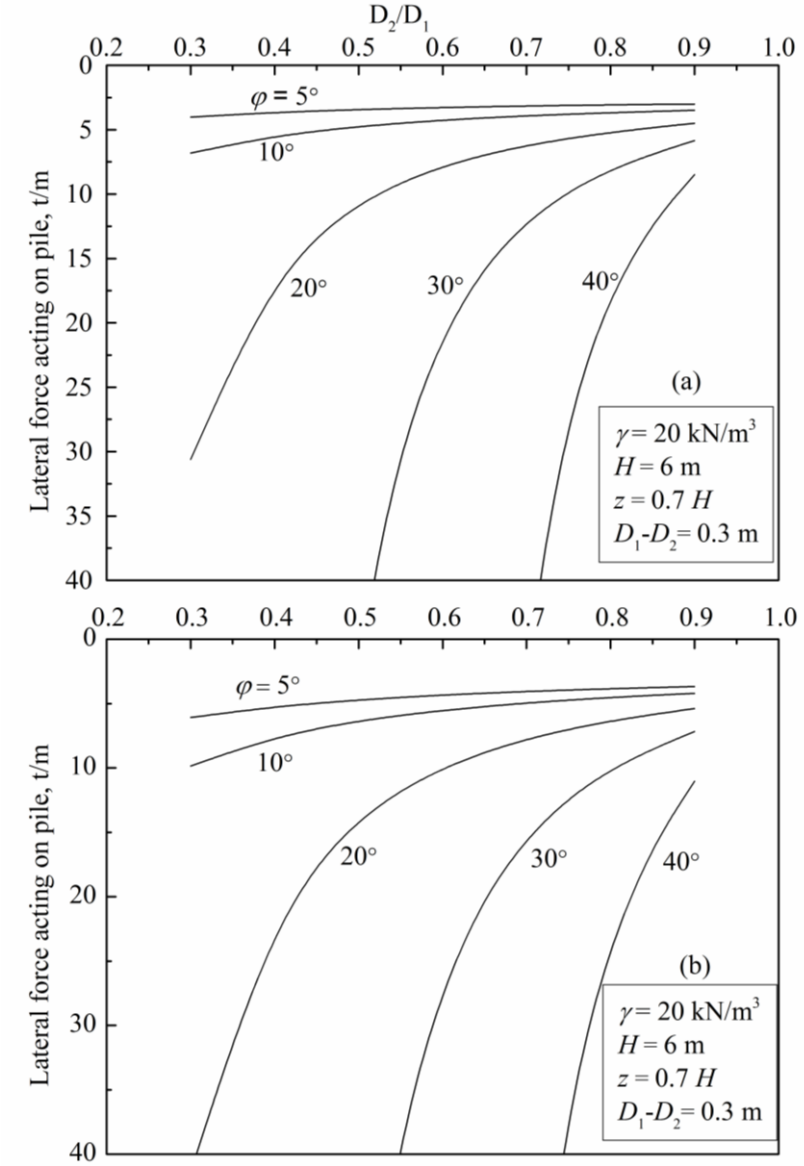

Figure 3.12 The effect of internal friction angle for (a) cohesionless soil (c = 0 kN/m^2) and (b) c-φ soil (c = 10 kN/m^2).

The total lateral force on a stabilizing pile is shown in **Figure 3.14**. It is clear that the toatal lateral force increases with the increase of internal friction angle φ and the cohesion c of the soil. Note that the four curves in **Figure 3.14** are nearly parallel to each other. It implies that the increment between two curves is nearly constant. For instance, when φ =10º, the increment of the force at c = 5 kN/m^2 and c=10 kN/m^2 is about 1.5 t. Comparing that when φ =30º, the increment is 1.6 t.

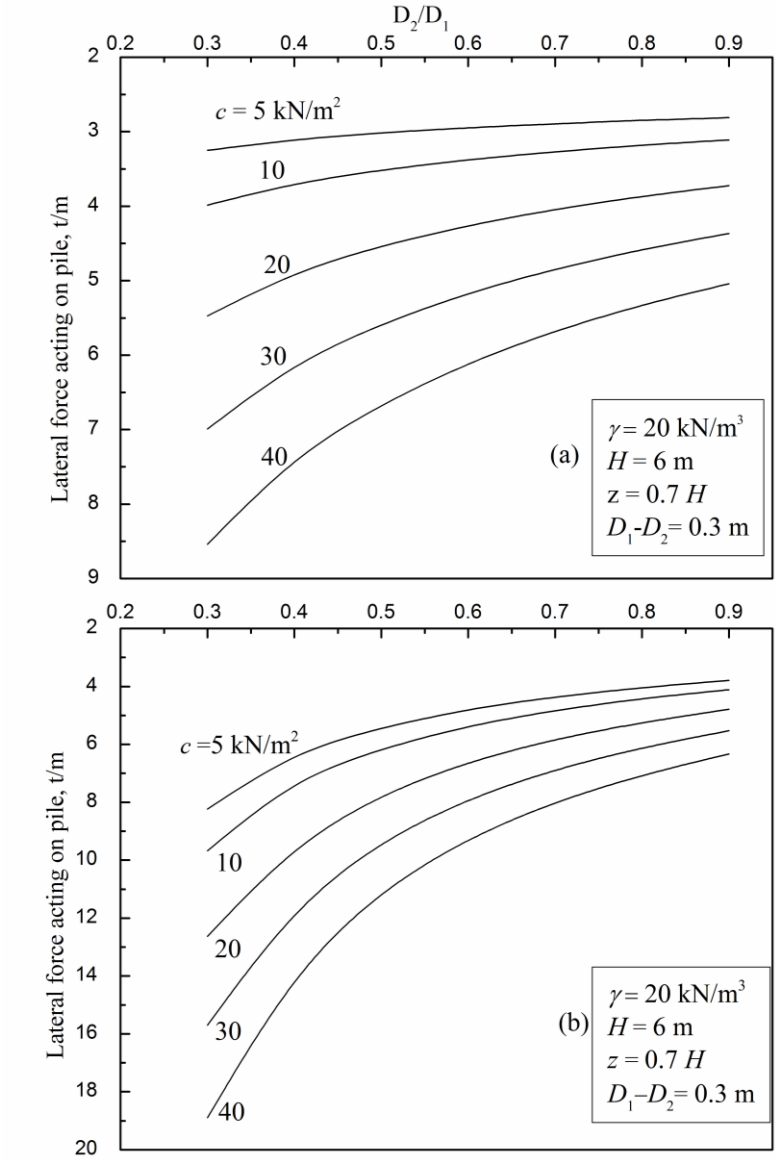

Figure 3.13 The effect of cohesion for (a) cohesive soil with internal friction angle approximates 0º (φ = 0.01º) and (b) c-φ soil with φ = 10º.

Pile diameter

The lateral force on the depth 0.7H with different pile diameter is presented in **Figure 3.15**. Both in cohesionless soil and c-φ soil, the increase of the pile diameter leads to the rise of the lateral force. Generally speaking, it means the piles in greater diameter provide more additional resistance than the smaller ones. For instance, **Figure 3.15(b)** shows that when the diameter is 0.3 m and D_2/D_1 = 0.3, the lateral force is

nearly 10 t/m; and when the diameter is 1.2 m and D_2/D_1 = 0.3, the lateral force is nearly 40 t/m, which is 4 times larger than the previous condition. It reveals that the lateral force increases in proportion to the pile diameter.

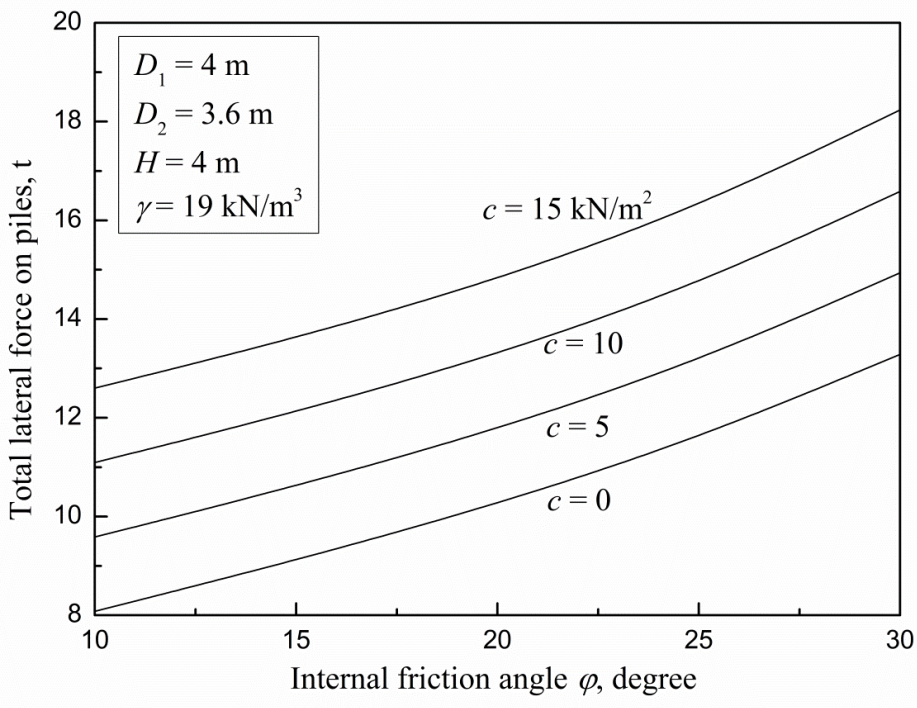

Figure 3.14 The total lateral force on the stabilizing piles.

The range of effective height

A limitation of Eq. (3.25) may exist when this equation is applied in c-φ soil in which the value of internal friction angle φ is small. It means that when Eq. (3.25) is utilized to calculate the lateral force acting on a stabilizing pile in c-φ soil with small value of internal friction angle, a negative value might be obtained in the depth that z is very close to the height of the sliding soil layer H. In this paper the critical depth in which the positive lateral force on piles can be calculated by Eq. (3.25) is defined as the effective height. What's more, the depth where the negative value exists is defined as the negative value area. In the negative value area, the lateral force is let equal to 0. That's because in many field experiments and numerical simulation results (Fukumoto, 1972 and 1974; Lirer, 2012), it is shown that when the depth that z is very close to the

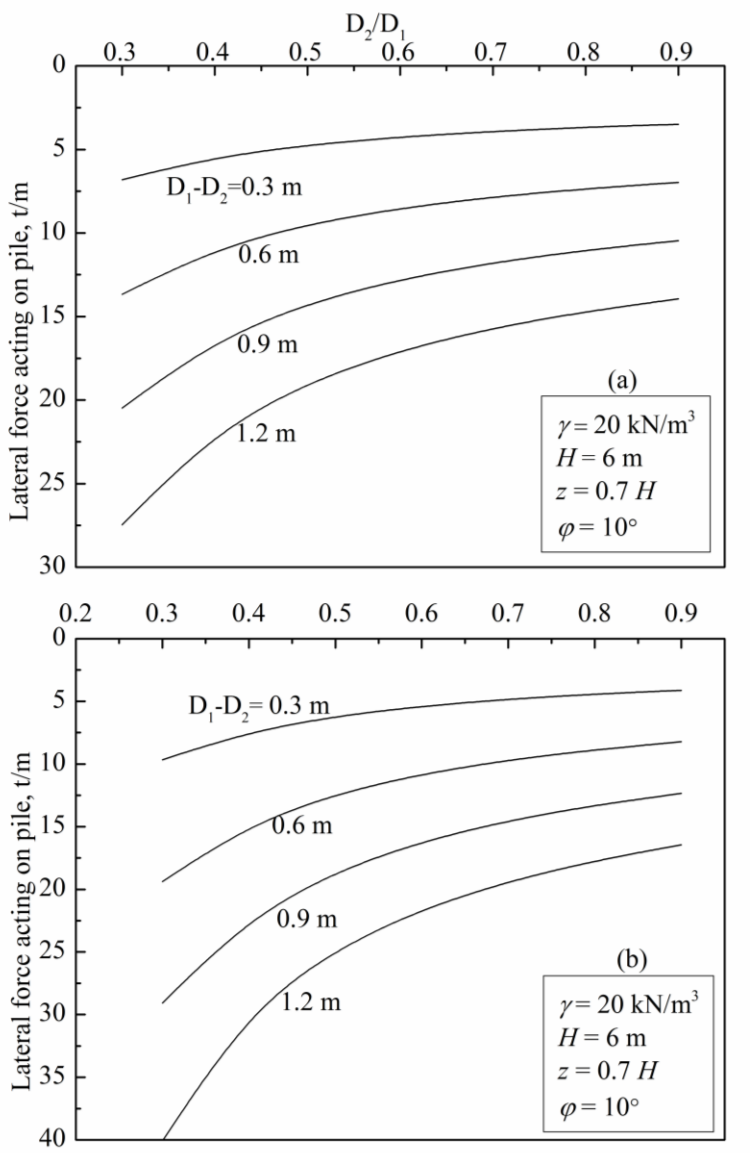

Figure 3.15 The effect of diameter of pile for (a) cohesionless soil (c = 0 kN/m^2) and (b) c-φ soil (c = 10 kN/m^2).

height of the sliding soil layer H, the value of lateral force on the piles is small. We will demonstrate in the following section that the negative value area is quite tiny that can be ignored so the treatment of the lateral force in the negative value area doesn't affect the prediction of the force. The calculated negative value between the effective height and the failure surface is considered to be a limitation of this approach because the

prediction of the lateral force on the pile in the ground above the failure plane should be positive. However this limitation can be neglected because the effective height always approximately equal to the real height of the sliding layer. The value of the effective height is studied as following.

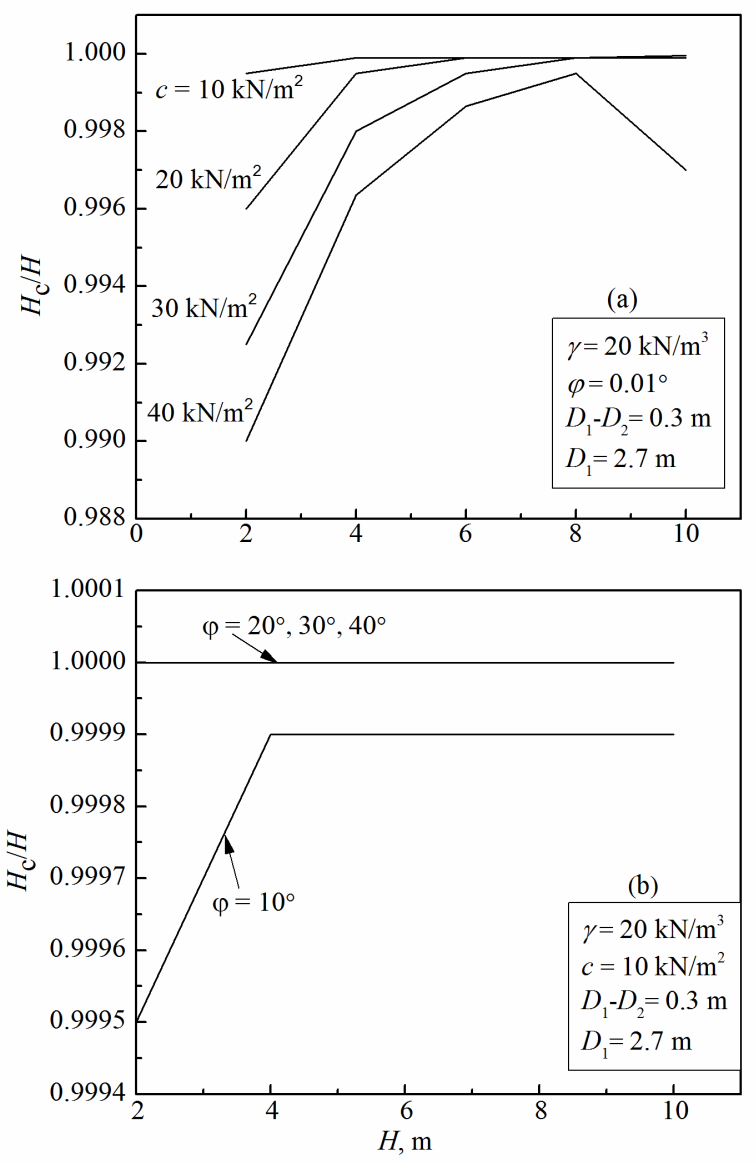

Figure 3.16 Change of effective height with mechanical parameters for (a) pure cohesive soil with internal friction angle approximates 0º and (b) c-φ soil with φ = 10º.

The ratio H_c/H versus H with respect to different mechanical parameters is shown in **Figure 3.16**, in which H_c is the effective height, H the height of the sliding soil layer. Fig. 13 displays that the effective height varies with the mechanical parameters, and the ratio H_c/H changes from 0.99 to 1. The variation of the ratio H_c/H indicates that the only a tiny discrepancy exists between effective height and the real height of sliding soil layer. It means that $H_c \approx H$.

It should be noted that if the calculated value on the failure plane is positive, it means there is no negative value area in these kinds of soils. In these soils the effective height H_c equals to H, and there is no need to modify the calculated value on the failure surface.

3.4 NUMERICAL AND EXPERIMENTAL VERIFICATION

In order to validate the proposed approach for cohesionless soil, the literature data is introduced. A numerical simulation on the response of piles subjected to mudslide was carried out by Lirer (2012). The dimensions of the numerical model are 300 m in length, 8 m in width, and 25 m in height. The sliding soil layer in this model is 4.5 m. The material properties are listed in **Table 3.1**. In which, γ is unit weight of the soil, E is the elastic modulus, c is cohesion of the soil, φ is the internal friction of the soil, ψ is the dilation angle of the soil. The pile used in the numerical simulation has a diameter of 0.4 m, and a length of 10 m. The center-to-center interval between two neighboring piles in a row is 1.3 m. The source reference gives details of the numerical model. The prediction of the lateral force and the numerical results are compared one another shown as **Figure 3.17**.

Table 3.1 Material properties in Lirer's numerical model (Lirer (2012)).

	Sliding body	Shear zone	Stable layer	Pile
γ (kN/m^3)	19	19	19	-
E (Pa)	$2\cdot10^7$	$1\cdot10^7$	$5\cdot10^7$	$2\cdot10^{11}$
v	0.34	0.34	0.34	0.25
c (Pa)	0	0	$1\cdot10^6$	$14\cdot10^7$
φ (º)	28	25	30	0
ψ (º)	0	0	0	0

Ignoring the negative force within the top few meter of the ground, Fig. 14 displays that in cohesionless soil the prediction by the proposed approach coincides with numerical results. Both the numerical results and the prediction show that the lateral force decreases near the sliding surface after the first gradually increases along the depth of the sliding soil layer. In the depth of 3.5 m ~ 4 m, both the prediction and the numerical results reach the peak value. The trend of the distribution of the force estimated by the proposed method shows a high degree of consensus with the numerical simulation data.

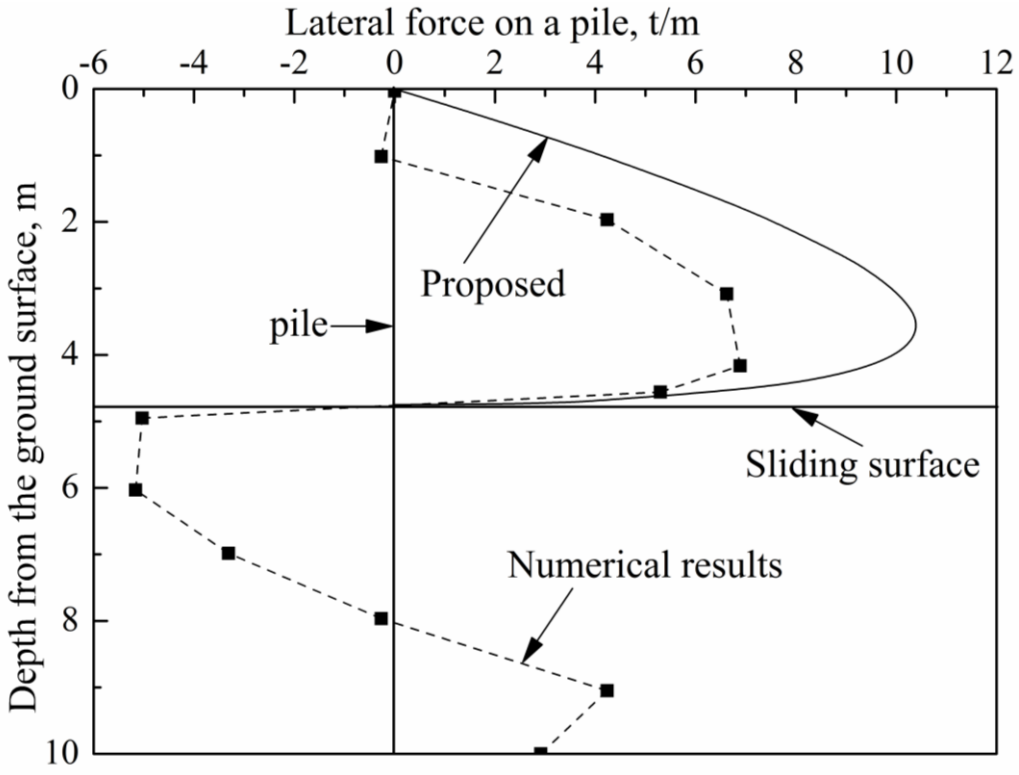

Figure 3. 17 Calculated and numerically simulated lateral force on a pile.

Verification for the c-φ-soil and cohesive soil

In Ito and Matsui's research (1975), the theoretical values were compared with the experimental results, which was originally given by Fukumoto (1972 and 1974) for the typical landsides areas in Japan, including Katamachi, Higashitono, and Kamiyana landsides areas. In this research, for the purpose of comparison, the measured data of

Fukumoto (1972 and 1974) is used again. The conditions of the stabilizing piles in these areas are summarized as follows. In Katamachi landslide area, the hollow concrete piles with diameter of 300 mm, and wall thickness of 60 mm were adopted. In the other landslide areas, the steel pipe piles with the diameter of 318.5 mm, and wall thickness of 6.9 mm were adopted. All the piles were set up zigzag in two rows at 4 m intervals, and the line space between two rows was 2 m. Furthermore, The head of the Katamachi B pile is 2.17 m depth under the ground, the Kamiyama No. 2 pile and the Higashitono No. 2 piles are both 1 m depth under the ground.

The soil properties are shown in **Table 3.2**. Note that the internal friction angles in Kamiyama and Higashitono landslide areas are 0.01º, while the original values of the angles are 0º. As mentioned previously, in the pure cohesive soil, when the internal friction angle equals to zero, a value approximated 0 is substituted.

Table 3.2 Soil properties of plastically deforming ground.

Pile	Kitamachi B	Kamiyama No.2	Higashitono No.2
Unit weight γ (kN/m^3)	19	19	19
Angle of internal friction φ (º)	2	0.01	0.01
Cohesion c (kN/m^2)	25	41	44

Generally speaking, in **Figure 3.18 (a) ~ (c)** the experimental results display the similar trend of the distributions of lateral force. Ignoring the negative force exerted on the pile within the top few meters, the lateral force by the experiment increases gradually, and then reduces near the sliding surface after reaching the peak value. The predictions of the lateral forces by the proposed method in several landslides area are almost in line with the experimental results.

In **Figure 3.18 (a) ~ (c)**, it is obvious that the distributions of the lateral force computed by Ito and Matsui's approach are linear along the stabilizing piles from top of the soil to the sliding surface. Furthermore, the maximum values calculated by Ito and Matsui's method are on the sliding surface. However, the experimental results show that the value of the force reduces radically when it reaches the maximum. Especially on the sliding

surface it usually appears to be a small value. The lateral force by the proposed method shows the nonlinear distribution, which results from the soil arching effect. Both the values due to the two theoretical methods are in the same order of magnitude with the observed ones. In **Figure 3.18 (a)**, the maximum force of the experimental result is about 3.18 t/m in the depth of 7 m below the ground, while the prediction of the proposed approach shows a maximum force of 4.97 t/m, which occurs in the depth of 7 m as well, comparing that the maximum force by Ito and Matsui's method is 6.46 t/m in the depth of 8.4 m, i.e. on the sliding surface. In **Figure 3.18 (b)**, the total lateral force on the pile in the sliding layer by the experiment the proposed approach and Ito & Matsui's method are about 14.85 t, 19.21 t, and 20.94 t. The peak value of the experimental result is about 4.30 t within the depth of 4.6 m ~ 5.5 m, while the maximum value by the prediction of the proposed approach is about 5.0 t within the depth of 4 m ~ 5 m, comparing the maximum force of 6.29 t in the depth of 6.47 m by the traditional prediction.

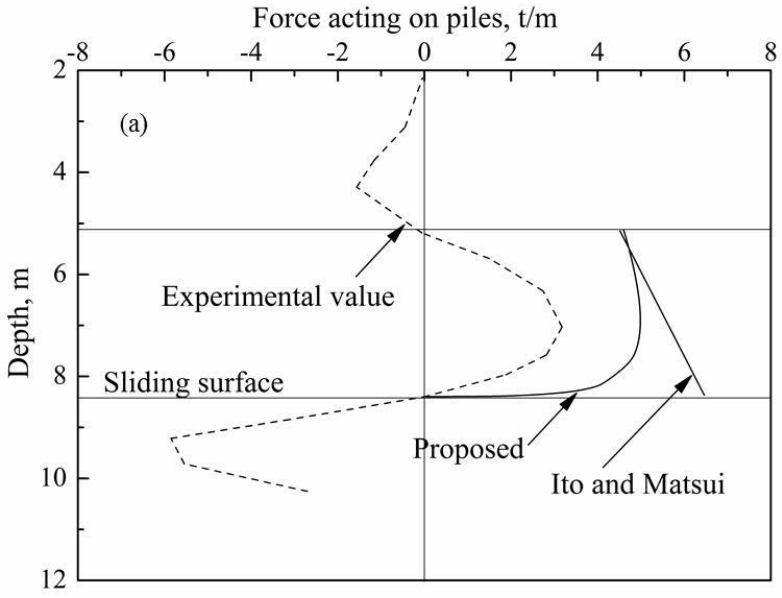

(a) Katamachi B pile, height of sliding soil layer H is 8.4m; effective height H_c is 8.399m;

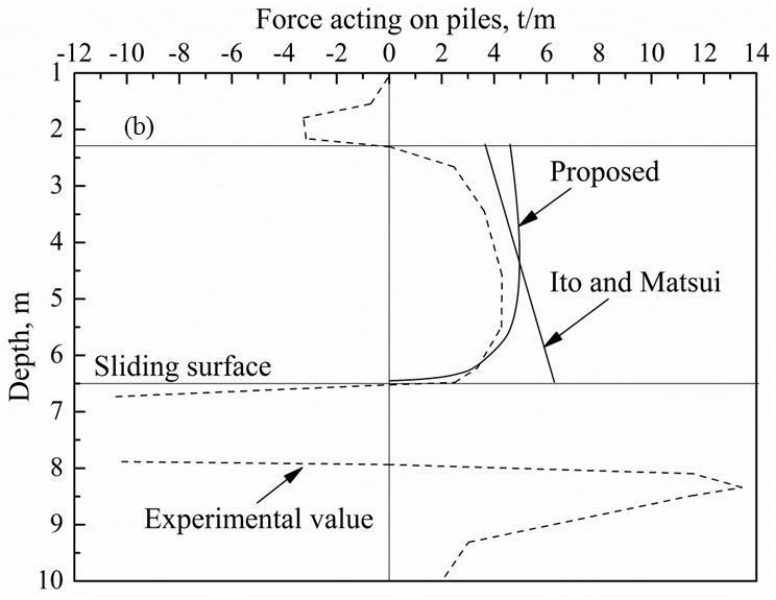

(b) Kamiyama No. 2 pile, height of sliding soil layer H is 6.47m; effective height H_c is 6.452m;

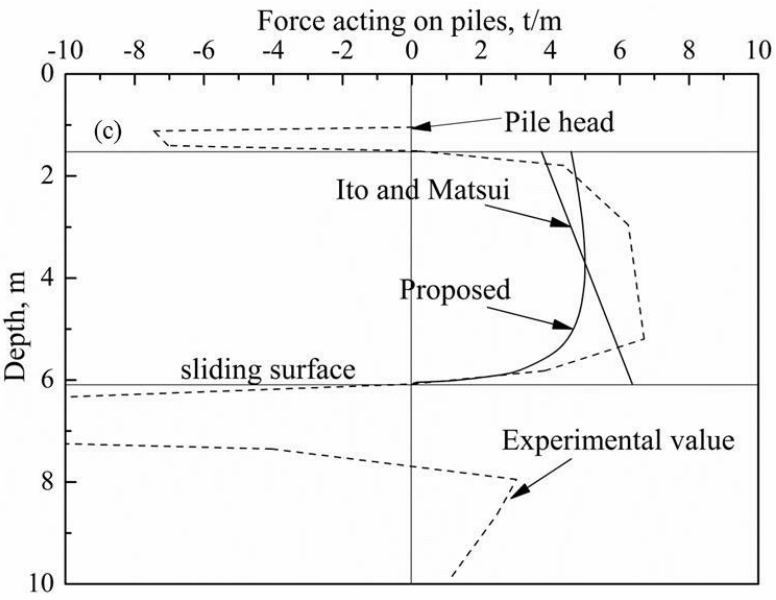

(c) Higashitono No. 2 pile, height of sliding soil layer H is 6.07m; effective height H_c is 6.045m.

Figure 3.18 Comparison between the observed and the theoretical values of lateral force acting on stabilizing piles.

The study of case histories indicates that the predictions by the proposed method are consistent with the field measurements for both *c*-*φ* soil and pure cohesive soil. Especially, the proposed method shows the nonlinear distribution of the force, i.e. the soil-pile pressure increases gradually and then decreases to 0 at the failure surface. This distribution compares well with the measurements.

3.5 CONCLUSIONS

The estimation of the lateral force acting on the stabilizing pile due to the soil layer movement is discussed in this chapter. The previous theoretical method shows the lineardistribution of the lateral force along the sliding soil layer, which can evaluate the magnitude of the lateral force. In this paper, the plastic deformation theory proposed by Ito and Matsui is modified by considering the soil arching effect between two neighboring piles. The prediction by the modified approach provides the nonlinear distribution of the lateral force, which is more consistent with the field measurement.

For cohesionless and *c*-*φ* soil, the lateral forces on the pile are discussed separately, and two new formulae are proposed. The parameters in these formulae are studied for each soil. Generally speaking, the parametric study shows the lateral force increase with the growth of the height of the unstable soil layer *H*, the internal friction angle *φ*, the cohesion *c*, and the pile diameter D_1-D_2.

The comparisons for cohesionless soil, *c*-*φ* soil and pure cohesive soil are carried out respectively. The calculated value shows highly consistent with the numerical simulation result. The comparisons in the *c*-*φ* soil and pure cohesive soil indicate that the prediction by the proposed approach compares well with the experimental result, especially the maximum force and the corresponding position calculated by the proposed method is in line with the field measurement. In addition, all the comparisons in this chapter display that in the flow mode the nonlinear distribution of the force on the stabilizing pile in the sliding soil layer is predicted by the proposed approach, which shows a satisfactory agreement with the experimental value. What's more, the proposed method reveals that the lateral force on the pile segment embedded in the sliding soil

layer would increase from the top of the ground surface, and then decrease to a small value on the sliding surface after culminates. This behavior of the distribution of the lateral force coincides with the experimental data, ignoring the negative force within the little depth below the ground surface.

REFERENCES

Ashour M., and Norris G., 2000. Modeling lateral soil-pile response based on soil-pile interaction. Journal of Geotechnical and Geoenvironment Engineering, ASCE 126(5): 420-428.

Ashour M., Pilling P., Norris G., 2004. Lateral behavior of pile groups in layered soils. Journal of Geotechnical and Geoenvironment Engineering, ASCE 130(6): 580-592.

Ashour M., and Ardalan H., 2012. Analysis of pile stabilized slopes based on soil-pile interaction. Computers and Geotechnics 39: 85-97.

Bosscher P J. and Donald H. G., 1986. Soil Arching in Sandy Slopes. Journal of Geotechnical Engineering 112(6), 626-645.

Cai, F. and Ugai, K., 2000. Numerical analysis of the stability of a slope reinforced with piles. Soils and Foundations 40(1), 73-84.

Cai, F. and Ugai K., 2004. Numerical Analysis of Rainfall Effects on Slope Stability. International Journal of Geomechanics, ASCE 4(2): 69-78.

Chen L. T, and Poulos H. G., 1997. Piles subjected to lateral soil movements. Journal of Geotechnical and Geoenvironment Engineering 123(9), 802-811.

Franx, C. & Boonstra, G.C. 1948. Horizontal pressures on pile foundations. Proc. 2nd Int. Conf. S.M. &F.E., 1: 131-135.

Fukumoto, Y., 1972. Study on the behavior of stabilization piles for landslides. Soils and Foundations, 12(2): 61-73. (In Japanese)

Fukumoto, Y., 1974. On the Lateral Resistance of Piles against a Land-sliding Erosion Control Section, Niigata Pref. Journal of the Japan Landslide Society, 11(2), 21-29. (In Japanese)

Guo W.D., 2013. Pu-Based Solutions for Slope Stabilizing Piles. International Journal of Geomechanics, ASCE 13(3): 292-310.

Hassiotis S, Chameau JL, Gunaratne M., 1997. Design method for stabilization of slopes with piles. Journal of Geotechnical Geoenvironment Engineering 123(4), 314–323.

Handy, R. L., 1985. The arch in soil arching. Journal of Geotechnical. Engineering, ASCE 111(3), 302-318.

Hazarika H, Terado Y, Hayamizu H., 2000. A new Approach to the Finite Element Slope Stability Analysis Incorporating the Slice and Pile Deformations. Proceeding of the Tenth International Offshore and Polar Engineering Conference, Seattle, Washiton, USA, 630-636.

Heyman, L. & Boersma, L. 1961. Bending moments in piles due to lateral earth pressures. Proc. 5th Int. Conf. S.M. & F.E., 2: 425-429.

Ito, T., and Matsui, T., 1975. Methods to estimate lateral force acting on stabilizing piles. Soils and Foundations 18(4), 43-59.

Janssen, H. A. 1895. Versuche uber getreidedruck in silozellen. Z. Ver. Deut. Ingr., Vol. 39, 1045-1049. (partial English translation in Proceeding of the Institute of Civil Engineers, London, England).

Jeong S., Kim B., Won J., Lee J., 2003 Uncoupled analysis of stabilizing piles in weathered slopes. Computers and Geotechnics 30(8): 671-682.

Kingsley, H. W., 1989. Arch in soil arching. Journal of Geotechnical Engineering 115(3), 415-419.

Krynine, D. P., 1945. discussion of "Stability and Stiffness of Cellular Cofferdams," by Karl Terzaghi, Transactions, ASCE, 110, 1175-1178.

Leussink, H. & Wenz, K.P. 1969. Storage yard foundations on soft cohesive soil. Proc. 7th Int. Conf. S.M. & F.E., 2: 149-155.

Livingston, C. W., 1961. The natural arch, the fracture pattern, and the sequence of failure in massive rock surrounding an underground opening. Proceedings of the symposium on rock mechanics, Pennsylvania State University, Bulletin 76, 197–204.

Lirer S., 2012. Landslide stability piles: Experimental evidences and numerical interpretation. Engineering Geology, 149-150(2): 70-77.

Liu F. and Zhao J., 2013. Limit Analysis of Slope Stability by Rigid Finite-Element Method and Linear Programming Considering Rotational Failure. International Journal of Geomechanics, ASCE 13(6): 827-839.

Marche, R. & Lacroix, Y. 1972. Stabilite des culees de ponts establies sur des pieux traversant une couche molle. Can. Geot. Jnl., 9(1): 1-24.

Marston, A., and Anderson, A. O., 1913. The Theory of Loads on Pipes in Ditches and Tests of Cement and Clay Drain Tile and Sewer Pipe, Iowa Engineering Experiment station Bulletin, Iowa State College, Ames, Iowa, No. 31.

Nian T.K., Chen G.Q., Luan M.T., Yang Q., Zheng D.F., 2008. Limit analysis of the stability of slopes reinforced with piles against landslide in nonhomogeneous and anisotropic soils. Canadian Geotechnical Journal 45(8): 1092-1103.

Nicu, N.D., Antes, D.R., & Kessler, R.S. 1971. Field measurements on instrumented piles under an over pass abutment. High Res. Rec., No. 345.

Paik K. H., and Salgado R., 2003. Estimation of active earth pressure against rigid retaining walls considering arching effects, Geotechnique 53(7), 643-653.

Poulus, H. G., 1973. Analysis of piles in soil undergoing lateral movement, Journal of Soil Mechanics and Foundation Engineering, ASCE,.99(5), 391-406.

Sokolovskii, V. V., 1965. Statics of Granular Media, Oxford: Pergamon Press, (translated from the Russian by J. K. Lusher).

Stevic´, M., Jasarevic´, I. & Ramiz, F., 1979. Arching in hanging walls over leached deposits of rock salt. Proceedings of 4th International Congress of Rock Mechanics, Montreaux 1, 745–752.

Suleiman M.T., Ni L., Helm J.D., Raich A., 2014. Soil-Pile Interaction for a Small Diameter Pile Embedded in Granular Soil Subjected to Passive Loading. Journal of Geotechnical and Geoenvironment Engineering, ASCE 140 (5): 1-15.

Terzaghi, K., 1936. A Fundamental Fallacy in Earth Pressure Computations. Journal of the Boston Society of Civil Engineers 23(2): 71-78.

Terzaghi, K., 1943. Theoretical Soil Mechanics, J. Wiley and Sons, Inc., New York, N.Y.

Walker, D. M., 1966. An approximate theory for pressure and arching in hoppers.

Chemical Engineering Science. 21(11): 975–997.

Wang, Y. Z., 2000. Distribution of earth pressure on a retaining wall, Geotechnique 50(1): 83-88.

Won J., You K., Jeong S., Kim S., 2005. Coupled effects in stability analysis of soil-pile system. Computers and Geotechnics, 32(4): 304-315.

Yamada, G., Watari, M. and Kobashi, S., 1971. Real Condition of Landslide and Slope Failure and Its countermeasure. Tokyo, Sankaido, 167-183 (in Japanese).

CHAPTER 4

ANALYSIS OF EFFECTS OF THE SLOPE ANGLE ON THE DISTRIBUTION OF SOIL-PILE PRESSURE

4.1 INTRODUCTION

In the past several decades, installing rows of drilled shafts for slope stabilization has proved to be a reliable and effective technique to prevent excessive slope movement (Ito and Matsui. 1975; De Beer 1977; Liang and Zeng 2002; Lirer 2012; Galli and Prisco 2013). Piles are installed through the unstable soil layer and embedded into the stable layer below the sliding surface. The slope is stabilized by piles, which are able to transfer part of the force from the failing mass to the stable soil layer. For passive piles, the soil-pile pressure applied on the piles by the unstable layer is dependent on the soil movement, which is in turn affected by the presence of the piles (Wei and Cheng 2009).

Evaluating soil-pile pressure acting on stabilizing piles is of great significance for the study of slope stabilization. In previous research, a horizontal semi-infinite soil ground was typically used for the theoretical analysis of the soil-pile pressure on piles (Ito and Matsui 1975; Poulos 1995; Viggiani 1981). Satisfactory results have been predicted by these methods. In subsequent research (Ito et al. 1981 and 1982; Hassiotis 1997; Ausilio 2001; Won et al. 2005; Li et al. 2010; Kourkoulis et al. 2011), these methods have been adopted and developed. The interaction between piles is governed by the so-called arching effect. Durrani et al. (2006) suggested that the Rankine passive and active pressure coefficients should be employed to estimate the maximum spacing resulting in arching between piles. Viggiani (1981) suggested designing slope stabilizing piles using the limit equilibrium method. With such an approach, the stabilizing

contribution given by a single pile depends on the pile characteristics (diameter, length, and ultimate bending moment), the soil strength and slide thickness (Lirer 2012).

Poulos (1995) presented an analysis method in which a simplified form of the boundary element method (Poulos 1973) was employed to study the response of a row of passive piles incorporated in limit equilibrium solutions of slope stability. This method revealed the existence of three modes of failure: (*i*) "flow mode", (*ii*) "short-pile mode", and (*iii*) "intermediate mode". This finding contributed to the practical design of stabilizing piles. Poulos (1995) highlighted that the flow mode created the least damage effect of soil movement on the pile; if the piles required protection, efforts should be made to promote this mode of behaviour.

Norris (1986) developed a strain wedge (SW) model to predict the response of a flexible pile under lateral loading. Generally speaking, the SW model allows the assessment of the nonlinear p-y curve response of a laterally loaded pile based on the envisioned relationship between the three-dimensional response of a flexible pile in the soil to its one-dimensional beam on elastic foundation parameters (Ashour et al. 1998). The SW model has been improved and modified to accommodate a laterally loaded pile embedded in multiple soil layers (Ashour et al. 1998 and 2000). Undoubtedly, great improvements have been made on the SW model to predict the response of flexible piles under lateral loading (Ashour et al. 2000 and 2004). In the SW model, the "flow mode" mechanism (Poulos 1995) mentioned previously was adopted in Ashour and Ardalan's research (2012). Such a slope-pile displacement mechanism is also adopted in the model presented here.

In this chapter, the author propose a simple method for estimating the ultimate soil-pile pressure per unit length of the pile, which is induced by flowing soil, assuming that the soil displacement is larger than the pile deflection (**Figure 4.1**). The theory of plastic deformation (Ito and Matsui 1975) is modified, and the soil arching effects between two neighbouring piles are considered, which leads to the nonlinear distribution of the soil-

pile pressure per unit length of piles. Furthermore, the theoretical analysis of the effect of the slope angle on the soil-pile pressure distribution in sandy slopes is carried out.

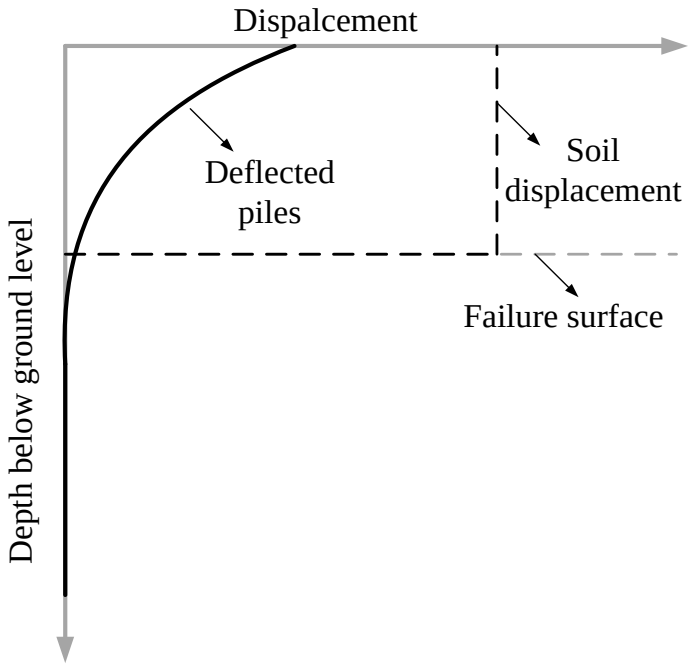

Figure 4.1 Soil-pile displacement as employed in the model presented here (Ashour and Ardalan, 2012).

In this chapter, the soil-pile pressure per unit length of the stabilizing pile is analysed in a semi-infinite sandy slope, as shown in **Figure 4.2**. The general analysis of the soil-pile pressure acting on the piles involves three main steps: (1) analysing the soil arching zone adjacent to the piles in the slope; (2) analysing the active lateral stress in the soil arching zone between two neighbouring piles; and (3) substituting the active lateral stress into Ito and Matsui's approach (1975) to estimate the soil-pile pressure acting on each pile. The piles are assumed to be flexible. In step 1, when the unstable soil layer slides along the potential sliding surface, the soil layer deforms. Additionally, soil arching occurs adjacent to the two neighbouring piles in the failing mass. The plan view of the soil arching zone between two neighbouring piles is shown by the hatched area in **Figure 4.3(a)**. A typical cross section UU′ is shown in **Figure 4.3(b)**. The area of the soil arching zone is dependent on the slope angle and the properties of the soil,

which are discussed later in this paper. In step 2, to simplify the analysis of the active stress on the plane AA′ (referring to **Figure 4.4**), an assumption is made that when the active stress on the plane AA′ is analysed, the area between the parallel lines AG and AG′ is considered to be the soil arching area. This soil arching area is shown as the shadowed portion in **Figure 4.4**, where σ_h is the active soil stress induced by the soil arching effects, D_1 is the centre-to-centre interval between two neighbouring piles, and D_2 is the clear interval between piles. In addition, the limit equilibrium condition of the differential element in the soil arching zone is analysed to obtain the active stress. In step 3, the approach proposed by Ito and Matsui (1975) is adopted, and the squeezing effects between the piles are evaluated. This procedure yields the soil-pile pressure per unit length of the pile.

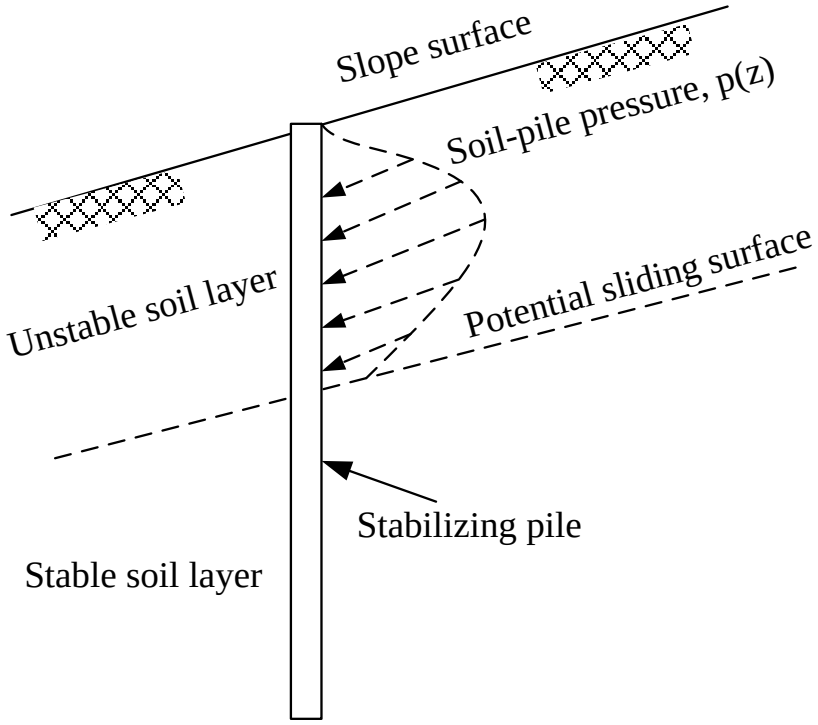

Figure 4.2 Stabilizing pile embedded into a semi-infinite slope (adopted from Ashour and Ardalan 2012).

For the purpose of verifying the proposed model, a numerical simulation was performed. The shear strength reduction method (SRM) is used in the code of FLAC^{3D}.

SRM has been used in the stability analysis of slopes without piles by many previous researchers (Zienkiewicz et al. 1975, Ugai and Leshchisky 1995, Griffiths and Lane 1999, Wei et al. 2009). This method is extended to analyse the safety factor of a slope stabilized with piles. In the studies by Martin and Chen (2005), Won et al. (2005), Wei

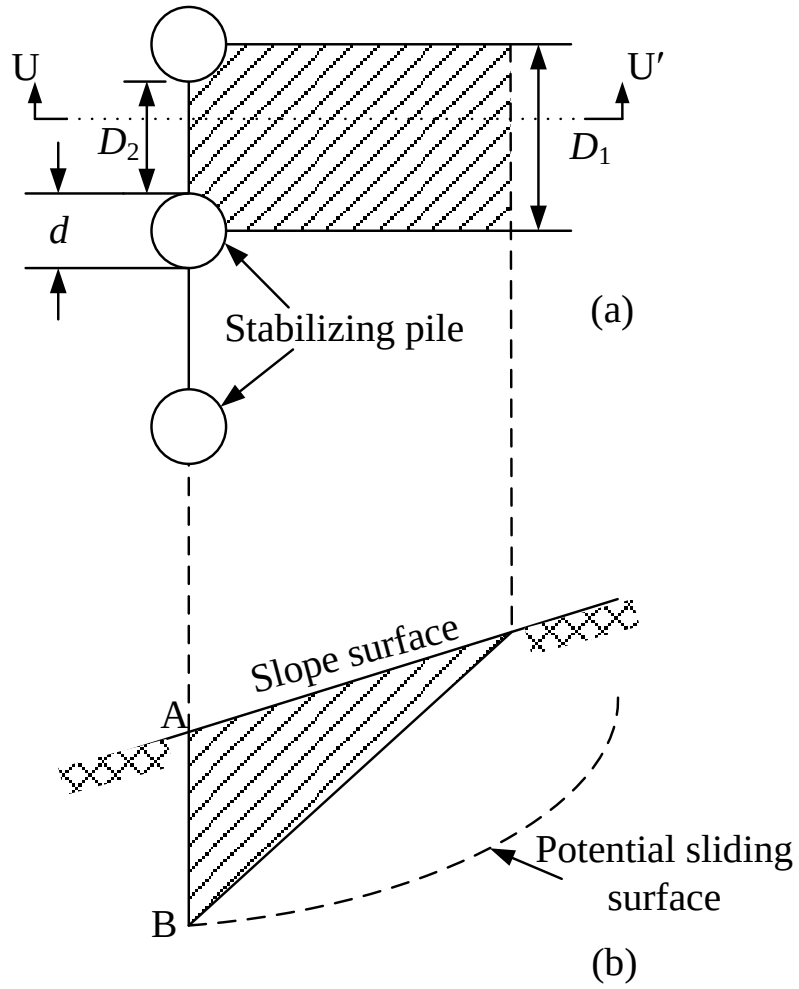

Figure 4.3 Soil arching adjacent to the stabilizing piles in a slope: (a) plan view of the soil arching zone; (b) cross section of the soil arching zone in the slope.

and Cheng (2009), and Lirer (2012), FLAC^{3D} is used to analyse the response of the stabilizing piles or the safety factor of the reinforced slope with piles. FLAC^{3D} is a widely used tool for estimating the response of the stabilizing piles. In this study, the authors use the three-dimensional finite difference code FLAC^{3D} by SRM to analyse the

soil-pile pressure acting on stabilizing piles during slope slides. The numerical simulation results are compared to the prediction obtained from the proposed model. Furthermore, the laboratory experiments carried out by Chen et al. (1997) and Guo and Ghee (2006) are introduced to evaluate the proposed model.

Finally, the validated model is used to evaluate the effect of slope angle on the distribution of the soil-pile pressure per unit thickness on the stabilizing piles. The main finding of this paper is that the distribution shape of the soil-pile pressure varies with the slope angle, while the magnitude of the soil-pile pressure remains in the same order.

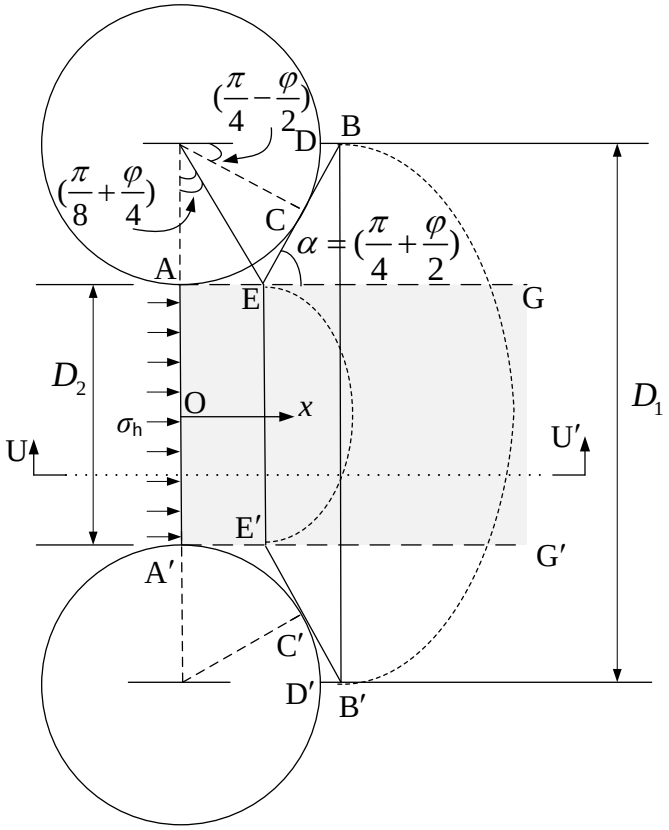

Figure 4.4 Plastic deformation of soil between neighbouring piles (adopted from Ito and Matsui, 1975).

4.2 LIMIT EQUILIBRIUM CONSIDERING SOIL ARCHING IN SLOPES

4.2.1 SOIL ARCHING ZONE IN SLOPES

In a semi-infinite inclined soil mass, the soil arching that occurs adjacent to stabilizing piles has been studied by Wang and Yen (1974). However, the area of the soil arching zone was not specified. Paik and Salgado (2003) assumed that the slip plane behind a retaining wall had an angle of $45^{o}+\varphi/2$ and that the area between the slip plane and the wall was the soil arching zone. In this section, the soil arching zone is analysed using geometry. It is assumed that when the unstable soil layer slides along the potential sliding surface, the soil layer deforms, and a slip plane occurs behind the piles, which is inclined at an angle θ_s with respect to the slope surface (**Figure 4.5**). The area ABC in **Figure 4.5** is the soil arching zone. The geometry in the soil arching zone is analysed using Mohr Circle, and shown as follows:

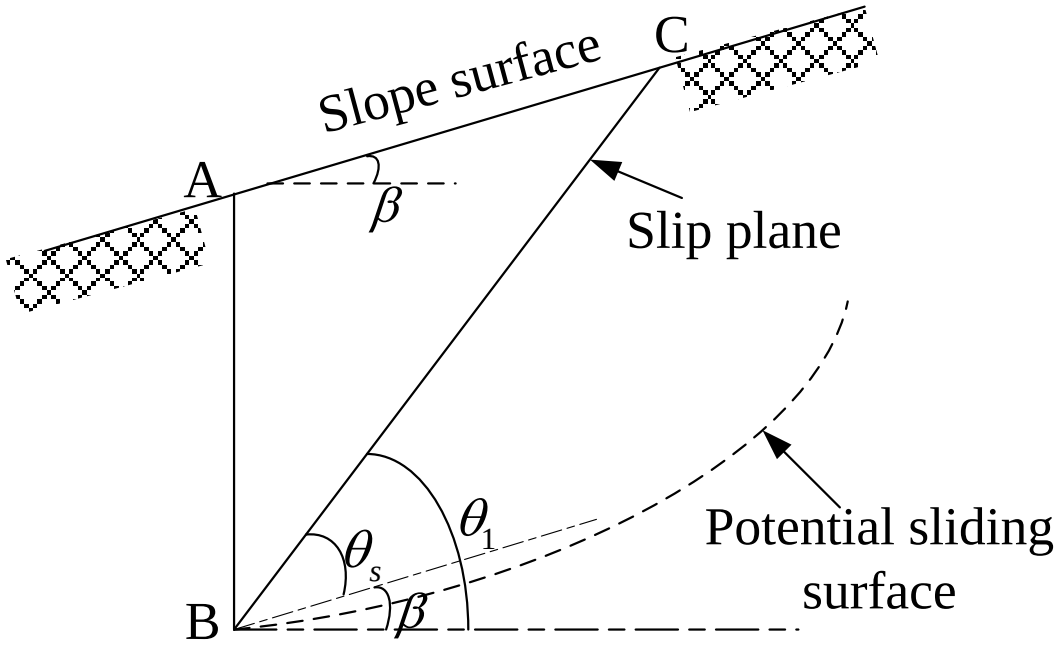

Figure 4.5 Profile of the soil arching zone and the geometric relationships in the zone.

When the soil stress on the line AB (**Figure 4.5**) is active, the differential element (**Figure 4.6**) and the corresponding Mohr's circle (**Figure 4.7**) are used to determine the geometric relationship between the stresses. The process of solving the angle θ is

(a) In a rectangular coordinate system, because the internal friction angle φ was investigated in advance, the strength envelope is determined as the line OP shown in **Figure 4.7**.

(b) The two lines OL and OL′ are drawn above and below the σ axis; the angle between each line and the σ axis is β.

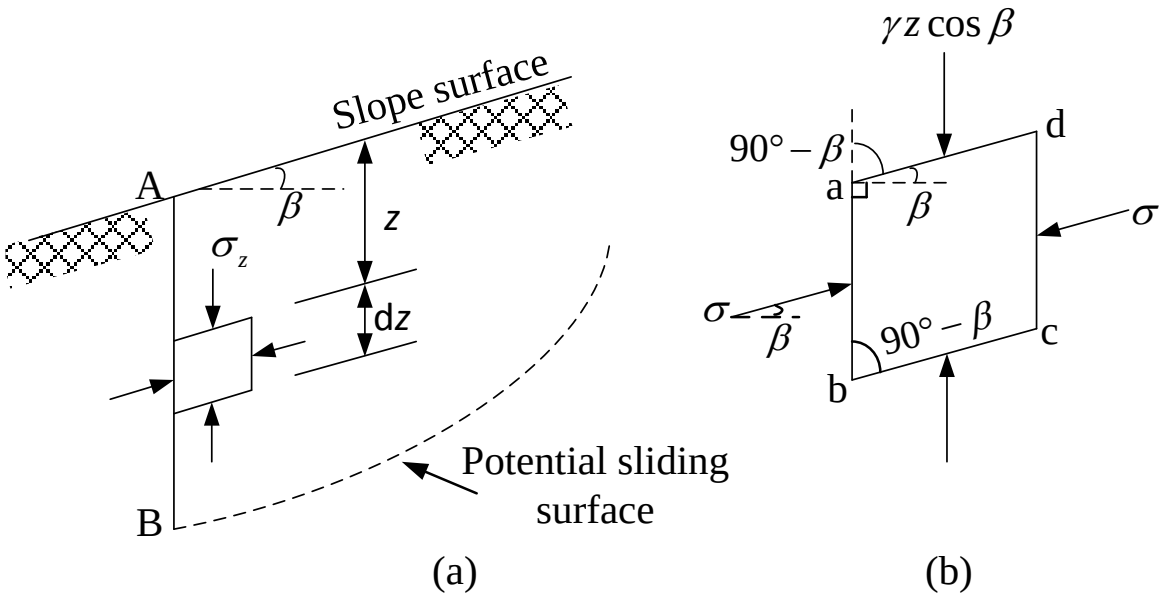

Figure 4.6 The stress state: (a) the stress state of a differential element in a semi-finite slope; (b) the generic element.

(c) On the line OL, we set OA = $\sigma_z = \gamma z\cos\beta$. Point A in **Figure 4.7** represents the stress acting on the surface (**Figure 4.6(b)**), including the normal stress and the shear stress.

(d) In the negative direction of the σ axis, an arbitrary point D′ is set. A circle can then be drawn with centre D′ and with tangency point B′ on the line OP′. The circle D′ and the line OE intersect at point A′.

(e) Parallel to A′D′, a line AD is drawn with the point D located on the σ axis. Taking AD as the radius and point E as the centre, a circle is drawn. This

produces the circle D, which is tangential to the line OP at point B.

(f) The angle between AD and BD is equal to $2\theta_1$.

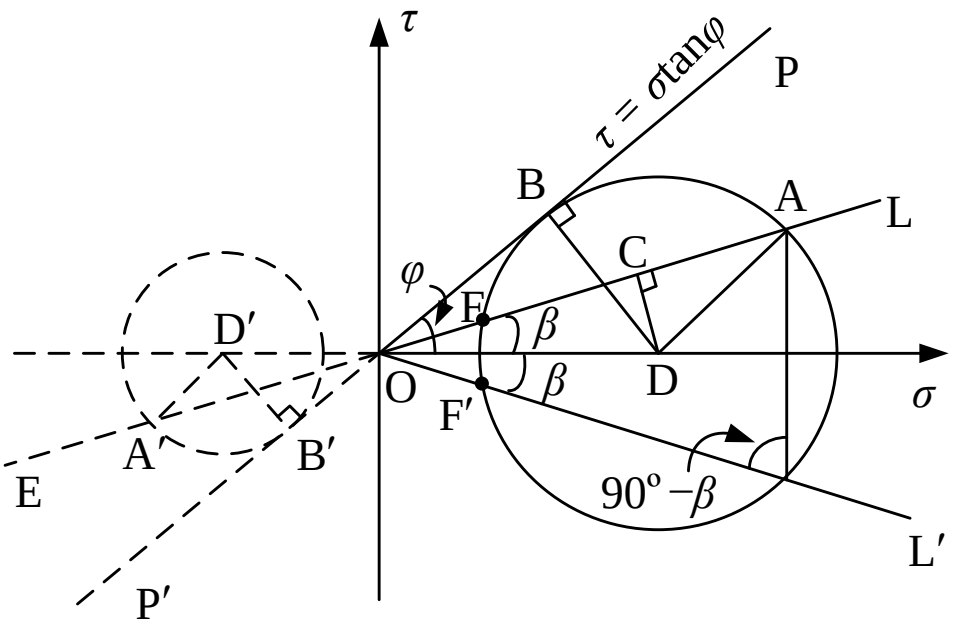

Figure 4.7 The geometric relationship in the soil arching zone illustrated by Mohr's Circle.

According to the geometric relationships in **Figure 4.7**, it is obvious that

$$CD = OD\sin\beta \tag{4.1}$$

$$AD = BD = OD\sin\varphi \tag{4.2}$$

$$\cos\angle ADC = \frac{CD}{AD} = \frac{OD\sin\beta}{OD\sin\varphi} = \frac{\sin\beta}{\sin\varphi} \tag{4.3}$$

$$\angle ADC = \arccos\frac{\sin\beta}{\sin\varphi} \tag{4.4}$$

$$\theta = \frac{1}{2}(\varphi - \beta + \arccos\frac{\sin\beta}{\sin\varphi}) \tag{4.5}$$

$$\theta_1 = \frac{1}{2}(\varphi + \beta + \arccos\frac{\sin\beta}{\sin\varphi}) \tag{4.6}$$

4.2.2 LIMIT EQUILIBRIUM EQUATION ON THE DIFFERENTIAL ELEMENT

In the study of retaining walls, soil arching is assumed to occur in a circular arc. Paik and Salgado (2003) have evaluated the active soil stress based on the soil arching theory. In this paper, the approach proposed by Paik and Salgado (2003) is adopted and extended to analyse an inclined soil mass. The rotation of the principal stress on the line AB (**Figure 4.5**) is described in **Figure 4.8(a)** and **(b)**. In the rear of line AB, the trajectory of the minor principal stress on the differential element is represented by dotted lines assumed as an arc, while the major principal stress is the normal to the arc. The active earth pressure acting on line AB includes two components: the active lateral stress σ_h and the shear stress τ.

As shown in **Figure 4.8(a)**, on the left side of the differential element, the force equilibrium in the triangular element at point E is considered. The lateral stress is calculated as follows:

$$\sigma_h = \sigma_1 \cos^2\theta_w + \sigma_3 \sin^2\theta_w \tag{4.7}$$

Similarly, at an arbitrary point D on the arc, whose original location is point F, the lateral force is given by

$$\sigma_{ah} = \sigma_1 \cos^2\psi + \sigma_3 \sin^2\psi \tag{4.8}$$

where ψ is the angle between the normal of the arc at point D and the horizontal, and σ_{ah} is the lateral stress at point D. Considering when the soil is in an active condition, substituting $\sigma_3/\sigma_1 = 1/N_1$ into Eq.(4.8) yields

$$\sigma_{ah} = (\cos^2\psi + \frac{1}{N_1}\sin^2\psi)\sigma_1 \tag{4.9}$$

where $N_1=\tan^2(45^o+\varphi/2)$.

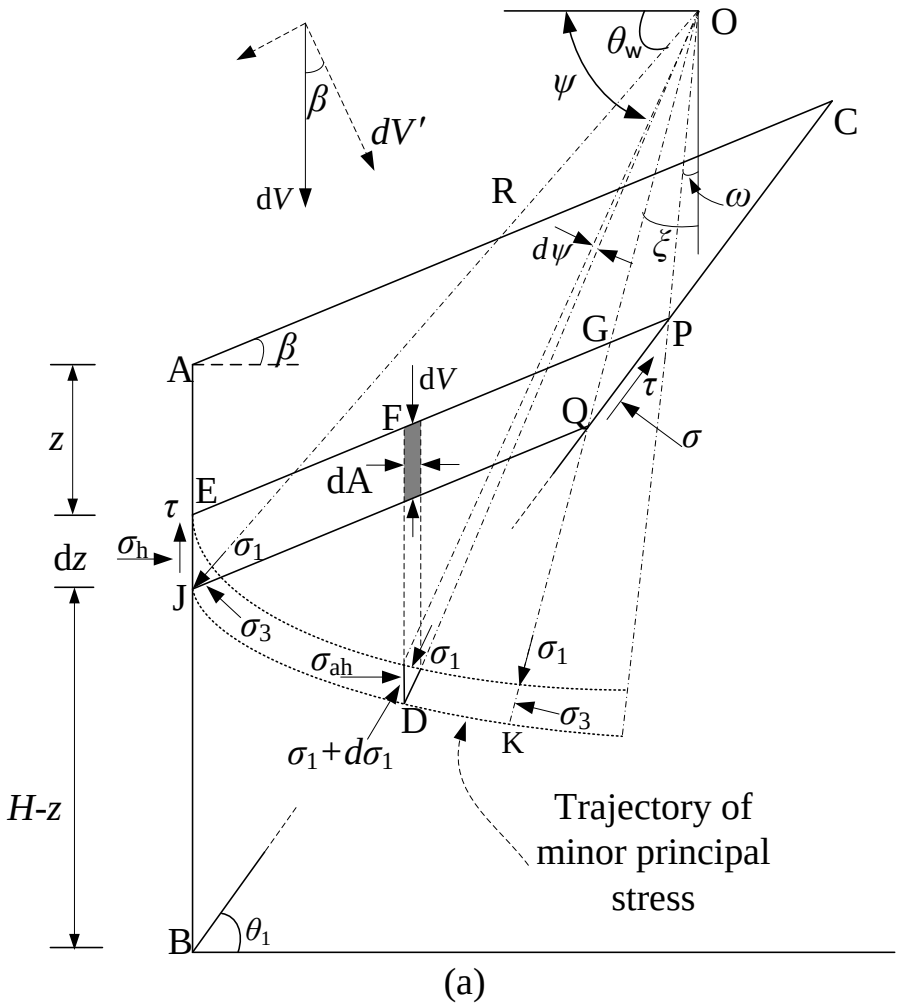

(a)

(a) The major and minor principal stresses

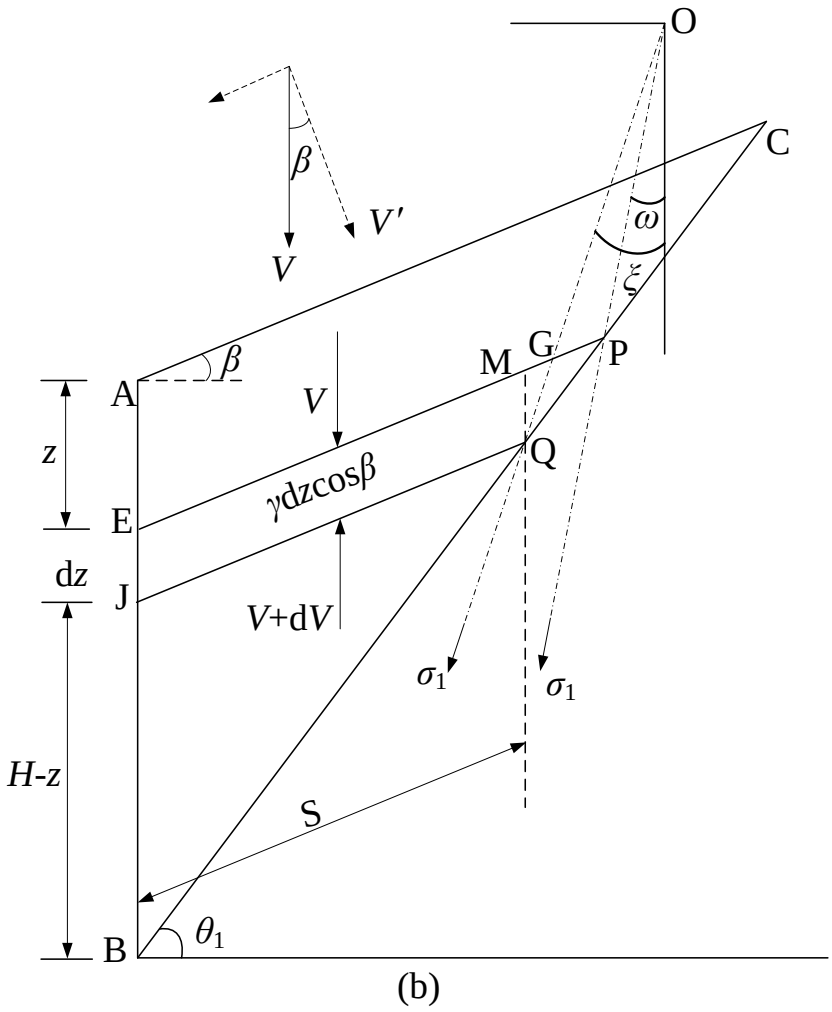

(b)

(b) Schematic of the vertical total force on the differential element

Figure 4.8 Stress on the differential element in the soil arching zone: (based on Paik and Salgado 2003).

In **Figure 4.9(a)**, the vertical stress σ_v, which is applied on the surface of the differential element, includes two components: one perpendicular to the line EP, σ_v', and one parallel to the line EP, σ_f. The ratio of σ_v to σ_v' is as follows:

$$\sigma_v / \sigma_v' = \frac{1}{\cos\beta} \tag{4.10}$$

Because $\sigma_{ah}-\sigma_3=\sigma_1-\sigma_v$, substituting for σ_{ah} yields

$$\frac{\sigma_v'}{\sigma_1} = \cos\beta(\sin^2\psi + \frac{1}{N_1}\cos^2\psi) \tag{4.11}$$

Because the angle ψ (**Figure 4.8(a)**) is not a constant, an average stress $\bar{\sigma}_v'$ is introduced to replace σ_v' at every point. This average stress is given by

$$\bar{\sigma}_v' = \frac{V'}{S} \tag{4.12}$$

where V' is a component of the total stress applied on the differential element, which is perpendicular to EP, and S is the width of the differential element (referring to **Figure 4.8(b)**). Considering the geometry depicted in **Figure 4.8(b)**, S is calculated by

$$S = \frac{\cos(\theta_w + \xi)}{\cos(\beta + \xi)} R \tag{4.13}$$

where ξ is the angle between the normal line OQ and the vertical and R is the radius of the circle.

The stress V' on the differential element can be calculated by

$$V' = \int_{\theta_w}^{\pi/2-\omega} dV' \tag{4.14}$$

where dV' is the differential force on the shaded element at point F, which is perpendicular to EP (referring to **Figure 4.8(a)**). This perpendicular differential force is expressed as

$$dV' = \sigma_v' dA = \sigma_1 \cos\beta(\sin^2\psi + \frac{1}{N_1}\cos^2\psi) \cdot \frac{Rd\psi\sin\psi}{\cos\beta} \tag{4.15}$$

Solving Eq. (4.12) to Eq. (4.45) yields

$$\bar{\sigma}_v' = \frac{\cos(\beta + \xi)}{\cos(\theta_w + \xi)} \cos\theta_w (1 - \frac{N_1 - 1}{3N_1}\cos^2\theta_w)\sigma_1 \tag{4.16}$$

To simplify the analysis process, the angle ω (referring to **Figure 4.8**) is assumed to

be 0.

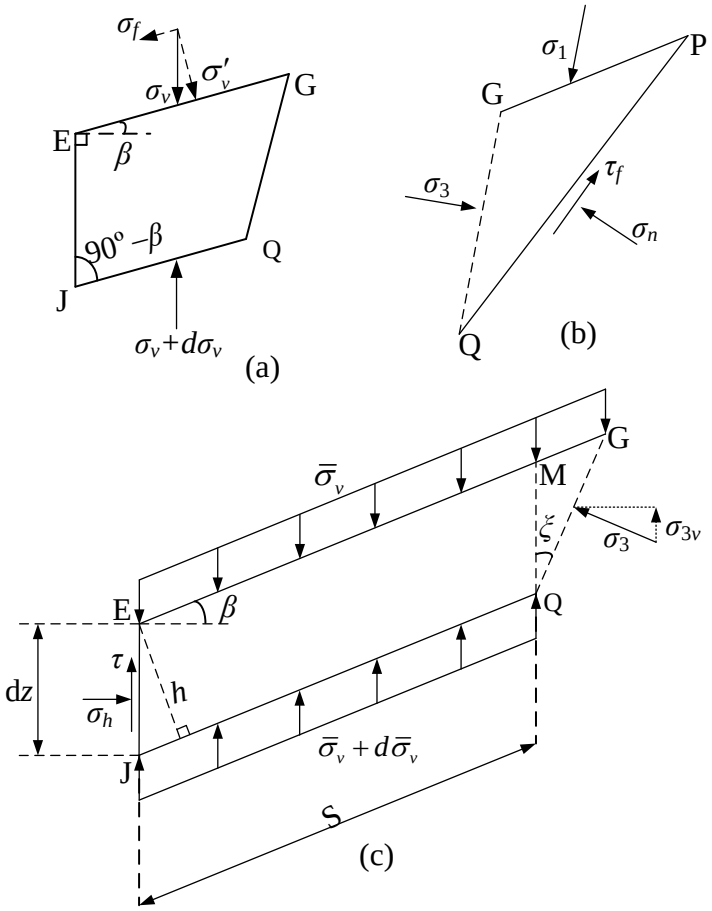

Figure 4.9 Stress on the differential element: (a) major and minor principal stresses applied on the right edge of the differential element; (b) two components of the vertical stress on the differential element; (c) stress on the main part of the differential element

Comparing this result to Eq. (4.10), it is reasonable to express the average vertical stress on the differential element as

$$\bar{\sigma}_v = \frac{1}{\cos\beta}\bar{\sigma}_v' \tag{4.17}$$

Substituting Eq. (4.16) into Eq. (4.17) yields

$$\bar{\sigma}_v = \frac{\cos(\beta+\xi)}{\cos(\theta_w+\xi)\cos\beta}\cos\theta_w(1-\frac{N-1}{3N}\cos^2\theta_w)\sigma_1 \tag{4.18}$$

Using Eq. (4.7) and Eq. (4.18), a ratio K_{an} of the active lateral stress acting on the plane AB to the average vertical stress over the differential element is derived:

$$K_{an} = \frac{\sigma_h}{\bar{\sigma}_v} = \frac{\cos(\theta_w+\xi)\cos\beta}{\cos(\beta+\xi)\cos\theta_w}\cdot\frac{3(N\cos^2\theta_w+\sin^2\theta_w)}{3N-(N-1)\cos^2\theta_w} \tag{4.19}$$

The limit equilibrium equation on the differential element

To evaluate the lateral stress on the line AB (**Figure 4.8(a)**), a detailed analysis of the differential element is required. On the right edge of the differential element (**Figure 4.8(a)**), because the direction of the major principal stress is along the line OG, the major and minor principal stresses are considered to be applied on surfaces GP and GQ, respectively, of the triangular differential element GPQ, which is shown in **Figure 4.9(b)**. In **Figure 4.9(b)**, the triangular element GPQ is shown in an equilibrium state, which allows this triangular element to be ignored when analysing the vertical stress for the entire differential element. In **Figure 4.9(c)**, the minor principal stress σ_3 is loaded on the line GQ, σ_{3v}, which is the vertical component of σ_3 and is expressed as

$$\sigma_{3v} = \sigma_3\sin\xi\frac{\cos\beta}{\cos(\xi+\beta)} \tag{4.20}$$

where ξ is the angle between the normal line OQ and the vertical. Based on the geometry between the slip surface and the major principal plane, ξ is calculated by

$$\begin{aligned}\xi &= \frac{\pi}{4}+\frac{\varphi}{2}-\theta_1 \\ &= \frac{1}{2}(\frac{\pi}{2}-\beta-\cos^{-1}\frac{\sin\beta}{\sin\varphi})\end{aligned} \tag{4.21}$$

In addition, on the left edge of the differential element, the shear stress is

$$\tau = \sigma_h\tan\varphi = \bar{\sigma}_v K_{an}\tan\varphi \tag{4.22}$$

Ignoring the stress loaded on the segment MG and considering the clear interval between the two neighbouring piles, the summation of all vertical forces acting on the main part of the differential element (**Figure 4.9(c)**) gives

$$d\bar{\sigma}_v \cdot SD_2 + \bar{\sigma}_v K_{an} \tan\varphi \cdot D_2 dz - \bar{\sigma}_v K_{an} \tan\beta \cdot D_2 dz + \sigma_3 \sin\xi \frac{\cos\beta}{\cos(\xi+\beta)} dz \cdot D_2 = \gamma S \cdot hD_2 \tag{4.23}$$

Using $\sigma_3 = \sigma_1/N$, Eq. (4.17) and Eq. (4.18), the minor principal stress is

$$\sigma_3 = \frac{K_{an}}{N\cos^2\theta_w + \sin^2\theta_w}\bar{\sigma}_v \tag{4.24}$$

Substituting Eq. (4.24) into Eq. (4.23) and considering that $S = (H\text{-}z)\cos\theta_1/\sin\theta$, $h=\cos\beta\cdot dz$, Eq. (4.23) is solved as

$$\bar{\sigma}_v = \frac{\gamma H\cos\beta}{1-(K_{an}\tan\varphi - K_{an}\tan\beta + m)\frac{\sin\theta}{\cos\theta_1}}\left[(1-\frac{z}{H})^{(K_{an}\tan\varphi - K_{an}\tan\beta+m)\frac{\sin\theta}{\cos\theta_1}} - (1-\frac{z}{H})\right] \tag{4.25}$$

where m is a function of β, given by

$$m = \frac{K_{an}\sin\xi\cos\beta}{(N\cos^2\theta_w + \sin^2\theta_w)\cos(\xi+\beta)} \tag{4.26}$$

where $\theta_w = \pi/4+\varphi/2$. Multiplying Eq. (4.25) by K_{an}, the lateral soil stress on the line AB (**Figure 4.8(a)**) is estimated by

$$\sigma_h = \frac{K_{an}\gamma H\cos\beta}{1-(K_{an}\tan\varphi - K_{an}\tan\beta + m)\frac{\sin\theta}{\cos\theta_1}}\left[(1-\frac{z}{H})^{(K_{an}\tan\varphi - K_{an}\tan\beta+m)\frac{\sin\theta}{\cos\theta_1}} - (1-\frac{z}{H})\right] \tag{4.27}$$

Note that as mentioned previously, the analyses of the active earth pressure σ_h are based on Paik and Salgado's outstanding work (2003), so that Eqs. (4.7) through (4.9) are similar to their research. However, the incline of the soil mass is considered in this paper, which leads to different boundary conditions and different expressions of the

earth pressure σ_h. Moreover, if $\beta = 0$, Eq. (4.27) simplifies to be the same as the equation proposed by Paik and Salgado (2003). This reveals that the equation in Paik and Salgado's research (2003) is the special case of this proposed model.

The squeezing effects between two neighbouring piles

Ito and Matsui (1975) have proposed a plastic deformation model to evaluate the squeezing effects between two neighbouring piles. In this paper, a similar concept is used; all of the assumptions for the soils implied by Ito and Matsui (1975) are also adopted. The soil-pile pressure per unit length of the stabilizing piles in sandy slopes is expressed as

$$p = \frac{\gamma H K_{an} \cos\beta}{1-(K_{an}\tan\varphi - K_{an}\tan\beta + m)\dfrac{\sin\theta}{\cos\theta_1}} \times [(1-\frac{z}{H})^{(K_{an}\tan\varphi - K_{an}\tan\beta + m)\frac{\sin\theta}{\cos\theta_1}} - (1-\frac{z}{H})]$$
$$\times \{D_1(\frac{D_1}{D_2})^{N_1^{1/2}\tan\varphi + N_1 - 1} \times \exp[\frac{D_1 - D_2}{D_2} N_1 \tan\varphi \tan(\frac{\pi}{8} + \frac{\varphi}{4})] - D_2\} \quad (4.28)$$

The details of the derivation of Eq. (4.28) are given in APPENDIX A. In addition, the details of the formulae used to calculate the total lateral force on a pile and the point application of the force are included in APPENDIX B.

4.3 NUMERICAL VALIDATION

A numerical model of the stabilized slope with piles was constructed in the numerical finite difference program FLAC^{3D}. Additionally, SRM was used to analyse the soil-pile pressure on the piles when the slope failed. In the numerical model, the piles were formatted by the intrinsic structure element. The slope model is shown in **Figure 4.10** with a vertical to horizontal gradient of 1:3. Three piles with a length of 9 m were installed in a row in the middle of the slope. The interval between two neighbouring piles was D_1 = 3 m and D_2 = 2.6 m. The width of the model was 9 m. At the bottom boundary of the model mesh, zero displacement was imposed. Stress boundary conditions were imposed at both the uphill and downhill truncation planes. The soil was

modelled using the Mohr-Coulomb model, and the material properties are shown in **Table 4.1**.

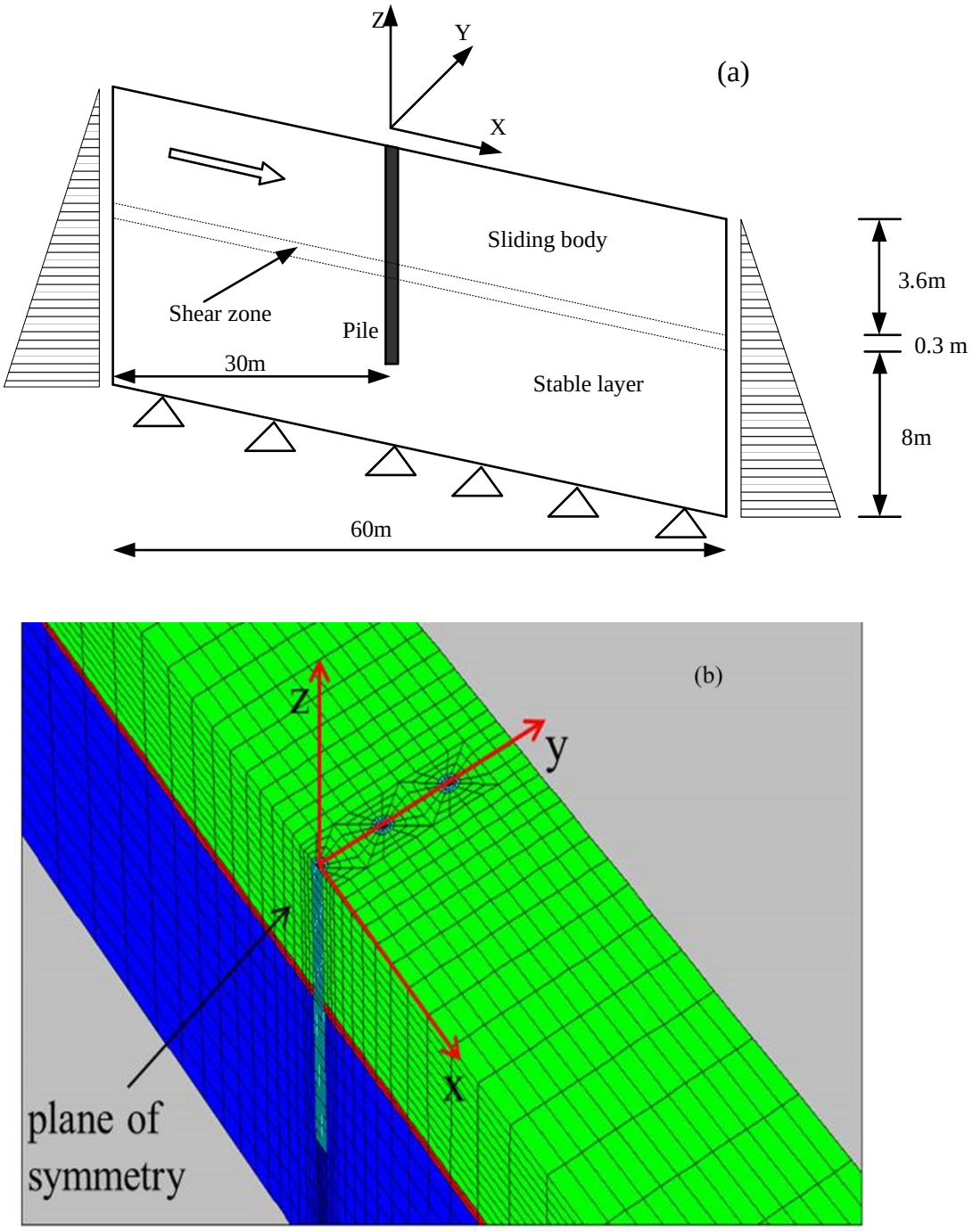

Figure 4.10 The slope model: (a) the two-dimensional schematic mode, (b) three dimensional mesh used in FLAC3D.

Table 4.1 Material properties adopted in the numerical model

	Sliding body	Shear zone	Stable layer	Pile
γ(kN/m^3)	19	19	20	25
E(Pa)	3.8e7	2e7	7.8e7	3e10
μ	0.32	0.32	0.32	0.2
c(kPa)	0	0	100	-
φ(°)	32	30	30	-
ψ(°)	0/2	0	0	0

The model was first brought to equilibrium under gravity loading. Next, a gradual reduction of the shear strength was imposed along the shear zone. To simulate the existence of an accumulation zone, the SRM was not imposed on the downslope final stretch of the shear zone for a length of 10 m. This method of simulating the resistance of the accumulation zone was proposed by Lirer (2012). Incorporating the soil properties, pile geometries and the height of the sliding soil above the shear zone, the soil-pile pressure acting on the piles was calculated by Eq. (4.28), and the results are shown in **Figure 4.10(a)**. For comparison, a prediction using Ito and Matsui's approach (1975) and the results from FLAC^{3D} are included in **Figure 4.10(a)** as well.

Table 4.2 Material properties adopted in Lirer's model

	Sliding body	Shear zone	Stable layer	Pile
γ(kN/m^3)	19	19	19	-
E(Pa)	2e7	1e7	5e7	2e11
μ	0.34	0.34	0.34	0.25
c(kPa)	0	0	1000	14e4
φ(°)	28	25	30	-
ψ(°)	0	0	0	0

A well-instrumented field trial was carried out by Lirer (2012) to study the influence of the row of piles on the local and overall mudslide displacement field, as well as to quantify the shear forces and bending moments within the piles. The experimental findings have been back analysed by numerical simulation (Lirer 2012). In this study, in addition to the numerical model mentioned above, both the observed data of the field trial and the numerical result obtained by Lirer (2012) were used to validate the proposed approach. The material properties used in Lirer's model are shown **in Table 4.2**. The section of Lirer's model was similar to **Figure 4.10**, replacing the dimensions

with 300 m in length, 25 m in height, and 8 m in width. In addition, the slope angle was 11º in Lirer's research. For more details of the field experiment and Lirer's numerical model, see the source reference. The comparison is shown in **Figure 4.11(b)**.

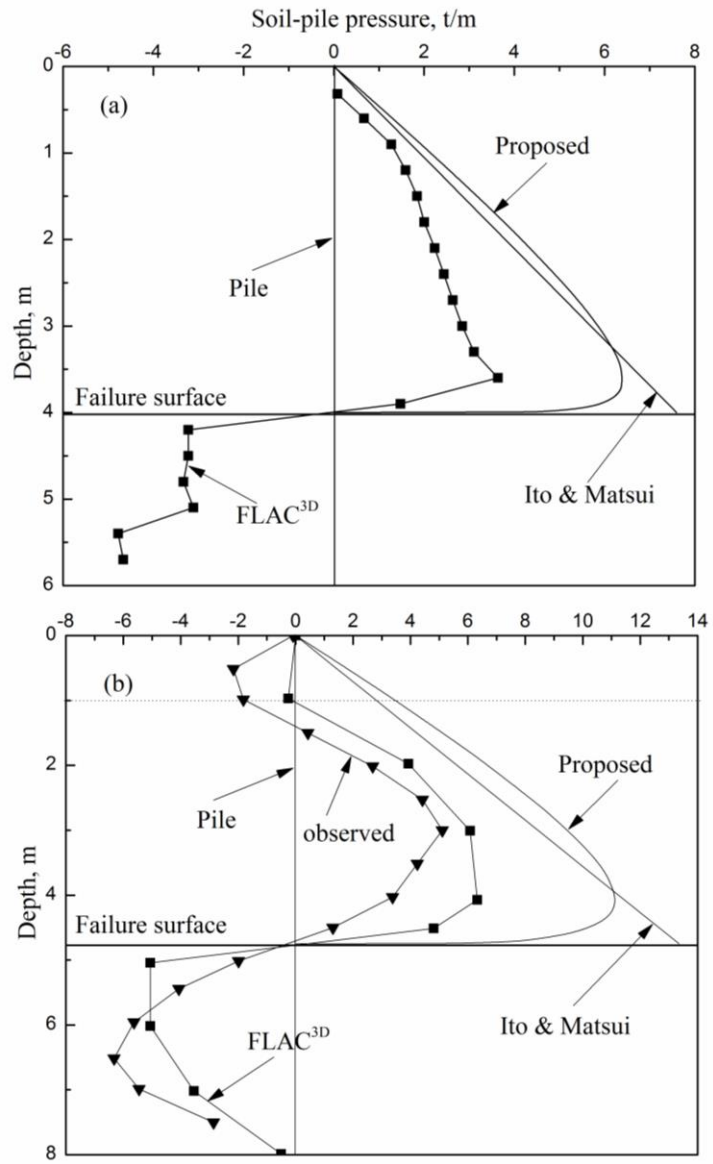

Figure 4.11 Comparison between the numerical results and predictions: (a) slope angle of 18.4º; (b) slope angle of 11º.

Figure 4.10(a) shows the comparison between the numerical simulation results and the prediction of two theoretical methods with a slope angle of 18.4º. **Figure 4.10(b)**

shows the observed data, the numerical results and the theoretical methods estimations with a slope angle of 11º. Both figures reveal that the distribution of the soil-pile pressure computed by the proposed model is nonlinear, while the prediction from Ito and Matsui's approach appears to be linear; however, the orders of magnitude of the two theoretical methods' results are in line with each other. In **Figure 4.10(b)**, the observed data shows that in the upper part of the sliding soil, within approximately 1 m depth, the soil-pile pressure is negative. Such a distribution of the soil-pile pressure on top of the pile is thought to have been obtained as a result of influences of the pile deformation and the non-uniform movements of the sliding soils. However, the prediction of the soil-pile pressure on the top of the pile is positive because the flow mode (Polous 1995) is considered in this proposed model, where the soil displacement is assumed to be larger than the pile deflection and the soil movement is uniform. Ignoring the negative force on the top of the piles, the distribution of the soil-pile pressure on the piles predicted by the proposed approach shows the same trends as the numerical results and the observed data. Particularly in the lower part of the sliding soil, the numerical results and the prediction of the proposed method show that the soil-pile pressure decreases after the first increase, while Ito and Matsui's approach shows linear increases of the soil-pile pressure. **Figure 4.11** reveals that the shape of the distribution of the soil-pile pressure estimated by the proposed model is similar to that of the numerical and observed results, while the values are overestimated. For instance, in **Figure 4.11(a)**, the maximum value provided by the numerical analysis is 3.64 t/m (z = 3.6 m), compared to 6.39 t/m (z = 3.5 m) and 7.6 t/m (z = 4 m) predicted by the proposed model and Ito and Matsui's approach, respectively. In addition, the order of magnitude of the predicted values agrees with that of the numerical and observed results. As presented in **Figure 4.11**, the proposed model allows the assessment of the soil-pile pressure based on soil and pile properties assuming that the soil movement is larger than the pile deflection. However, the limited accuracy of the prediction implies that the proposed model needs to be improved in the future.

A simulation with the piles formatted by a number of zones is carried out. The piles with a diameter of 0.6 m and a centre-to-centre interval of 2 m were installed in the

slope. The stress contour around the stabilizing piles is plotted in **Figure 4.12**. The passive soil wedge behind each pile and the arching zone between neighbouring wedges are apparent. The shape of the soil arching zone in the stress contours from the plane view appears to be sector. However, as mentioned previously, the soil arching zone in the plane is assumed to be a rectangle for the purpose of simplifying the analysis of the active stress.

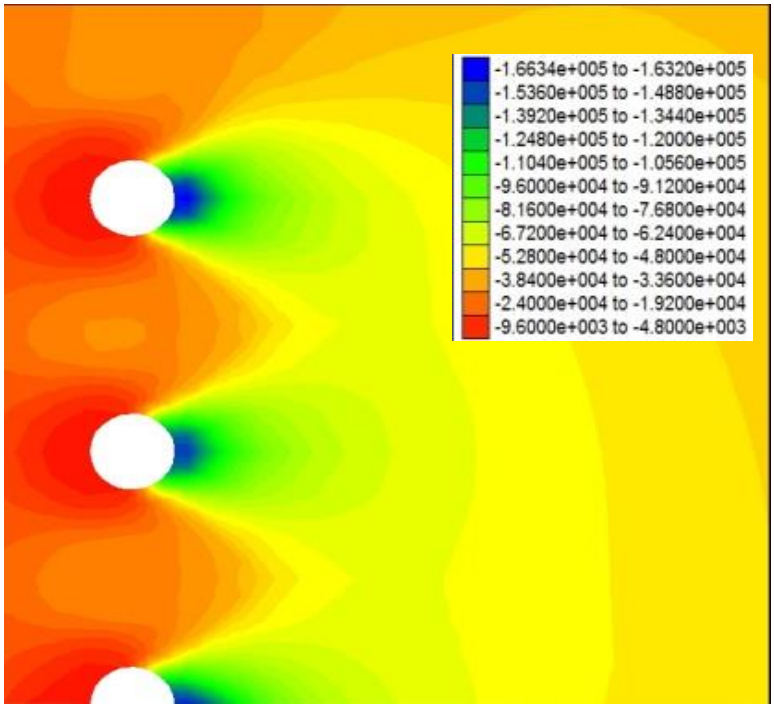

Figure 4.12 The stress contours (σ_{xx}) around the piles.

4.4 PUBLISHED EXPERIMENTAL STUDIES

Chen et al. (1997) have reported on the model tests of pile groups subjected to lateral soil movement. The experimental setup is briefly described below and more details can be found in Polous et al. (1995). The main part of the apparatus consisted of a testing vessel made from a steel sheet and having internal dimensions of 450 mm wide by 565 mm long and 700 mm high. Two vertical steel plates, consisting of two parts hinged at mid-height, were placed across the width inside the box. With a loading system attached to the steel vessel, the upper part of each steel plate could be rotated

simultaneously around its hinge and consequently cause the upper part of the sand to move (Chen et al. 1997). The model piles were made from aluminium tubes and were 1 m in length and 25 mm in diameter with a 1.2 mm wall thickness. On the instrumented piles, ten full bridge circuit strain gauges were placed at 100 mm intervals inside each pile for measuring the bending moments in the pile. Based on the measured bending moments M(z), the shear forces T(z) and the soil-pile pressure per unit thickness p(z) can be computed by successive derivations as follows:

$$T(z) = \frac{dM(z)}{dz} \tag{4.29}$$

$$p(z) = \frac{d^2M(z)}{d^2z} \tag{4.30}$$

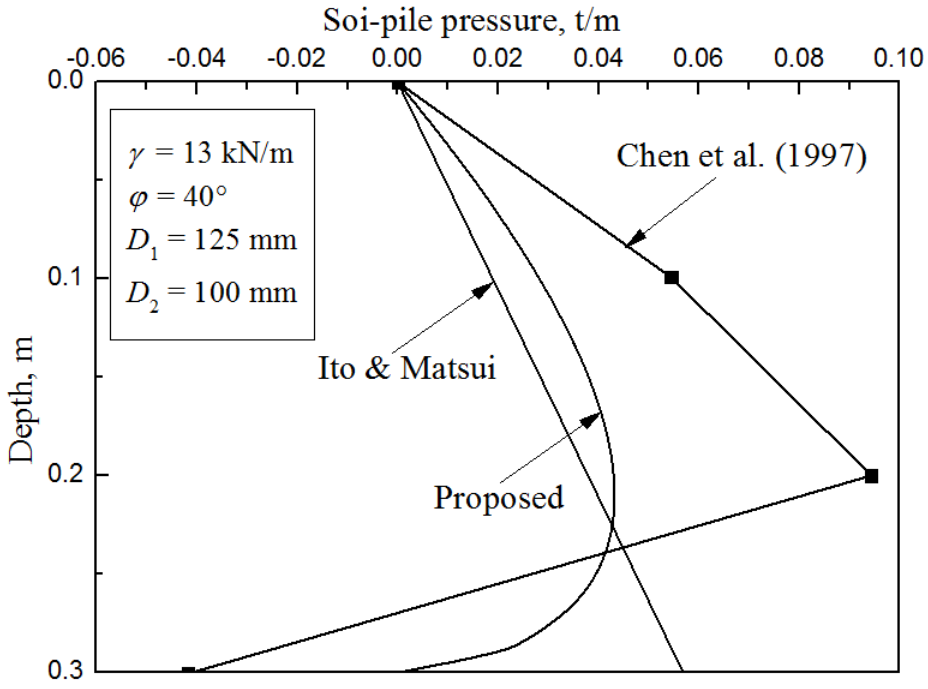

Figure 4.13 Comparison of the prediction and the experimental values based on the research of Chen et al. (1997).

The dry sand used in the model test was calcareous sand taken from Bass Strait, Australia (Chen et al. 1997). The piles were installed into the sand bed in a row. The properties of the sand and the pile spacing are shown in **Figure 4.13**. The soil-pile

pressure per unit length of the pile is calculated based on Eq. (4.30), which implies that the depth of the real failure surface around the piles is approximately 0.3 m. The comparison of the predicted and the experimental values is shown in **Figure 4.13**.

In **Figure 4.13**, the prediction using the proposed approach shows a similar trend of soil-pile pressure distribution as the experimental data. The maximum soil-pile pressure obtained by the experiment is 0.094 t/m at a depth of 0.2 m. Meanwhile, the calculated maximum soil-pile pressure is at the same depth and is 0.043 t/m. **Figure 4.13** shows that the maximum value from the experiment is approximately two times larger than that of the prediction. The sand in the test was subjected to a triangular profile of horizontal movement with depth, while the proposed model is based on a mode of the uniform soil movement. However, compared to Ito and Matsui's approach, the proposed model provides a relatively similar distribution shape of the soil-pile pressure as the experimental data, although some value discrepancy does exist.

Guo and Ghee (2006) conducted the experiment on group effects of piles due to lateral soil movement. The apparatus consisted of a shear box and a loading system that allow different soil movement profiles and vertical loading to be applied simultaneously. The experimental setup is briefly introduced here.

The shear box has internal dimensions of 1 m by 1 m and is 0.8 m in height. The upper moveable part of the box consisted of the desired number of 25 mm thick square laminar aluminium frames to achieve a thickness of L_m (< 400 mm). They were moved together by a rectangular loading block to generate uniform lateral soil movement. The lower fixed section of the box was a timber box 400 mm in height with a number of laminar aluminium frames to achieve a stable sand layer of thickness L_s ($\geq$ 400 mm). For details of the apparatus and tests, see the source reference.

The sand used in the test was oven-dried medium-grained quartz, Queensland sand. The model piles used in the tests were made of aluminium tube, 1200 mm in length and 32 mm in outer diameter with a 1.5 mm wall thickness (Guo and Ghee 2006). Two piles were installed into the fixed timber box. The centre-to-centre "joining" line of the piles

was perpendicular to the direction of the soil movement. The properties of the sand and the pile spacing are shown in **Figure 4.14**.

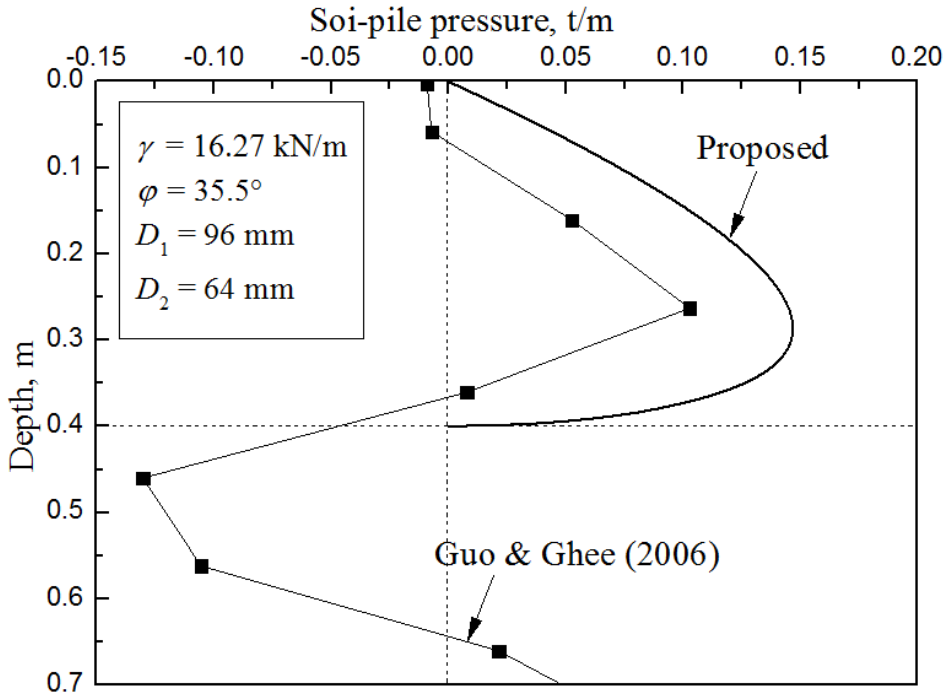

Figure 4.14 Comparison of the prediction and the experimental values based on the research of Guo and Ghee (2006).

Figure 4.14 compares the predicted and the experimental values. Above the failure surface, the soil-pile pressure per unit length of the pile predicted by the proposed approach shows the same distribution as the experimental values. In the upper half of the moveable soil, the predicted soil-pile pressure increases linearly until the increment slows down at the depth of 0.2 m–0.3 m. The maximum soil-pile pressure obtained by the experiment is approximately 0.103 t/m at a depth of 0.26 m, while the predicted maximum value is 0.147 t/m at 0.28 m. **Figure 4.14** indicates that the order of magnitudes of the soil-pile pressure from the prediction and the experiment are in line with each other.

4.5 PARAMETRIC STUDY

A parametric analysis is carried out based on the proposed analytical model to investigate the influence of the slope angle and the internal friction angle on the distribution of the soil-pile pressure per unit length of the piles. Because the proposed model aims to predict the distribution of the soil-pile pressure on stabilizing piles embedded in a semi-infinite slope, which differs from the models designed for horizontal soil grounds, the angle of the semi-infinite slope is considered to be one of the governing factors. In addition, because the internal friction angle of soils is a primary mechanical property, its effect on the soil-pile pressure distribution of the piles also needs to be analysed.

In the following discussion, the soil-pile pressure distribution, the soil-pile pressure on different pile depths, the total lateral force and the point application of the force with respect to different slope angles and different internal friction angles are analysed. Additionally, for comparison, the corresponding values from Ito and Matsui's approach are also calculated.

4.5.1 THE INFLUENCE OF SLOPE ANGLE

Figure 4.15 shows the distribution of the soil-pile pressure along the stabilizing piles when the sliding soil layer is 4 m thick. The soil properties and geometric parameters are also shown in **Figure 4.15**. The soil-pile pressure on the pile has a nonlinear distribution at every slope angle β. Additionally, with a slope angle β varying from 0º to 30º, the order of magnitude of the soil-pile pressure does not change. The maximum soil-pile pressure and the height of the centroid of the soil-pile pressure increases while the slope angle β increases from 0º to 25º. However, when β varies from 25º to 30º, the maximum soil-pile pressure decreases. Furthermore, **Figure 4.15** implies that if the magnitude of the soil-pile pressure on a pile is the only factor considered, ignoring the change of the point application of the force with slope angle, it is reasonable to use a horizontal soil model ($\beta = 0º$) as a simplified way to estimate the response of stabilizing piles in slopes ($\beta \neq 0º$).

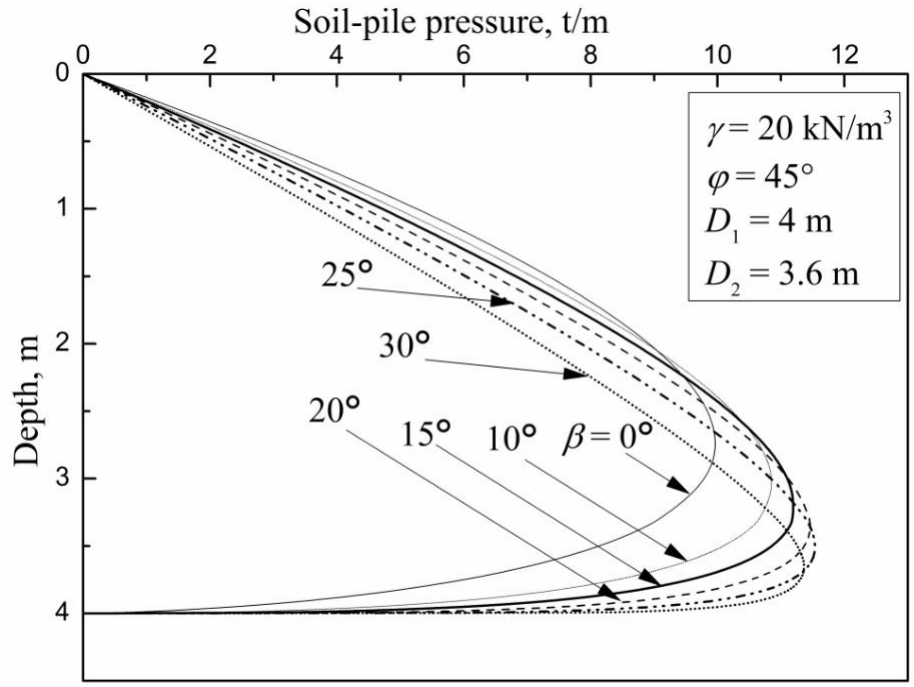

Figure 4.15 Distribution of the soil-pile pressure along the piles with respect to different slope angles.

Figure 4.16 shows the soil-pile pressure at different pile depths with respect to different internal friction angles. The calculated soil-pile pressure denoted by the solid line remains the same while the slope angle varies from 10º to 0º. Moreover, the soil-pile pressures at different depths are almost parallel to each other, which is consistent with the linear distribution of the soil-pile pressure on a pile above the failure surface based on Ito and Matsui's approach. Conversely, the dotted lines intersect with each other, which reveals the nonlinear distribution of the soil-pile pressure along the pile. For instance, in **Figure 4.16(b)**, when the depth z is equal to 1.5 m and 2.5 m, the soil-pile pressures are nearly parallel to each other, which indicates that on the top of the pile, the soil-pile pressure increases linearly. However, when z is 3.95 m (close to the failure surface), the soil-pile pressure is less than that at z = 2.5 m and 3.5 m, which indicates a sharp decrease near the failure surface.

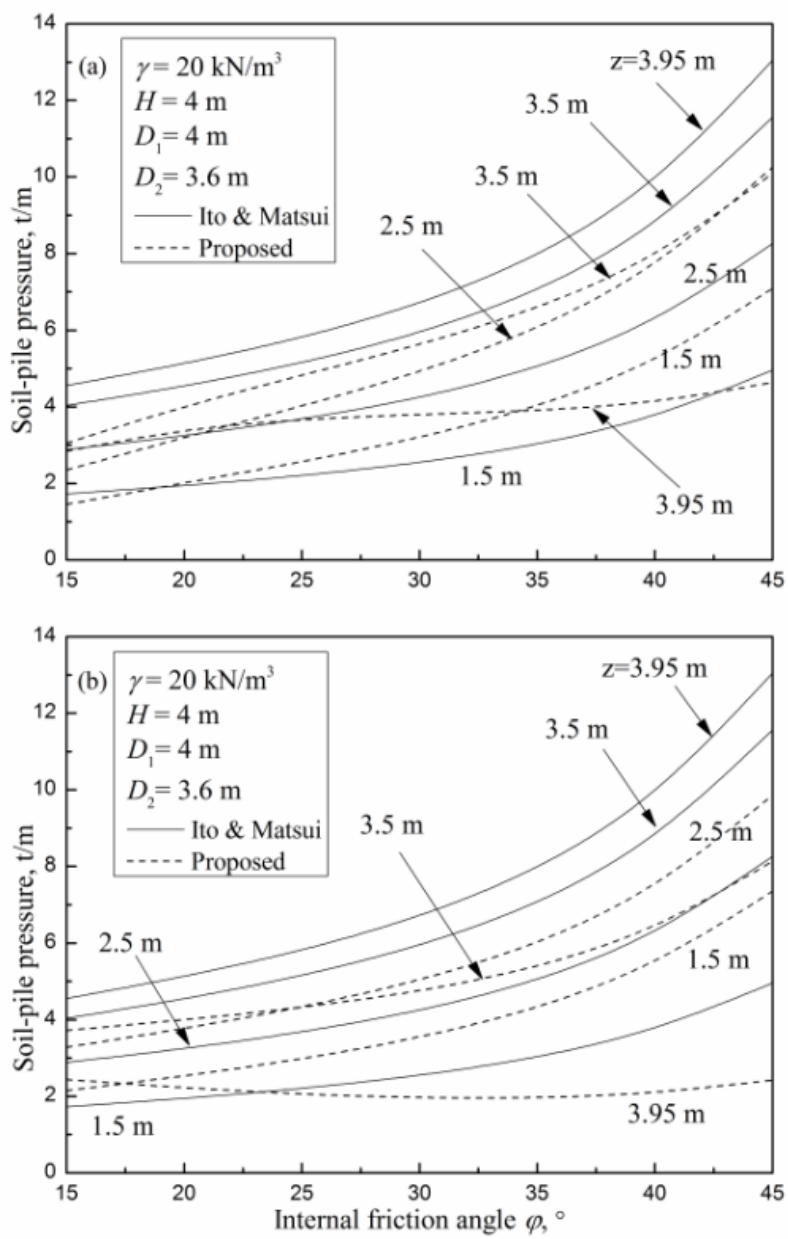

Figure 4.16 Soil-pile pressure at different depths of the pile with respect to different internal friction angles: (a) β = 10º; (b) β = 0º.

In **Figure 4.15**, the area enclosed by the nonlinear distribution of the soil-pile pressure and the vertical coordinate axis represents the total force acting on the pile, which can be obtained by Eq. (B-2). The prediction of the total force as the slope changes is shown in **Figure 4.17**. According to the proposed model, the total force

decreases after the first increase when the slope angle varies from 0º to 30º. As the slope angle increases, the total force increases because of the increase of the component of the gravity along the direction of sliding. However, when the slope angle is approximately equal to the internal friction angle, the total force decreases because of the decrease in slope stability.

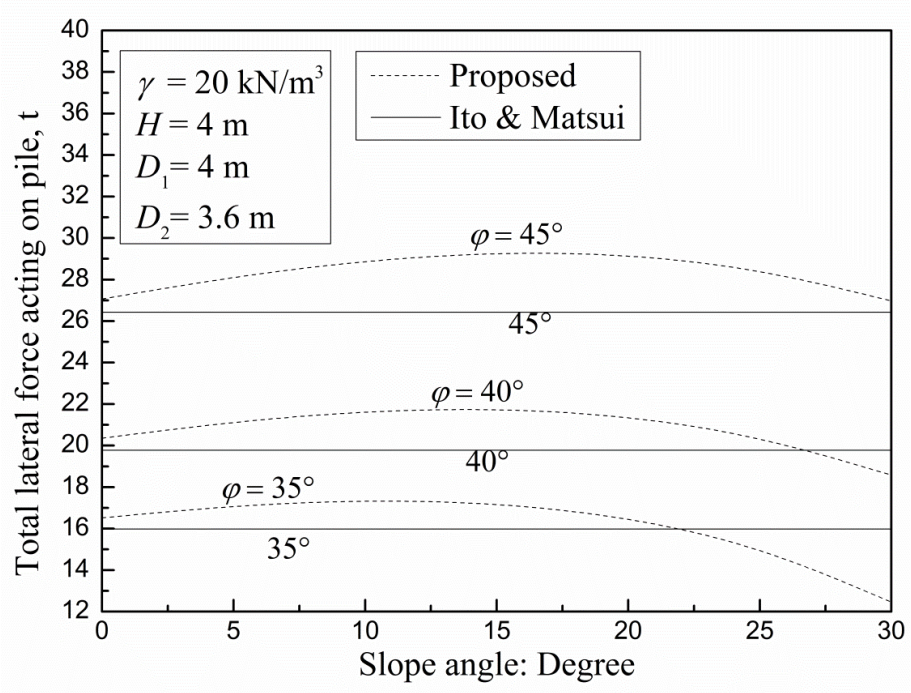

Figure 4.17 Effect of the slope angle on the total force on a pile.

The height of the resultant lateral force versus the slope angle is displayed in **Figure 4.18**. The height of the resultant lateral force predicted by Ito and Matsui's approach remains constant at 0.33H, even if the slope angle varies from 0º to 30º. However, the height of the resultant lateral force is a function of the slope angle and the internal friction angle based on the proposed model (Eq. (B-4)). For instance, when φ = 45º, the height of the resultant lateral force varies from 0.423H to 0.351H when the slope angle changes from 0º to 30º. The height of the resultant lateral force appears to be affected by the soil arching that occurs between two neighbouring piles.

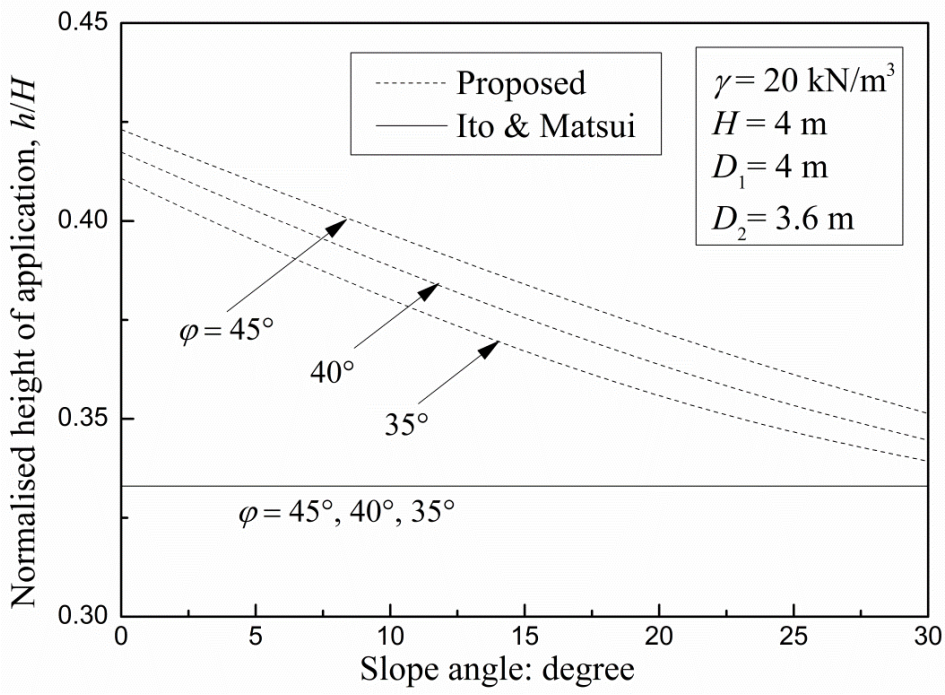

Figure 4.18 Change in the height of the resultant lateral force.

4.5.2 THE INFLUENCE OF THE INTERNAL FRICTION ANGLE

The soil-pile pressure acting on a pile with respect to different internal friction angles is shown in **Figure 4.17**, and the soil properties and geometric parameters are shown in **Figure 4.19**. The distribution shapes of the soil-pile pressure are similar to each other when the internal friction angle varies from 25º to 40º. Additionally, the maximum soil-pile pressure appears in the range of 0.7*H* (2.8 m) to 0.9*H* (3.6 m). The maximum soil-pile pressure for φ = 40º is nearly twice as large as that for φ = 25º. Additionally, the soil-pile pressure on the pile increases when the internal friction angle increases. Compared to **Figure 4.15**, **Figure 4.19** shows that the internal friction angle has a greater effect on the magnitude of the soil-pile pressure on the pile than the slope angle does.

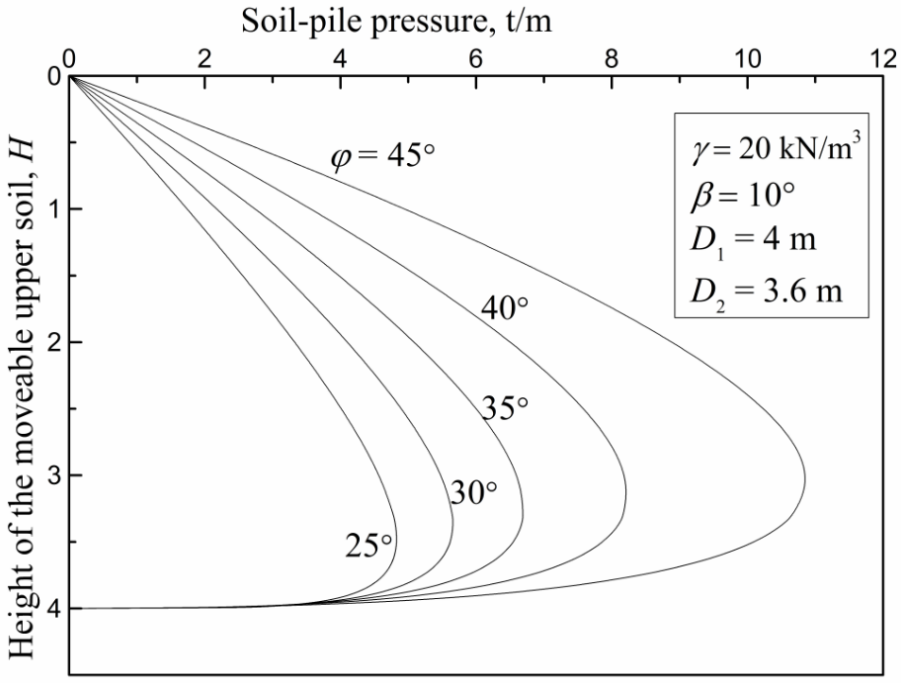

Figure 4.19 Effect of the internal friction angle on the soil-pile pressure acting on a pile.

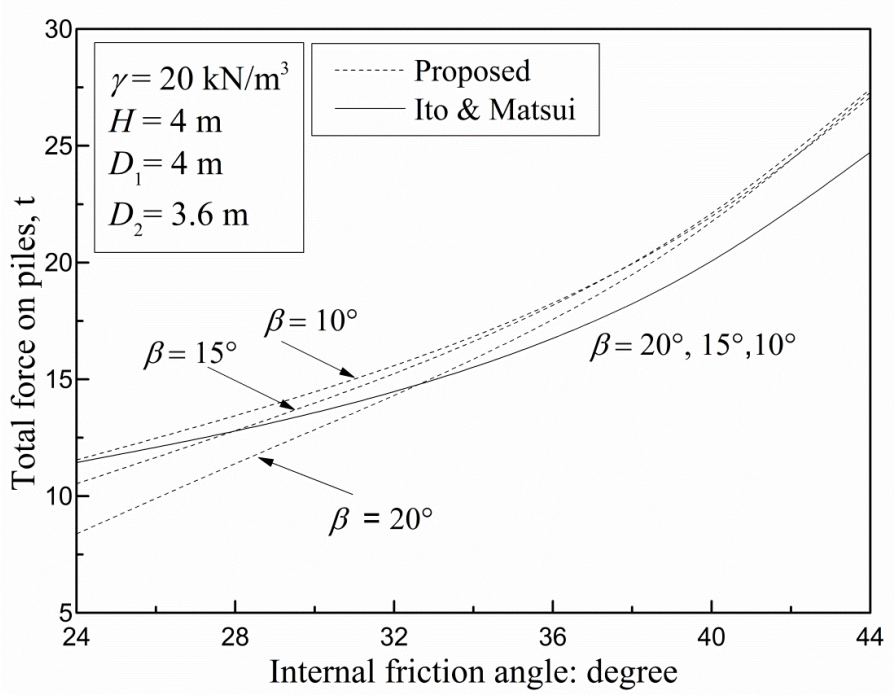

Figure 4.20 Effect of the internal friction angle on the total force on a pile.

Figure 4.20 displays the effect of the internal friction angle on the total force on the

pile. The trends of the total force on the pile from both Ito and Matsui's approach and the proposed model are similar: when the internal friction angle increases, the total force increases. Additionally, when φ = 24º, the dotted line reveals that the closer that the slope angle approximates the internal friction angle, the smaller the total force estimates. Furthermore, when φ is much larger than β, such as when φ = 44º, the total force appears to approach to the same value among the three different slope angles.

Figure 4.21 shows the effect of the internal friction angle on the height of the resultant lateral force. The height of the resultant lateral force remains constant (0.33H) according to Ito and Matsui's approach. However, based on the proposed model, for instance when β = 10º, the height of the resultant lateral force varies from 0.375H to 0.395H as the internal friction angle increases from 24º to 44º. This difference occurs because in Ito and Matsui's approach, Rankine theory is used to estimate the lateral active stress, which leads to the constant height of the resultant lateral force. Conversely, when the effects of soil arching are considered, the proposed model displays a height that changes with respect to different internal friction angles.

Figure 4.22 displays the soil-pile pressure at different pile depths with respect to different slope angles. The internal friction angle φ is 45º. **Figure 4.22** shows the same trends of the distribution of the soil-pile pressure as **Figure 4.16**. Moreover, along the upper half of the pile, the soil-pile pressures calculated by Ito and Matsui's approach are always less than that calculated using the proposed method. Along the lower half of the pile, changeover of the soil-pile pressure occurs.

4.5.3 DISCUSSION

This work attempts to develop a simple method to analyse the soil-pile pressure per unit length of the pile. The model is based on the theory of plastic deformation and is modified by considering both the inclination of the sliding ground and the soil arching effects along the depth of the sliding soil between two neighbouring piles. Comparisons have been made previously between the predicted results and the data from literature, as

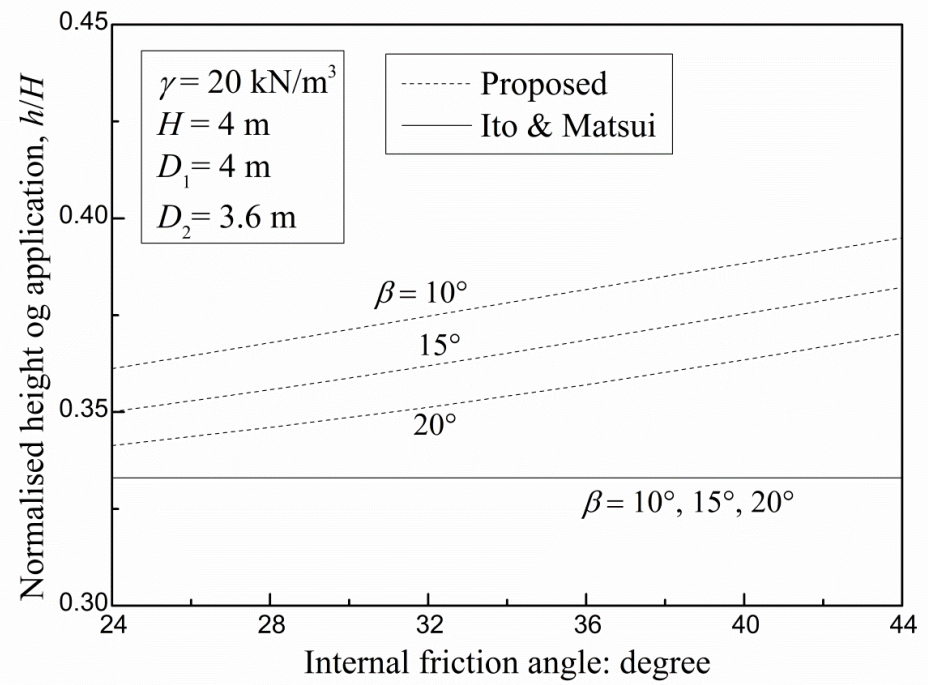

Figure 4.21 Effect of the internal friction angle on the height of the resultant lateral force.

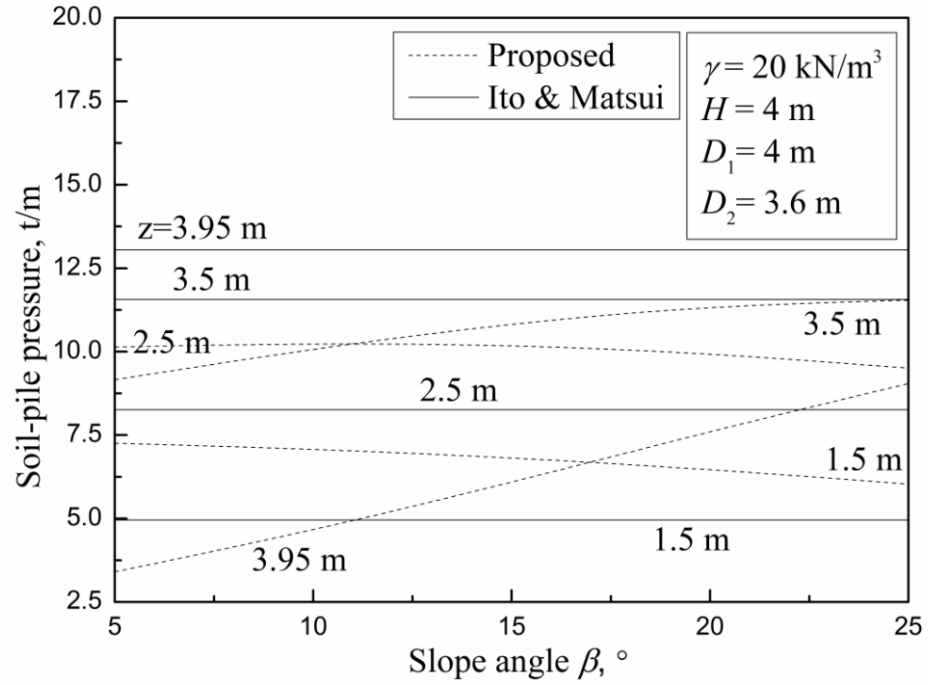

Figure 4.22 Soil-pile pressure at different pile depths with respect to different slope angles.

well as the results from Ito and Matsui (1975). The proposed model performs better than that of Ito and Matsui when predicting the soil-pile pressure per unit length of the pile in the slope. However, the prediction using the proposed method shows limited accuracy. **Figure 4.11**, **Figure 4.13** and **Figure 4.14** show some differences between the predictions and the numerical and experimental results. The assumption of neglecting the deformation of the piles during the movement of the soil is thought to result in the limited prediction. Furthermore, because the "squeezing effects" between two neighbouring piles are adopted from the theory of plastic deformation, the limitation of this theory is inherited as well (Poulos 1995; Lee et al. 1995). The comparison mentioned above indicates that the proposed model is able to describe the distribution of the soil-pile pressure varying with the slope angle and that the trends of the soil-pile pressure are consistent with the literature data, but some differences in the values exist. To improve the prediction results, the model needs further modification in the future.

4.6 CONCLUSION

In this chapter, the interaction between stabilizing piles and granular soil is analysed in a semi-infinite inclined sandy slope. A new theoretical model is proposed to evaluate the soil-pile pressure on stabilizing piles in a sandy slope based on the assumption that the soil displacement exceeds the pile deflection. In the proposed model, the soil arching zone is analysed using stress geometry. The soil arching effects are then considered to estimate the lateral active stress between two piles. Furthermore, the squeezing effects (Ito and Matsui 1975) between two neighbouring piles due to the deformation of the surrounding soils are adopted. To evaluate the proposed model, numerical simulations are implemented by FLAC^{3D}. Comparing the predicted results from the proposed model, Ito and Matsui's approach and the simulations results reveals that Ito and Matsui's approach provides a linear solution for estimating the soil-pile pressure, while a nonlinear solution is obtained from the proposed model, which shows better agreement with the simulation results. In addition, the limited accuracy of the proposed model is also evaluated through comparison to the experimental data from the published literature.

A parametric analysis is also carried out on the slope angle and the internal friction angle. Both the slope angle and internal friction angle affect the distribution of the soil-pile pressure per unit length of the pile; the shape of the distribution of the soil-pile pressure is mainly affected by the slope angle, whereas the internal friction angle has a greater effect on the magnitude of the soil-pile pressure on the pile than the slope angle. Additionally, the height of the resultant lateral force varies with the slope angle and the internal friction angle in the proposed model, whereas it remains constant in Ito and Matsui's approach.

REFERENCES

Ashour M, Norris G, Pilling P. (1998). Lateral loading of a pile in layered soil using the strain wedge model. Journal of Geotechnical and Geoenvironmental Engineering. ASCE 124(4):303–15.

Ashour M, and Norris G. (2000). Modeling lateral soil–pile response based on soil–pile interaction. Journal Geotechnical and Geoenvironmental Engineering ASCE,126(5):420–8.

Ashour M, Pilling P, and Norris G. (2004). Lateral behavior of pile groups in layered soils. Journal Geotechnical and Geoenvironmental Engineering ASCE 130(6):580–92.

Ashour M, and Ardalan H. (2012). Analysis of pile stabilized slopes based on soil-pile interaction. Computers and Geotechnics 39:85-97.

Ausilio E, Conte E, and Dente G. (2001). Stability analysis of slopes reinforced with piles. Computers and Geotechnics 28(8):591–611.

Chen L. T., Poulos H. G., Hull T. S. (1997). Model tests on pile groups subjected to lateral soil movement. Soils and Foundations 37(1): 1-12.

De Beer, E., (1977). Piles subjected to static lateral loads. Proceedings of the 9th International Conference on Soil Mechanics and Foundation Engineering, Special Session No. 10, Tokyo.

Durrani, J.K., Ellis, E.A., Reddish, D.J. (2006). Modelling lateral pile–soil interaction for a row of piles in a frictional soil. 4th International FLAC Symposium Numerical Modelling Geomechanics. 231–238.

Griffiths DV, and Lane PA. (1999). Slope stability analysis by finite elments. Geotechnique, 49(3):387–403.

Galli A, and Prisco C. di. (2013). Displacement-based design procedure for slope-stabilizing piles. Canadian Geotechnical Journal, 50(1):41-53.

Guo W., and Ghee E. (2006). Behavior of Axially Loaded Pile Groups Subjected to Lateral Soil Movement. Foundation Analysis and Design: 174-181.

Hassiotis S, Chameau JL, and Gunaratne M. (1997). Design method for stabilization of slopes with piles. Journal of Geotechnical and Geoenvironmental Engineering., 123(4):314–323.

Kourkoulis R., Gelagoti F., Anastasopoulos I. and G. Gazetas (2011). Slope Stabilizing Piles and Pile-Groups: Parametric Study and Design Insights. Journal of Geotechnical and Geoenvironmental Engineering, ASCE, 137, (7):663-677

Ito, T. and Matsui, T. (1975). Methods to estimate lateral force acting on stabilizing piles. Soils and foundations.,15(4): 21-37.

Ito T, Matsui T, and Hong WP (1981). Design method for stabilizing piles against landslide one row of piles. Soils and Foundations, 21(1):21–37.

Ito T, Matsui T, and Hong WP (1982). Extended design method for multi-row stabilizing piles against landslide. Soils Found., 22(1):1–13.

Lee, C.Y., Hull, T.S., and Poulos, H.G. (1995). Simplified pile-slope stability analysis. Computers and Geotechnics, 17(1): 1-16.

Li X. P., He S. M., Wu, Y. (2010). Seismic Displacement of slopes reinforced with piles. Journal of Geotechnical and Geoenvironmental Engineering, 136(6):880-884.

Liang, R., and Zeng, S. P. (2002). Numerical study of soil arching mechanism in drilled shafts for slopes stabilization. Soils and foundations., 42(2): 83-92.

Lirer S. (2012). Landslide stabilizing piles: Experimental evidences and numerical interpretation. Engineering Geology. 149-150: 70-77.

Martin G R, Chen C Y. (2005). Response of piles due to lateral slope movement. Computers and Structures, 83(8-9): 588-598.

Norris G (1986). Theoretically based BEF laterally loaded pile analysis. In: Proceedings of third international conference on numerical methods in offshore piling. Nantes, France; 361–86.

Paik K. H., and Salgado R. (2003). Estimation of active earth pressure against rigid retaining walls considering arching effects, Geotechnique, 53(7): 643-653.

Poulos, H.G., (1995). Design of reinforcing piles to increase slope stability. Canadian Geotechnical Journal 32(5): 808–818.

Ugai K, and Leshchinsky D. (1995). Three-dimensional limit equilibrium and finite element analysis: a comparison of results. Soils Found 35(4):1–7.

Viggiani, C., (1981). Ultimate lateral loads on piles used to stabilized landslides. Proceedings of 10th International Conference on Soil Mechanics and Foundation Engineers; Stockholm, 3:555-560.

Wang W. L, and Yen B. C. (1974). Soil arching in slopes. Journal of Geotechnical and Geoenvironmental Engineering ASCE, 100(1): 61-79.

Wei, W. B and Cheng, Y. M. (2009): Strength reduction analysis for slope reinforced with one row of piles. Computers and Geotechnics, 36: 1176-1185.

Won J, You K, Jeong S, Kim S (2005). Coupled effects in stability analysis of pile-slope systems. Computers and Geotechnics 32(4):304–15.

Zienkiewicz OC, Humpheson C, Lewis RW. (1975). Associated and non-associated visco-plasticity and plasticity in soil mechanics. Geotechnique, 25(4):671–89

CHAPTER 5

THREE DIMENSIONAL SLOPE REINFORCED WITH PILES SUBJECTED TO SEISMIC LOAD

5.1 INTRODUCTION

Earthquake induced slope failure and landslides occur extensively in the world and frequently result in a tremendous toll of death and destruction of properties. Records show that these kinds of earthquake induced landslides occur most frequently on sloping earth masses. They are observed on the slopes of dams, embankments, and other man made cuts; on the banks of rivers, lakes, reservoirs, and along coasts as well as on mountain slopes (Koh and Chen, 1978). For simplicity, such sloping earth masses will be referred to as 'earth slopes' throughout this chapter.

Earthquake induced permanent displacement or deformation can be estimated by a number of approaches of varying degrees of sophistication. On one hand, stress-deformation methods can be used to model the dynamic deformation of geotechnical structure (e.g. Elgamal et al., 1987; 1990; Prevost et al., 1981; 1985; Seed et al., 1975; Serff et al., 1976). On the other hand, dynamic sliding block methods based on Newmark's original double-integration approach (Newmark, 1965) can also be used to provide a measure of permanent displacement of a potentially sliding block (e.g. Chen 1980; Seed et al. 1969; Seed, 1979; Sarma 1975; Makdisi and Seed, 1978; Constantinou and Gazetas, 1987; Franklin and Chang, 1977; Lin and Whitman, 1983; Ambraseys and Menu, 1988; Ling et al. 1997; Michalowski 1998; Michalowski and You 2000). However, stress-deformation methods with the drawbacks of complex input parameters and high computational requirements only suit for site-specific investigations where high density and high quality soil property data can be obtained. By contrary, dynamic block methods have a

wide range of applications because of its advantages in simple input parameters and relatively low computational complexity.

An analysis based on upper bound limit analysis and Newmark's (1965) analytical procedure was implemented to assess the soil displacement of 2D slopes without reinforcement (Chang et al. 1984). This method was later adopted to analyze the directed sliding mechanism for geosynthetics reinforced soil structures (Ling et al. 1997). Applications of Newmark model to the development of a permanent displacement analysis for geosynthetics reinforced slopes subjected to seismic loads was found in literatures (Ling et al. 1998; Michalowski and You 2000). Additionally, the seismic displacement of slopes reinforced with piles was analyzed by Li et al. (2010). All the literatures mentioned above analyzed two-dimensional (2D) plane-strain failure mechanisms. However, it was commonly acknowledged that 2D solutions were conservative to analyze slope stability compared with 3D solutions (Cavounidis 1987; Gao et al. 2012). In order to provide a more accurate prediction of the displacement of the reinforced slopes subjected to seismic loads, 3D analysis of the slopes should be considered.

Michalowski and Drescher (2009) have proposed a class of 3D admissible rotational failure mechanisms for slopes (referring to Fig. 1), which definitely promotes the application of the limit analysis method in 3D stability of earth slopes (Gao et al. 2012). In this chapter, the 3D failure mechanism is adopted for estimating the permanent displacement of earth slopes reinforced with a row of piles subjected to seismic load. Furthermore, the random iteration method (Hammersley and Handscomb 1964) is used to find the critical failure surface. The kinematic approach of limit analysis is used to calculate the yield acceleration of the reinforced slope. Considering the seismic loads applied on the slope, the cumulative displacement induced by the earthquake is estimated by Newmark model. Therefore, the 3D admissible rotational failure mechanisms for slopes proposed by Michalowski & Drescher (2009) are introduced and summarized in following section.

5.2 REVIEW OF THE 3D ROTATIONAL FAILURE MECHANISMS

5.2.1 KINEMATIC METHOD OF LIMIT ANALYSIS IN SLOPE STABILITY

Limit analysis aims at evaluating bounds on the limit load inducing or resisting failure in structures built of perfectly plastic materials. In application to slopes, the limit load can be identified with forces acting on top of the slope, or the weight of the soil, alternatively, a bound on the geometry of the slope (e.g. height) can be sought if the unit weight of the soil is given. An upper bound on the load or height can be obtained from the kinematic method, the essential element of which is a kinematically admissible velocity field defining the possible mechanism of failure. The term admissible implies that the strain rates resulting from the velocity field must satisfy the flow rule that is associated with the yield condition (strength criterion) of the material, and the velocities satisfy the boundary conditions.

The Mohr-Coulomb criterion is usually used as the yield condition for soils. It contains two material constants: the internal friction angle φ and the cohesion intercept c. This yield condition is used here to describe the strength of overconsolidated soils. Reduced tensile strength can be accounted for by postulating a tension cut-off. Incorporating this modification, however, increases the complexity of admissible kinematic field, and is not considered in this chapter. Because the flow rule associated with the Mohr-Coulomb yield condition (for soils with $\varphi > 0$) predicts large dilation than that measured in experiments, the non-associated flow rule is often postulated. Although no rigorous bounds on limit loads can be found for non-associated materials, an upper bound for an associated material is also an upper bound for a non-associated one with the same yield condition (Radenkovic, 1962), and this warrants the construction of admissible kinematic solutions satisfying the normality flow rule.

In the case of a 3D and continuous deformation field, the flow rule requires the following relationship among the principal strain rates

$$\dot{\varepsilon}_1 + \dot{\varepsilon}_2 + \dot{\varepsilon}_3 + (\dot{\varepsilon}_1 - \dot{\varepsilon}_2 - \dot{\varepsilon}_3)\sin\varphi = 0 \tag{5.1}$$

The velocity fields satisfying equation (5.1) is a difficult task, and no solutions other than axisymmetric have been reported in the literature (Drescher, 1986). The task simplifies greatly if the material is purely cohesive ($\varphi = 0$), the problem is of the plane strain-type ($\dot{\varepsilon}_2 = 0$), or the failure mechanism is of the rigid-block motion type. In the last case, strain rates are zero within the rigid block, and equation (5.1) is satisfied within blocks identically. The blocks are separated as limits of thin material layers undergoing shear and possibly dilation. When equation (5.1) is applied to these thin layers, it leads to the condition where the velocity jump vectors must be inclined at angle φ to the discontinuities: that is

$$[v_n] = [v_t] \tan \varphi \tag{5.2}$$

where $[v_n]$ and $[v_t]$ are the normal and tangential components of the velocity jump vector $[v_i]$ respectively. This requirement is equally mandatory in 2D and 3D mechanisms. Numerous 2D translational and rotational mechanisms have been considered in the literature for $\varphi \geq 0$, when the velocity discontinuities are straight lines (planes) or logarithmic spirals (circles for $\varphi = 0$). Baligh & Azzouz (1975) and Gens et al. (1988) considered 3D rotational mechanisms for purely cohesive soils ($\varphi = 0$), for which any surface of revolution is an admissible velocity discontinuity, and the velocity jump vectors are tangential. These surfaces are generated by rotating a straight line or a curve about an axis of rotation parallel to the slope crest: examples are a cylinder, a cone, and a paraboloid. 3D translational mechanisms with planar surfaces for $\varphi > 0$ can be found in Drescher (1983) and Michalowski (1989). Solutions with three-dimensional blocks undergoing rotation for soils discontinuity surfaces in such mechanisms are neither planar nor surfaces of revolution. A class of admissible rotational mechanisms proposed by Michalowski & Drescher (2009) is discussed in this chapter.

For a kinematically admissible velocity field an upper bound on the limit load (or on the slope height) is determined by equating the rate of work of externally forces W to the rate of work D, dissipated internally in the failure balance, with no forces on the slope surface, the rate of external work is provided only by the weight if the soil, and it

is calculated as an integral of the dot product of the unit weight vector γ_i and the velocity vector v_i. In rotational mechanisms, the work rate of the weight (W_γ) can be calculated as the dot product of the total weight of a block W_i and the velocity of the block centroid v_i^c

$$W_\gamma = \int_V \gamma_i v_i dV = W_i v_i^c \tag{5.3}$$

with V being the volume of the rotating block. In general, the rate of dissipated work D is the sum of dissipation within volume V, D_v, and over the velocity discontinuity surface S_t, D_t. In term of the principal strain rates, the dissipation with the deformation volume can be expressed as

$$D_v = \int_V c \cos\varphi(\dot{\varepsilon}_1 - \dot{\varepsilon}_2 - \dot{\varepsilon}_3) dV \tag{5.4}$$

whereas for velocity discontinuity surface S_t the dissipation rate can be written as

$$\begin{aligned} D_v &= \int_{S_t} c[v_t] dS_t \\ &= \int_{S_t} c \cos\varphi[v] dS_t \end{aligned} \tag{5.5}$$

In the case of planar discontinuities (translational mechanisms) it is relatively simple to calculate D_t. It becomes more involved if the boundaries are complex curvilinear surface, typical of rotational mechanisms. For materials with $\varphi > 0$ an advantageous alternative to the integration given in equation 5.4 and 5.5 is use of the methodology suggested by Michalowski (2001). This methodology is based on the observation that, using the divergence theorem, the sum if volumetric strain rates in the failure mechanism can be expressed as

$$\begin{aligned} \int_V (\dot{\varepsilon}_1 + \dot{\varepsilon}_2 + \dot{\varepsilon}_3) dV &= \int_V \dot{\varepsilon}_{ii} dV = -\int_V \frac{\partial v_i}{\partial x_i} dV \\ &= -\int_S v_i n_i dS \\ &= -\int_{S_t} v_i n_i dS_t - \int_{S_r} v_i n_i dS_r \end{aligned} \tag{5.6}$$

where the surface S bounding the mechanism is divided into kinematic discontinuities S_t

and the remaining part S_r; n_i is the outward unit vector normal to surface S, and v_i is the corresponding velocity. Making use of equation 5.1 and 5.6, equation 5.4 can be written as

$$\begin{aligned} D_V &= c\cot\varphi \int_S v_i n_i dS \\ &= c\cot\varphi \int_{S_t} v_i n_i dS_t + c\cot\varphi \int_{S_r} v_i n_i dS_r \end{aligned} \tag{5.7}$$

At the discontinuity surface St bounding the mechanism $v_i = [v_i]$, and the dot product $v_i n_i = -[vt]\sin\varphi$. Thus the first term on the right-hand side in equation 5.7 is opposite in sign, and equal in magnitude, to the dissipation given in equation 5.5. This implies that the total dissipation in the mechanism $D = D_V + D_t$ on the right-hand side in equation 5.7. in the case of a slope, surface S_r consists of two planar surface (part of the top surface of the slope, and the face of the slope). This procedure is equally valid if the mechanism contains kinematic discontinuities within volume V.

Note that equation 5.7 cannot be used when $\varphi = 0$, and the dissipation must be determined from equation 5.4 and equation 5.5, for continuous deformation and for discontinuities respectively.

In evaluating an upper bound to the height H of a slope at failure (*critical height*), it is convenient to introduce a dimensionless group $\gamma H/c$, and seek its minimum as a function of slope geometry and friction angle φ. The dimensionless group is sometimes referred to as the stability factor, and it is a reciprocal of the stability number $c/\gamma H$, used earlier by Taylor (1937). Alternatively, for a slope of given geometry, it is possible to evaluate the safety factor, defined as

$$F = \frac{c}{c_d} = \frac{\tan\varphi}{\tan\varphi_d} \tag{5.8}$$

where c_d and φ_d are developed soil strength parameters required for the slope to become unstable. In seeking the factor of safety, the energy balance yields $\gamma H/c_d$ as a function of φ_d, and F is determined by using equation 5.8. Finding F is explicit when $\varphi = 0$, and implicit (iterative) otherwise.

5.2.2 THREE DIMENSIONAL ROTATIONAL FAILURE MECHANISMS IN SLOPES

A class of kinematically admissible three-dimensional rotational mechanisms for slopes is discussed in this section. Both frictional/cohesive and purely cohesive soils are considered.

Frictional/cohesive soil (c > 0, φ = 0)

As implied in equation (5.1) and (5.2), the plastic yielding of soils with φ > 0 is accompanied by dilation, and this causes difficulties in constructing kinematically admissible fields. More specifically, in a rigid rotation mechanism (no volume changes within the rotating block), equation (5.2) must be satisfied across the velocity discontinuity surface bounding the rotating volume.

Among the various admissible mechanisms a particular class is suggested now in which all radial cross-sections are circular. An example of such a mechanism is illustrated in **Figure 5.1(a)**. The linear velocity in the mechanism is a function of radius ρ and angle θ, tis direction is perpendicular to radius ρ, and its magnitude is given by

$$v = \omega\rho \tag{5.9}$$

where ω is the angular velocity about the axis passing through point O. The shape of this mechanism resembles that for continuous and translational velocity limit load on rectangular footings.

This mechanism has the shape of a curvilinear cone (a 'horn') with apex angle 2φ. This surface is smooth (with the exception of the apex), and has one symmetry plane, a portion of this surface intersects the slope. The trace if the mechanism (discontinuity surface) on the symmetry plane is described by two log-spirals, AC

$$r = r_0 e^{(\theta-\theta_0)\tan\varphi} \tag{5.10}$$

and A′C′

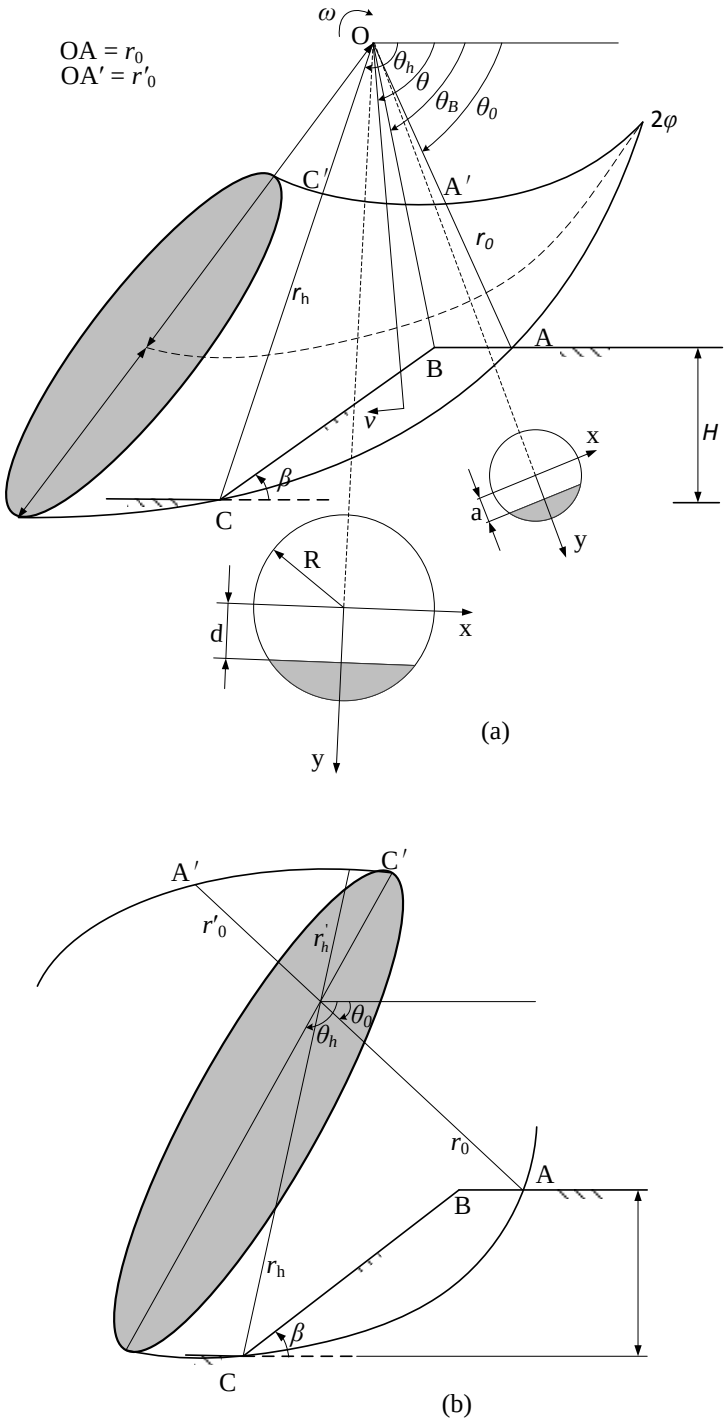

Figure 5.1 Three-dimensional rotational mechanism: (a) a 'horn-shape' surface; (b) alternative mechanism (Michalowski & Drescher (2009)).

$$r' = r_0' e^{-(\theta-\theta_0)\tan\varphi} \tag{5.11}$$

with r_0 and θ_0 as shown in **Figure 5.1(a)**. With the trace of the surface intersecting the toe point C, angle θ_0 and θ_h, and ration r_0'/r_0 uniquely determine the location of the 'horn' surface in the space.

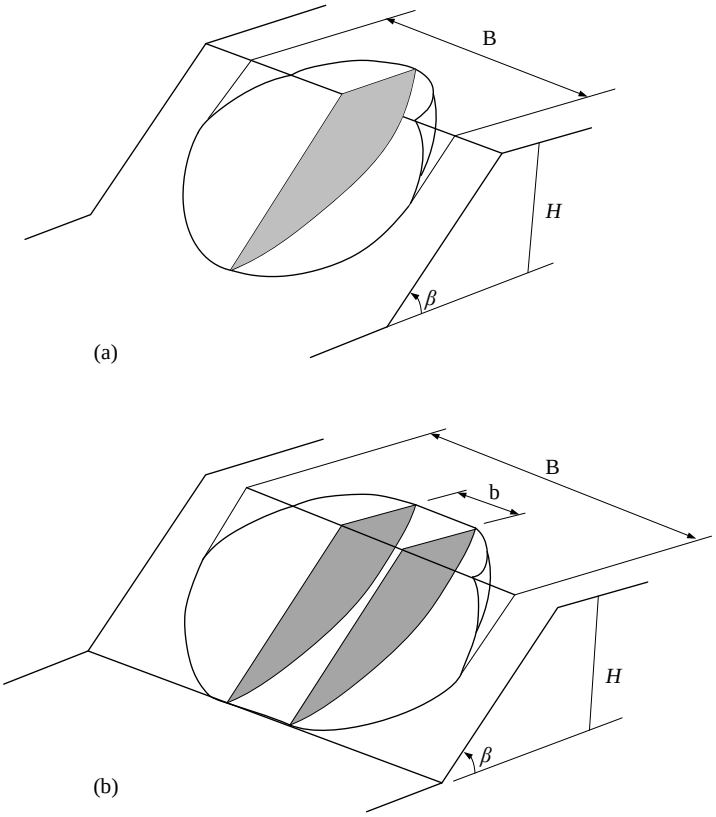

Figure 5.2 (a) Schematic diagram of the 3D mechanism; (b) mechanism with plane insert (Michalowski & Drescher (2009)).

The rate of work of the external forces (weight) and the dissipation rate were calculated from equation 5.3 and the second term of equation 5.7 respectively. The best (lowest) estimate of ratio $\gamma H/c$ was obtained by varying the ratio r_0'/r_0 and angles θ_0 and θ_h.

The shape of this mechanism can be regarded as being generated by rotating a

circle of increasing diameter (shaped area in **Figure 5.1(a)**) about an axis passing through point O outside the circle. If the circle is rotated about an axis passing through the circle, a different mechanism is generated (**Figure 5.1(b)**). This time, however, the upper contour A′C′ of the generated block is defined by the log-spiral

$$r' = -r'_0 e^{(\theta-\theta_0)\tan\varphi} \tag{5.12}$$

Previous experience (e.g. Duncan, 1996) has shown that plane-strain mechanisms of failure are more critical than three-dimensional ones. Calculations for the mechanisms in Figure 1 have shown, however, that the minimum ratio $\gamma H/c$ is found at some finite width of the mechanism, even if no constraints are placed on the width of the slope. To allow transition to plane-strain mechanisms, the three-dimensional failure patterns (**Figure 5.2(a)**) were modified with a 'plane insert', by splitting and separating laterally the halves of the 3D surface, as illustrated in **Figure 5.2(b)**.

Cohesive soil (undrained shear strength $c > 0$, $\varphi = 0$)

Soils are described as purely cohesive when their shear strength is independent of the level of stress. This is typical of clays subjected to undrained conditions. Constructing rotational mechanisms for such soils is relatively simple, as their deformation occurs without volume change (incompressibility). Consequently, any surface of revolution provides an admissible surface of sliding. An example of such a surface is illustrated in **Figure 3(a)**. The rotating block has the shape of a portion of a torus, and it is a special case of the first mechanism considered in the previous section. **Figure 3(b)** shows the case where the axis of rotation passes through the circle generating the surface. These mechanisms can be modified with cylindrical inserts, to ensure transition to a plane

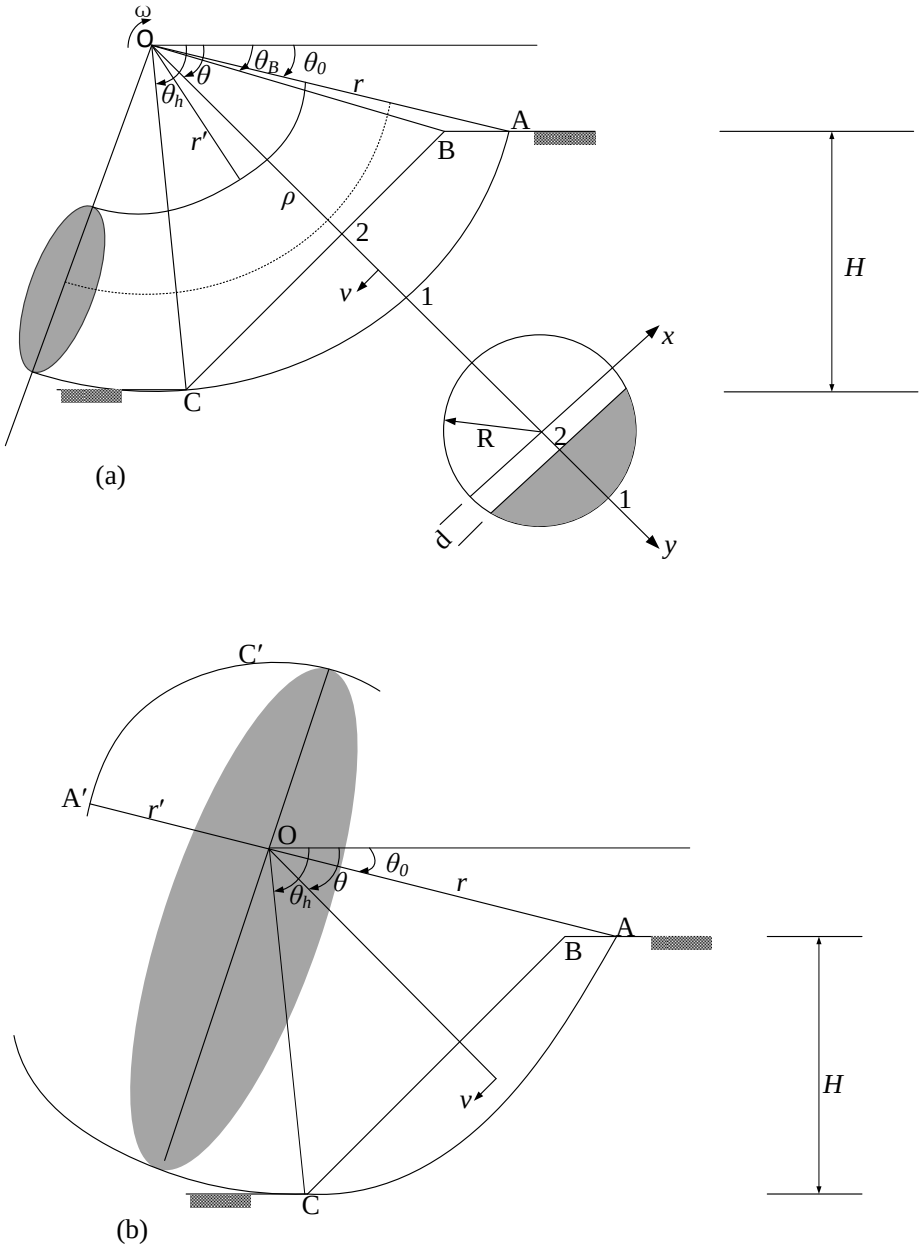

Figure 5.3 Rotational failure mechanisms for soil under undrained conditions (incompressible): (a) torus-type failure surface; (b) alternative mechanism (Michalowski & Drescher (2009)).

mechanism with an increase in the width of the insert. The mechanisms in **Figure 5.3** are particular examples if the mechanisms considered earlier by Baligh & Azzouz

(1975). Baligh & Azzouz considered a cylindrical mechanism in 'cohesive slopes', with a variety of 'ends' to form an overall three-dimensional mechanism. Similar failure patterns were also considered by Gen et al. (1988).

5.3 LIMIT ANALYSIS APPROACH

5.3.1 CRITICAL ACCELERATION FOR 3D SLOPES REINFORCED WITH PILES

In this section, the soil of the slopes is considered to be homogeneous and isotropic. The failure surface in the 3D slopes is assumed to be the curvilinear cone (the shape is similar to a horn), with upper and lower contours defined by log-spirals (Michalowski 2009), as shown in **Figure 5.4**. The shape of the failure surface is smooth, and has one symmetry plane. The trace of the mechanism on the symmetry plane is described by two log-spirals, which is the same to equation 5.10 and 5.11, namely:

AC

$$r = r_0 e^{(\theta-\theta_0)\tan\varphi} \tag{5.10}$$

and A′C′

$$r' = r_0' e^{-(\theta-\theta_0)\tan\varphi} \tag{5.11}$$

where r_0 is the radius of the log spiral with respect to angle θ_0, shown as **Figure 5.4(a)**. φ is the internal friction angle of the soil. The location of the 'horn' for a specified slope is uniquely determined by the angles θ_0, θ_h, the ratio r_0'/ r_0, and the resistance force F_P. The failure soil mass rotates as a rigid body about the point O with angles velocity ω. In order to allow the 3D failure surface to transitioned to plane-strain mechanisms, the 3D failure surface model is split from the symmetry plane (**Figure 5.4(a)**), and then separated laterally into two halves. Additionally, an 'insert plane' with a width of b is inserted (**Figure 5.5(b)**). This 'plane insert' modification has been proposed by Michalowski and Drescher (2009)).

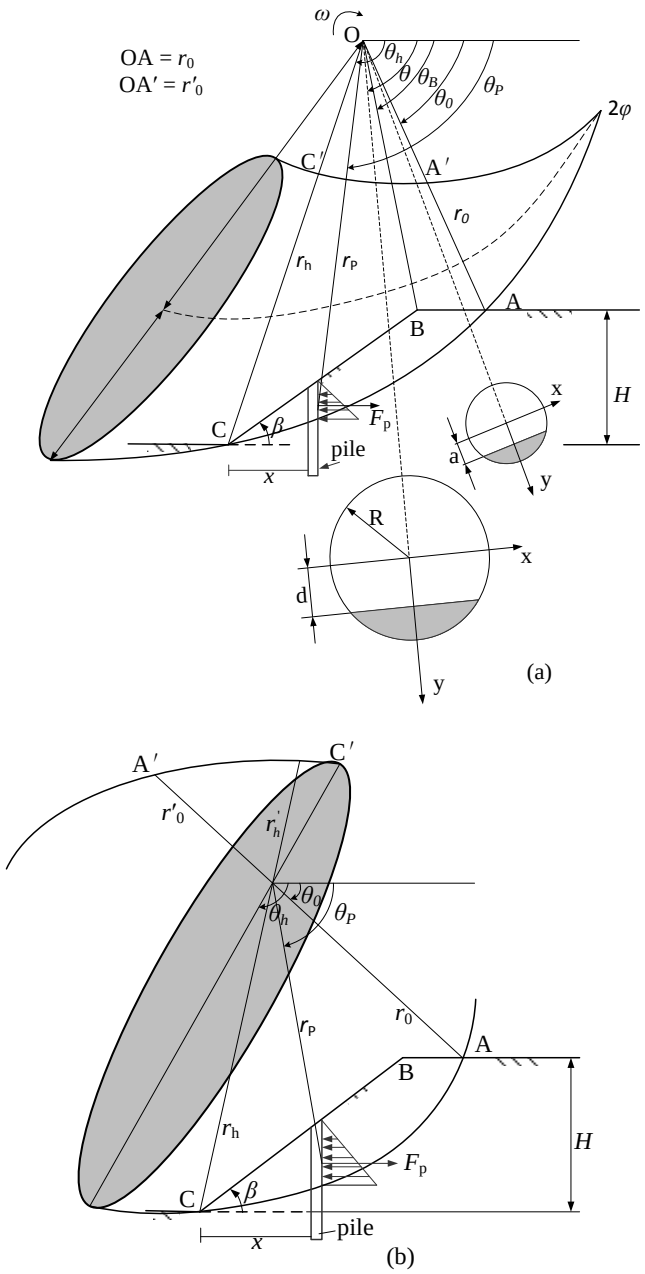

Figure 5.4 Three-dimensional rotational toe-failure mechanism in stabilized slopes: (a) a 'horn-shape' surface; (b) alternative mechanism (based on Michalowski & Drescher, 2009).

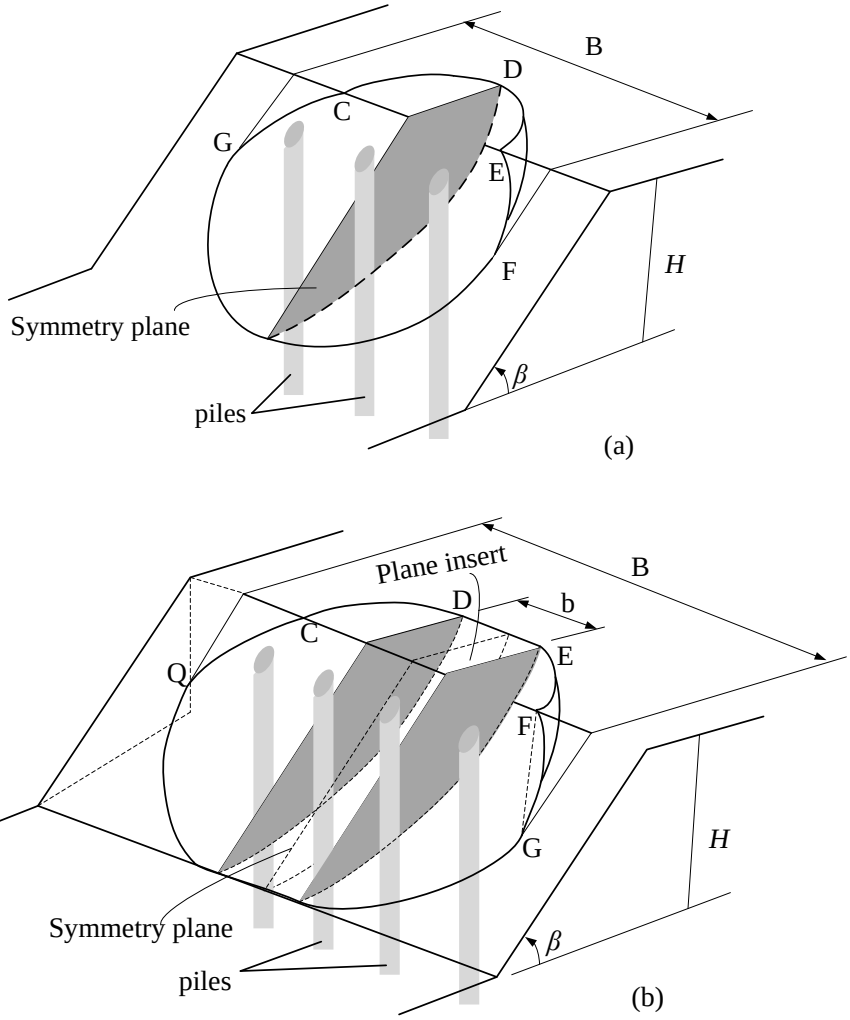

Figure 5.5 Schematic diagram of 3D rotational failure mechanism with limited width B for slopes stabilized with piles: (a) 3D mechanism; (b) mechanism with plane insert (based on Michalowski & Drescher, 2009).

The rate of work of the failing soil weight in block CDEFGQ (Fig. 2(b)) during an incipient rotation about point O is calculated as

$$W_\gamma = W_\gamma^{2D} \cdot b + W_\gamma^{3D} \tag{5.13}$$

where the superscript 3D denotes the work rates for the 3D portion of the failure mechanism (block CDEFG in **Figure 5.5(a)**)and 2D relates to the plane insert (**Figure 5.5(b)**). The details of the equation used in calculations are shown in Appendix.

Once the slope is subjected to horizontal shaking, the rate of the inertial force W_s should be considered in the energy balance equation. According to the pseudo-static approach, the horizontal force acting at the center of gravity is calculated as the product of a seismic coefficient k and the weight of potential failing soil mass to represent the effect of the earthquake loading on the failing soil mass. The rate of external work due to the inertial force can be written as

$$\begin{aligned} W_s &= W_s^{2D} \cdot b + W_s^{3D} \\ &= k\gamma r_0^3 \omega b(f_1^s - f_2^s - f_3^s) + 2\omega\gamma k f_4^s \end{aligned} \tag{5.14}$$

where the superscript has the same meaning with Eq. (5.13), k is the seismic coefficient, γ is the unit weight of the soil. The coefficient $f_1^s \sim f_4^s$ can be found in Appendix.

Considering the resistance provided by the piles, the total energy dissipation rate D is the sum of D_c and D_p, shown below

$$\begin{aligned} D &= D_c + D_P \\ &= D^{2D} \cdot b + D^{3D} + D_P \end{aligned} \tag{5.15}$$

where D_p is the dissipation rate induced by the reinforcement, D_c is the rate of work dissipation caused by soil cohesion. Additionally, the work dissipation rate caused by soil cohesion involves two terms: the 3D term (D^{3D}) and the plain-strain term ($D^{2D} \cdot b$). The soil reinforcement plastically deforms at the slope limit state, and the rate of dissipated work associated with the reinforcement plastic deformation depends on its distribution throughout the unstable soil height. In order to simplify the calculation, the work dissipation rate induced by each pile is assumed to be the same, which equals to that caused by the pile embedded on the symmetry plane of the composite 3D slope (referring to **Figure 5.5(b)**). Based on the distribution of the lateral force acting on piles (referring to **Figure 5.4**) the rate of work dissipation caused by the piles can be calculated as follow

$$D_P = F_p n \sin\theta_p r_p \omega \tag{5.16}$$

in which F_p is the total lateral force exerted on a stabilizing pile due to the plastically deforming layer around the pile; θ_p specifies the position of the stabilizing piles; r_p is the

radius of F_p about the rotation center; n is the number of the piles. In this chapter a trade-off is made that we ignored the vertical resistance. In fact, vertical resistance of the pile is still a scientific challenge in this field, and currently, no method is available (Ito and Matsui 1975; Polous 1995; Ashour and Ardalan 2012; Ausilio, et al. 2001; Li et al. 2010). For this reason, this study majorly focuses on the lateral force acting on piles, and has to ignore the effect of vertical resistance to slope.

To evaluate the force F_p, a theory developed in **Chaper 2** to specifically estimate the pressure acting on the passive piles is chosen in this present work. The lateral force per unit thickness of the layer acting on the pile proposed in their work is integrated here to calculate the force F_p, which is shown as

$$\begin{aligned} p = AcH\{&\frac{(2N_1^{1/2}\tan\varphi+1)}{N_1\tan\varphi}\times[\exp(\frac{D_1-D_2}{D_2}N_1\tan\varphi\tan(\frac{\pi}{8}+\frac{\varphi}{4}))-1] \\ &+\frac{2\tan\varphi+2N_1^{1/2}+N_1^{-1/2}}{N_1^{1/2}\tan\varphi+N_1-1}\}-cHD_1\frac{2\tan\varphi+2N_1^{1/2}+N_1^{-1/2}}{N_1^{1/2}\tan\varphi+N_1-1} \\ &+\int_0^H\sigma_h dz\times[D_1(\frac{D_1}{D_2})^{N_1^{1/2}\tan\varphi+N_1-1}\times\exp(\frac{D_1-D_2}{D_2}N_1\tan\varphi\tan(\frac{\pi}{8}+\frac{\varphi}{4}))-D_2] \end{aligned} \tag{5.17}$$

in which D_1 is the center-to-center interval between neighboring piles; D_2 is the clear interval between neighboring piles; γ is the unit weight of soil; H is the height of the unstable soil layer from ground surface to the failure surface; $N_\varphi = \tan^2(\pi/4+\varphi/2)$; A= $D_1(D_1/D_2)(N_\varphi^{1/2}\tan\varphi+ N_\varphi-1)$. Additionally, when the spacing between two neighboring piles is small, i.e., that the ratio D_2/D_1 is below to about 0.5~0.6, the Eq. (5.17) provides an overestimation of the total force on a pile. A suggestion given by Li et al. (2010) is adopted, which implies that the simple passive earth pressure should be introduced to check the applicability of Eq. (5.17) in using this method.

In order to obtain the critical acceleration coefficient k_c, according to the limit analysis theory, we let the rate of internal work dissipation equal to the external rate of work

$$W_\gamma + W_s = D \tag{5.18}$$

Substituting Eqs. (5.13) ~ (5.16) into Eq. (5.18) yields:

$$k' = \frac{D^{2D} \cdot b + D^{3D} + F_P n \sin\theta_P r_P \omega - (W_\gamma^{2D} \cdot b + W_\gamma^{3D})}{\gamma r_0^3 \omega b (f_1^s - f_2^s - f_3^s) + 2\omega\gamma f_4^s} \tag{5.19}$$

Note that k' is the function of the independent variable parameters θ_0, θ_h, r_0'/r_0, b/H. So the critical acceleration coefficient k_c can be obtained when the parameters θ_0, θ_h, r_0'/r_0, b/H satisfy the following conditions

$$\frac{\partial k'}{\partial \theta_0} = 0\,,\ \frac{\partial k'}{\partial \theta_h} = 0\,,\ \frac{\partial k'}{\partial (r_0'/r_0)} = 0\,,\ \frac{\partial k'}{\partial (b/H)} = 0 \tag{5.20}$$

Eq. (5.17) accompanied with Eq. (5.20) is used to calculate the best value of k'. The minimum value k' equals to k_c. When the seismic coefficient k' reaches its critical value k_c, the slope will be in limit equilibrium, then the work rate balance equation becomes

$$W_\gamma + k_c \gamma r_0^3 \omega b (f_1^s - f_2^s - f_3^s) + 2\omega\gamma k_c f_4^s = D^{2D} \cdot b + D^{3D} + D_P \tag{5.21}$$

5.3.2 ASSESSMENT OF SEISMIC DISPLACEMENT OF SLOPES REINFORCED WITH PILES

When the ground acceleration exceeds the critical value, the block CDEFGQ will start rotating with acceleration. An equation has been proposed to analyze the rotating acceleration by Chang et al. (1984) for the 2D slopes with rotational failure mechanism. This method was adopted by other researchers to analyze the 2D slope reinforced with geosynthetics or piles (Michalowski and You 2000; Ling et al. 1997; Li et al. 2010). Recently, this method was utilized by Nadukuru and Michalowski (2013) to analyze the displacement of 3D slope subjected to seismic loads. In this present work, this approach is developed to 3D slopes reinforced with on row of piles, so balancing the work rate equation yields

$$W_\gamma + k\gamma r_0^3 \omega b (f_1^s - f_2^s - f_3^s) + 2\omega\gamma k f_4^s = D^{2D} \cdot b + D^{3D} + D_P + \omega l^2 \frac{G}{g} \ddot{\theta} \tag{5.22}$$

where G = weight of block CDEFGQ; l = distance from gravity center of CDEFGQ to point O; g = gravity acceleration. The expressions of G and l can be found in Appendix.

The block CDEFGQ stats sliding when the seismic coefficient k exceeds its critical value k_c, simultaneously, the velocity of the failing block increases from 0 to its maximum while the ground acceleration drops down to its critical level. Additionally, according to the Newmark's model (1965), when the ground acceleration decreases to a certain value, the block velocity decreases to 0, but will never be negative. It is because the Newmark's model indicated that the uphill resistance was taken as infinitely large in the calculation. In this situation, the negative velocity or velocity heading uphill is not allowed in this work.

Eq. (5.21) is subtracted from Eq. (5.22), so the rotating acceleration of 3D block CDEFGQ can be written as

$$\ddot{\theta} = (k - k_c) g \frac{\gamma r_0^3 b(f_1^s - f_2^s - f_3^s) + 2\gamma f_4^s}{Gl^2} \tag{5.23}$$

This expression is similar to the ones developed by other researchers for slopes without reinforcement (Chang et al. 1984) and those for 2D slopes reinforced with geosynthetics and piles (Michalowski and You 2000; Li et al. 2010). Comparing with these researches mentioned above, it is clear that both in 2D and 3D conditions, the block accelerations are not directly related to the reinforcement. However, the reinforcement impacts the critical acceleration coefficient k_c and the optimization process of the failure mechanism.

For a selected earthquake, Chang et al. (1984) has proposed a procedure to assess the cumulative displacement of 2D slopes. Michalowski and You (2000) summarized this procedure with an integration equation. In this work, the integration equation is extrapolated from 2D to 3D, which is shown as follow

$$\begin{aligned} u_x &= \int_t \int_t r_h \sin\theta_h \ddot{\theta} dt dt \\ &= C \int_t \int_t g(k - k_c) dt dt \end{aligned} \tag{5.24}$$

where

$$C = \frac{\gamma r_0}{Gl^2} e^{(\theta_h - \theta_0)\tan\varphi} [r_0^3 b(f_1^s - f_2^s - f_3^s) + 2 f_4^s] \sin\theta_h \tag{5.25}$$

Note that Eq. (5.25) contains the 2D seismic coefficient terms $f_1^s \sim f_3^s$, and the 3D term f_4^s. So it is clear that the geometry of the slopes and the failure mechanism are both contained in coefficient *C*. what's more, the properties of the soil and reinforcement have effect on the value of *C* as well. According to Newmark's theory, this integration interval starts from the time at which the first positive motion acceleration occurs (Eq. (5.23) > 0). Simultaneously, the slope starts to slide downhill. Since a small displacement is allowed in this work, the total rotation θ is assumed to be small enough (<0.25rad or 15º) so that the approximation $\tan\theta = \theta$ is valid (Michalowski and You 2000).

5.3.3 MONTE-CARLO METHOD

A random search approach (Hammersley and Handscomb 1964) is used to find the critical acceleration coefficient k_c. This approach has been utilized to find the minimum factor of safety by other researchers (Boutrup and Lovell 1980; Siegel et al. 1981). As mentioned in Chen's research (1992), a large number of searches are needed to obtain sufficiently accurate solution when the random search approach is used. So in this work, 400,000 trials are performed to find k_c for each condition.

For a specified slope (the properties and geometry are given), different upper bound values to the critical height $\gamma H/c$ have been provided by Michalowski and Drescher (2009) and Gao et al. (2012) using different computational approaches for 3D toe-failure mechanism. In order to validate the random search approach, the critical height $\gamma H/c$ computed by the random trials method is compared with the results obtained by the researchers mentioned above. The comparison is shown in **Table 5.1**. It can be seen from **Table 5.1** that the values of the critical height $\gamma H/c$ by this study are between the estimation obtained by Michalowski & Drescher (2009) and Gao et al. (2012). In addition, a comparison is carried out between the critical values of $c_u/\gamma HF$ calculated by random search approach and those presented by others for undrained slopes. It is shown in **Figure 5.6** that the trends of upper-bound results are similar to those of Gens et al. (1998) and (Gao et al. 2013), but the critical values of $c_u/\gamma HF$ obtained by this method are slightly lower than those presented by Gens et al. (1998). This means that the factors of safety

derived from the limit analysis method are higher than those calculated from the limit equilibrium method. The limit equilibrium method leads to conservative estimates of the safety of 3D slopes. This is in good agreement with the research of Gao et al. (2013). Moreover, comparing to the critical seismic acceleration coefficient k_c analyzed by Li et al. (2010) for 2D slopes, under the condition of the parameter B/H = 15 in 3D mechanism, a verification of the accuracy of k_c using the random trials method is shown in **Table 5.2**. Additionally, it is validated that for finding k_c, the transition from the 3D toe-failure mechanism with a 'plane insert' to 2D mechanism is feasible. (This transition has been illustrated by researchers for finding the critical value of $\gamma H/c$, considering that the constraint on the width of the mechanism is sufficiently large, e.g. $B/H > 10$. (Michalowski and Martel (2011); Gao et al. (2013)).

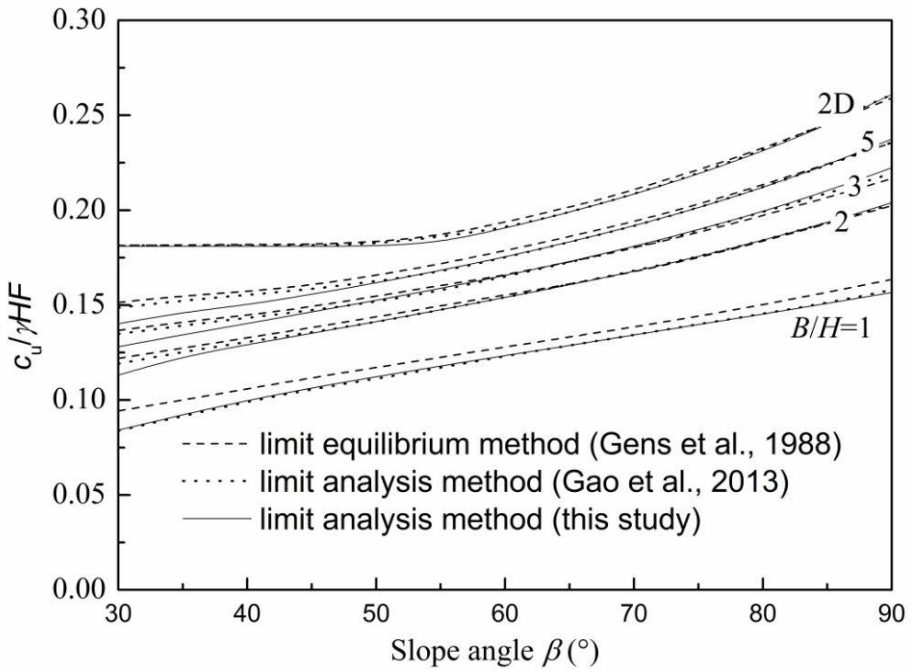

Figure 5.6 Comparisons between the critical values of $c_u/\gamma HF$ obtained by this study and those presented by others for undrained slopes.

Recently, Nadukuru and Michalowski (2013) employed the kinematic theorem of limit analysis and described the 3D displacement of slopes subjected to seismic loads. The critical seismic acceleration coefficient is calculated for 3D slope failures. In this

paper, the critical seismic acceleration coefficients on two example slopes calculated by random iteration method are compared with Nadukuru and Michalowski's results (2013). The characteristics of the two slopes are listed in **Table 5.3** and **Table 5.4** respectively. **Table 5.3** shows that the critical seismic acceleration coefficients obtained by this method are in line with those presented by Nadukuru and Michalowski's results (2013). In addition, it is shown in **Table 5.4** that the calculation from this method is slightly lower than the results of Nadukuru and Michalowski (2013). This implies that a higher estimation of the displacement is obtained by this method when slope B is subjected to seismic loads. All the comparisons shown in **Table 5.1 ~ 5.4** imply that the random iteration method is available in finding the critical seismic acceleration coefficient for 3D toe-failure mechanism.

Table 5.1. Comparison of the results of critical height (vertical slope)

	θ_0: degrees	θ_h: degrees	r_0'/r_0	b/H	$\gamma H/c$		
					Present study	Michalowski & Drescher (2009)	Gao et al. (2012)
$\varphi = 15^o$, $B/H = 1.5$	22.20	59.65	59.65	0.409	6.776	7.124	6.783
$\varphi = 15^o$, $B/H = 5.0$	35.04	60.58	60.58	3.493	5.473	5.504	5.456
$\varphi = 30^o$, $B/H = 0.8$	16.03	62.94	62.94	0.004	12.444	14.368	12.263
$\varphi = 30^o$, $B/H = 3.0$	40.68	66.01	66.01	1.762	7.640	7.974	7.632

Table 5.2 Results of critical seismic acceleration coefficient

	B/H	b/H	k_c	
			Present study	Li et al. (2010)
$\varphi = 10^o$, $c = 23.94$	15	13.10	0.060	0.061
$\varphi = 15^o$, $c = 23.94$	15	12.63	0.165	0.182
$\varphi = 15^o$, $c = 18$	15	12.96	0.087	0.089

Table 5.3 Comparison of the results of critical seismic acceleration coefficient (Slope A)

B/H	θ_0: degrees	θ_h: degrees	r_0'/r_0	b/H	k_c	
					Nadukuru and Michalowski (2013)	Present study
1.5	37.0214	112.4188	0.4917	0.1916	0.27	0.2691
2	36.72	114.4241	0.3954	0.5301	0.21	0.2149
3	35.0919	115.9807	0.3324	1.4702	0.17	0.1704
5	35.5194	115.777	0.1125	3.2229	0.14	0.1403

Slope A with characteristics $\beta = 30^o$, $\varphi = 10^o$, $c = 18.1$ kN/m^2, $\gamma = 17$kN/m^3, $H = 10$ m.

Table 5.4 Comparison of the results of critical seismic acceleration coefficient (Slope B)

B/H	θ_0: degrees	θ_h: degrees	r_0'/r_0	b/H	k_c	
					Nadukuru and Michalowski (2013)	Present study
1.5	45.4282	107.3830	0.3974	0.1072	0.61	0.5706
2	49.5788	106.3162	0.4650	0.5517	0.52	0.4934
3	51.8178	107.5518	0.4512	1.4288	0.44	0.4317
5	52.5442	107.3106	0.3868	3.3483	0.39	0.3912

Slope B with characteristics $\beta = 45^o$, $\varphi = 20^o$, $c = 45$ kN/m^2, $\gamma = 20$ kN/m^3, $H = 15$ m.

5.4 EXAMPLE

Based on the previously derived equations, the displacements of the 3D slopes subjecting to seismic load are analyzed by kinematic theory within the frame of the pseudo-static approach. The slopes with/without reinforcement are considered respectively. Furthermore, the results including the effect of the reinforcement on the 3D conditions and

the plane-strain conditions are compared herein.

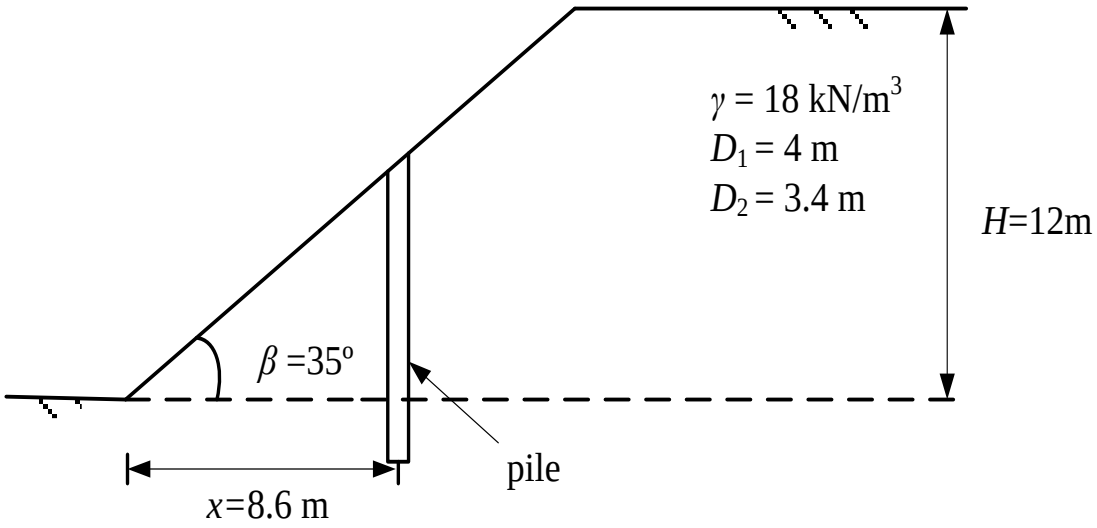

Figure 5.7 The reinforcement in the symmetry plane of the 3D composite slopes.

Figure 5.7 shows the reinforcement in the symmetry plane of the composites 3D slopes. The properties of the slope soil and piles are shown as well. In this section, the displacement of this slope is analyzed when the seismic load is subjected to it. The consideration of progressive block rotation is based on the premise that the rotating angular acceleration in Eq. (5.23) can be integrated over time to yield the angular velocity of the sliding block, and the time integrated velocity will yield the angular displacement (angle of rotation). Seismic acceleration varies during the seismic event, and integration of acceleration is carried out for intervals with positive angular velocity $\dot{\theta}$. For a single interval, the velocity increases rapidly, encounters an inflection point when the acceleration is at its peak, and reaches its maximum when the ground acceleration drops down to the yield level. Past that point, the angular velocity of the sliding block will start decreasing, to reach zero at some level of ground acceleration below the yield acceleration (further decreases in ground acceleration will produce the reversal of the inertial force, but the acceleration causing upward failure in slope is uncommon). The time integral of the angular velocity yields the angular displacement,

and the total angular displacement is the sum of displacements calculated during interval when the velocity was not zero (Nadukuru and Michalowski (2013)).

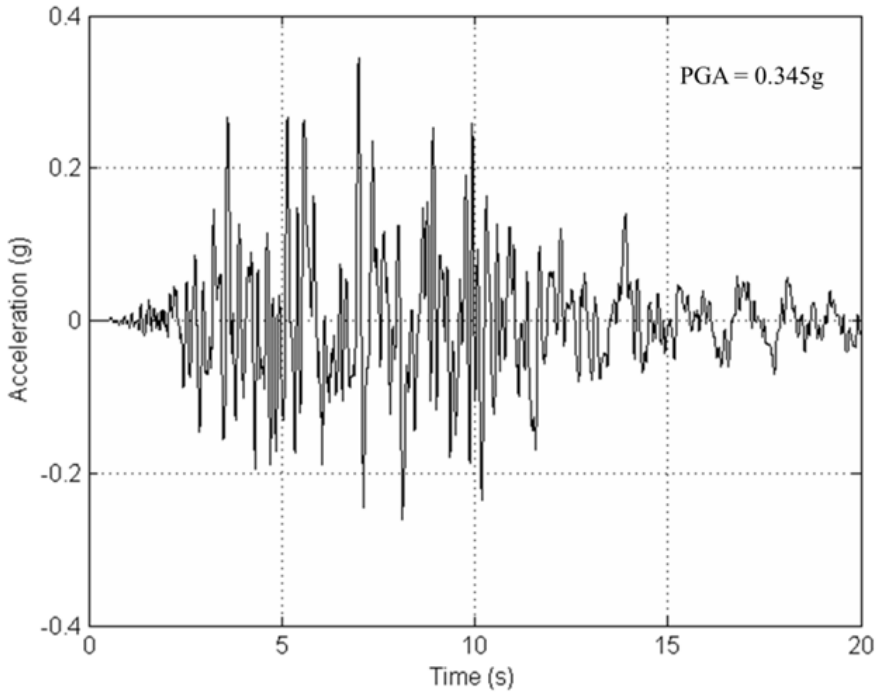

Figure 5.8 Acceleration Records of Kobe Earthquake (Kakogawa Station) with PGA = 0.345 g, $D_{5\text{-}95}$ = 13.2 s.

Figures. 5.8~5.10 show the earthquake records used for calculating the displacements of slopes ($D_{5–95}$ is the duration, in seconds, of the motion from 5% to 95% of Arias intensity). **Figure 5.8** is the Kobe earthquake record (Kakogawa station) with PGA = 0.345 g. **Figure 5.9** is the Imperial Valley-06 earthquake records (Aeropuerto Mexicali station) with PGA = 0.307 g. The constant time interval of each earthquake record mentioned above is 0.01 second. **Figure 5.10** is the Parkfield-02 earthquake record (Parkfield-Cholame 2WA station) with PGA = 0.373 g. and a constant time interval of 0.005 second. These three earthquake records are used one after another to estimate the performance of the slopes (with or without reinforcement) subjected to seismic loads. The results are listed in **Table 5.5**.

Table 5.5 indicates that for the same soil properties, the constraint of the width

significantly affects the results of the critical acceleration coefficient and seismic displacement. When B/H = 2, and φ = 15º, the seismic forces of Kobe earthquake, Imperial Valley-06 Earthquake and Parkfield-02 Earthquake are exerted on the slope, resulting in the displacement of 0.25 cm, 0 cm, and 3.33 cm respectively. So for this small-displacement slope, there is no need to embed any pile to enhance the stability. When B/H = 5, the number of the piles n is designed differently for different internal friction angle. For example, when φ = 15º (B/H = 5), the displacement of the slope (without reinforcement) induced by Parkfield-02 Earthquake is only 16.78 cm, so the width of the 'plane insert' is considered when the number of the piles is determined (12 piles with the interval D_1 =4 m can roughly cover the width of 'plane insert' b, which is about 42 m). However when φ = 10º (B/H = 5), the displacement of the slope is quite large (83.21 cm), which implies that the total width B should be taken into account (16 piles are embedded to cover the total width). When B/H = 10, the 2D failure mechanism is considered to be acting on the slopes. **Figures 5.11** and **5.12** display the response of the example slope (with/ without reinforcement) subjected to Kobe Earthquake. It is clear that the displacement of the slope induced by the seismic load is significantly reduced by the stabilizing piles. Furthermore, using the composite 3D mechanism, it is able to calculate the different numbers of the needed piles for stabilizing slopes based on different soil properties.

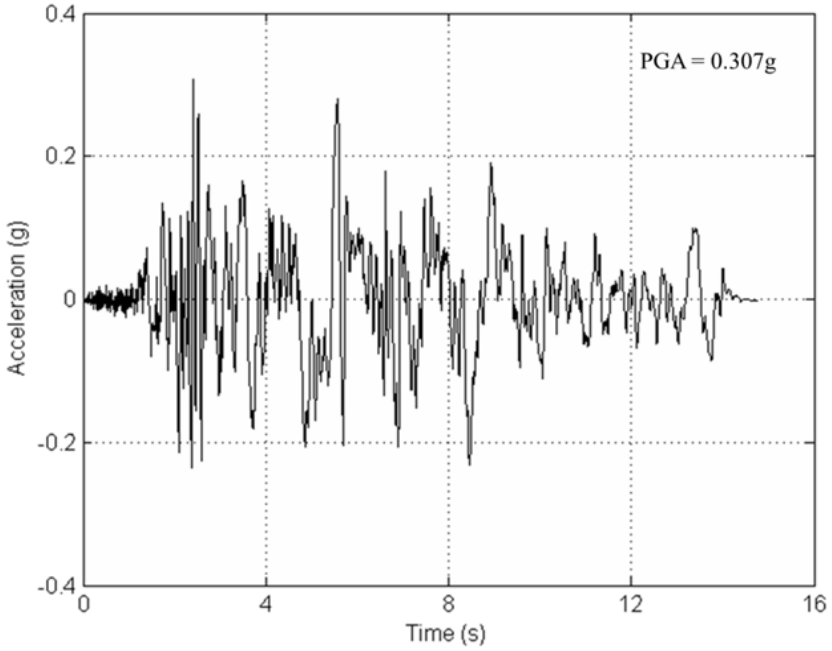

Figure 5.9 Acceleration Records of Imperial Valley-06 Earthquake (Aeropuerto Mexicali Station) with PGA = 0.307 g, $D_{5\text{-}95}$ = 9.8 s.

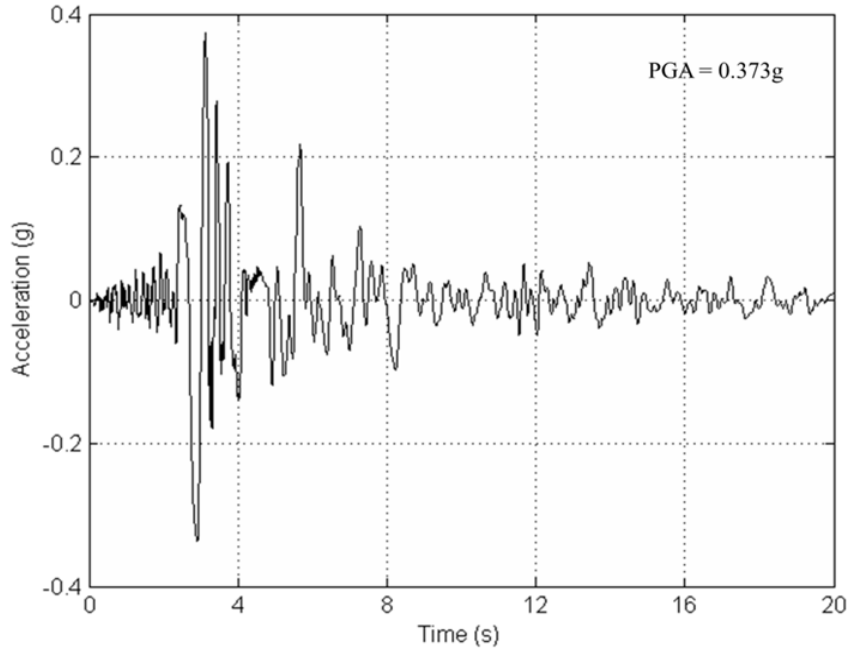

Figure 5.10 Acceleration Records of Parkfield-02, CA Earthquake (Parkfield - Cholame 2WA Station) with PGA = 0.373 g, $D_{5\text{-}95}$ = 7.0 s.

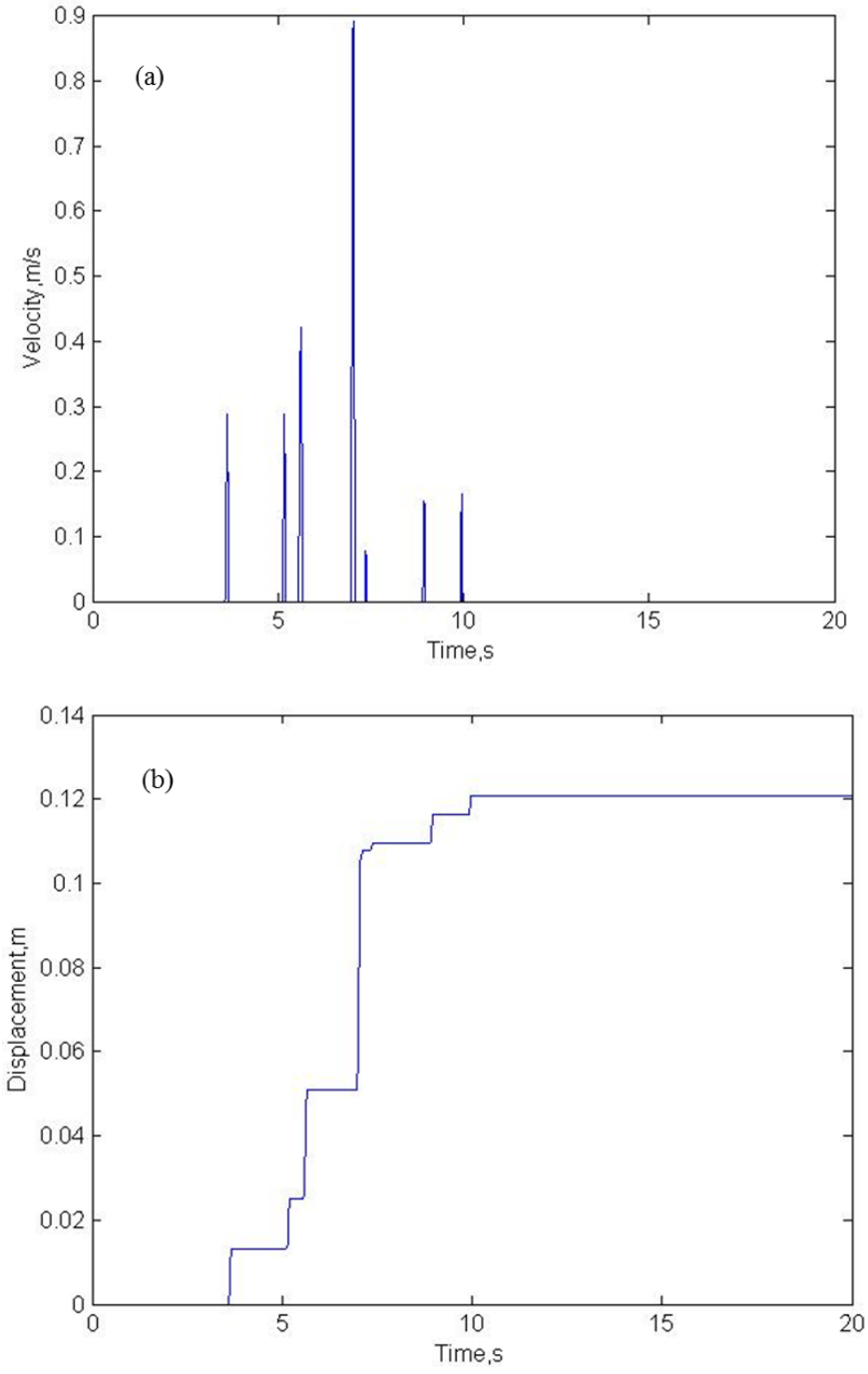

Figure 5.11 The response of example slope (γ = 18kN/m^3, c = 24 kPa, φ = 15º, b/H = 10) without reinforcement subjected to Kobe Earthquake: (a) the velocity of the failure block, (b) the irreversible displacement.

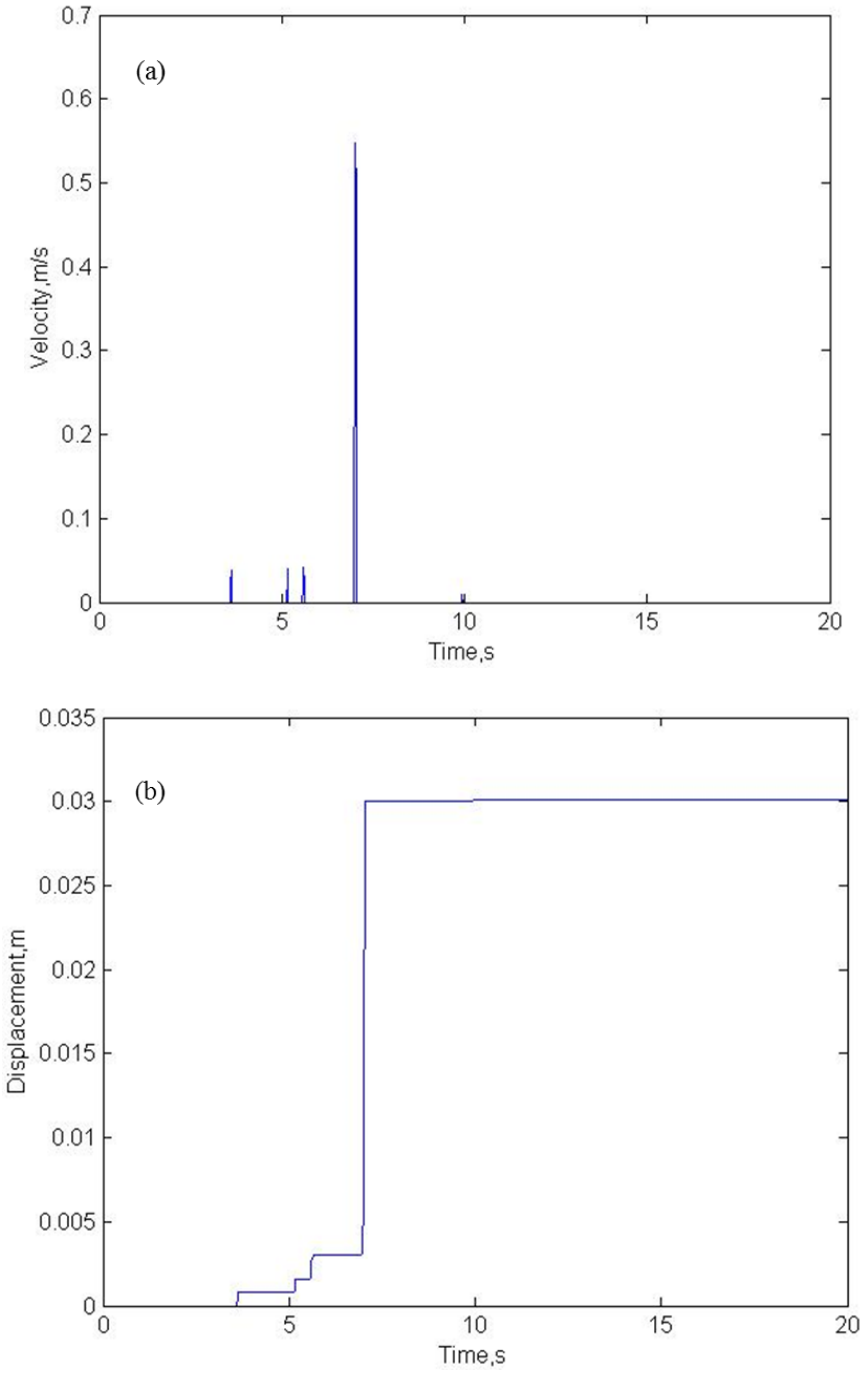

Figure 5.12 The response of example slope (γ = 18kN/m^3, c = 24 kPa, φ = 15º, b/H = 10) stabilized with one row of 24 piles subjected to Kobe Earthquake: (a) the velocity of the failure block, (b) the irreversible displacement.

5.5 CONCLUSIONS

This model is an extension and modification of the 3D rotational failure mechanisms and the pseudo-static slope analysis. It should be viewed as a useful estimating approach for the displacement of the reinforced slopes with constraint on the width. In addition, since a 'plane insert' with width b is inserted into the 3D mechanism, it is possible to assess the displacement on the condition of 2D mechanism when b is sufficient large. In this chapter, the following two phase of the work are presented: (1) the determination of the yield acceleration and its corresponding failure mechanism (especially the width of the 'plane insert' is determined) in 3D mechanism; (2) the estimation of the seismic displacement of the 3D reinforced slope.

In order to calculate the yield acceleration, the limit analysis theory is utilized for the first phase. Additionally, the proposed approaches in Chapter 3 and 4 are introduced to evaluate the lateral force and work dissipation of the piles. Based on the calculated yield acceleration and its corresponding failure mechanism, Newmark's analytical procedure is employed to estimate the soil displacement of the earth slope which is subjected to design earthquakes. Furthermore, the random trials method is used for the computational proceeding, which is validated by the literature data. A simple example is given herein, and the findings are: the yield accelerations of 2D mechanism (B/H = 10) are less than that in 3D mechanism with the same soil properties; the displacements in 2D mechanism are much large than that in 3D conditions; it is possible to reduce the seismic displacement of the soil slopes using stabilizing piles both in 2D and 3D conditions.

Table 5.5 Numerical results of the critical coefficient and seismic displacement for different soil properties

		Without piles						With piles					
B/*H*		2		5		10		2		5		10	
c (kPa)		24		24		24		24		24		24	
φ (degree)		15	10	15	10	15	10	15	10	15	10	15	10
b/*H*		0.646	0.633	3.442	3.547	8.184	8.317	-	0.710	3.532	3.571	8.317	8.295
k_c		0.307	0.199	0.2278	0.125	0.208	0.105	0.307	0.244	0.275	0.184	0.252	0.159
n		-	-	-	-	-	-	-	4	12	16	24	30
u (cm)	Earthquake 1[a]	0.25	14.5	6.24	80.69	12.09	31.03	0.25	3.44	1.26	28.74	3.01	50.03
	Earthquake 2[b]	0	5.05	2.04	35.09	4.17	59.24	0	0.93	0.071	10.34	0.67	18.95
	Earthquake 3[c]	3.33	24.07	16.78	83.21	22.51	119.68	3.33	13.32	8.45	41.46	14	61.92

Example slope characteristics: $\beta = 35^o$, $\gamma = 18$ kN/m^3, $H = 12$ m.

a: Kobe Earthquake (Kakogawa station) with PGA = 0.345 g, constant time interval of 0.01 second.

b: Imperial Valley-06 Earthquake (Aeropuerto Mexicali station) with PGA = 0.307 g, constant time interval of 0.01 second.

c: Parkfield-02 Earthquake (Parkfield-Cholame 2WA station) with PGA = 0.373 g, constant time interval of 0.005 second.

REFERENCES

1. Ambraseys, N., and Menu, J. 1988. Earthquake - induced ground displacements. Earthquake Engineering & Structural Dynamics, 16(7): 985-1006.
2. Ashour M., Ardalan H. (2012). Analysis of pile stabilized slopes based on soil-pile interaction. Computers and Geotechnics, 39:85-97.
3. Ausilio E., Conte E., and Dente G. (2001). Stability analysis of slopes reinforced with piles. Computers and Geotechnics, 28 (8): 591-611.
4. Boutrup, AW., and Lovell, C.W. (1980). Search technique in slope stability analysis. Engineering Geology, 16(1-2):51-61.
5. Chang, C. J., Chen, W. F., and Yao, J. T. P. (1984). Seismic displacements in slopes by limit analysis. Journal of Geotechnical and Geoenvironmental Engineering, ASCE, 110(7): 860–874.
6. Chen, W. F., (1980). Plasticity in Soil Mechanics and Landslides. Journal of the Engineering Mechanics Division, ASCE, 106(3): 443-464.
7. Chen, Z.Y., (1992). Random trials used in determining global minimum factors of safety of slopes. Canadian Geotechnical Journal, 29, 225-233.
8. Constantinou, M., and Gazetas, G. 1987. Probabilistic seismic sliding deformations of earth dams and slopes. In: Probabilistic Mechanics and Structural Reliability, ASCE, pp: 318-321.
9. Elgamal, A.-W.M., Abdel-Ghaffar, A.M., and Prevost, J.-H. 1987. 2-D elastoplastic seismic shear response of earth dams: applications. Journal of Engineering Mechanics, 113(5): 702-719.
10. Elgamal, A.-W.M., Scott, R.F., Succarieh, M.F., and Yan, L. 1990. La Villita dam response during five earthquakes including permanent deformation. Journal of Geotechnical Engineering, 116(10): 1443-1462.
11. Franklin, A.G., and Chang, F.K. 1977. Permanent displacements of earth embankments by Newmark sliding block analysis. Earthquake Resistance of Earth and Rock-Fill Dams. Report 5.
12.. Gao, Y. F., Zhang, F., Lei, G. H., and Li, D. Y. (2012). An extended limit analysis of

three-dimensional slope stability. Geotechnique, 63(6): 518–524.

13.. Gao, Y.F., Zhang, F. Lei, G.H., Li, D.Y.,Zhang, N., (2013). “Stability charts for 3D failure of Homogeneous slopes.” Journal of Geotechnical and Geoenvironmental Engineering, ASCE, 139(9): 1528-1538.

14. Hammersley, J.M., and Handscomb, D.C., (1964). “Monte Carlo method.” Methuen Co. Ltd., London.

15. Ito, T., and Matsui, T., (1975). Methods to estimate lateral force acting on stabilizing piles. Soils and Foundations, 15(4): 43–59.

16. Li, X., He, S., and Wu, Y., (2010). Seismic displacement of slopes reinforced with piles. Journal of Geotechnical and Geoenvironmental Engineering, ASCE, 136(6): 880-884.

17. Lin, J.S., and Whitman, R.V. 1983. Decoupling approximation to the evaluation of earthquake‐induced plastic slip in earth dams. Earthquake Engineering & Structural Dynamics, 11(5): 667-678.

18. Ling, H. I., Leshchinsky, D., and Perry, E. B. (1997). Seismic design and performance of geosynthetic-reinforced soil structures. Geotechnique, London, 47(5): 933–952.

19. Ling, H. I., and Leshchinsky, D. (1998). Effects of vertical acceleration on seismic design of geosynthetic reinforced soil structures. Geotechnique, 48(3): 347–373.

20. Makdisi, F.I., and Seed, H.B. 1978. Simplified procedure for estimating dam and embankment earthquake-induced failures. Journal of the Geotechnical Division, ASCE, 104: 849–861.

21. Michalowski, R. L. (1998a). Soil reinforcement for seismic design of geotechnical structures. Computers and Geotechnics, 23(1–2): 1–17.

22. Michalowski, R. L., and Drescher, A. (2009). Three-dimensional stability of slopes and excavations. Geotechnique, 59(10): 839–850.

23. Michalowski, R. L., and Martel, T., (2011). Stability charts for 3D failure of steep slopes subjected to seismic excitation. Journal of Geotechnical and Geoenvironmental Engineering,2, 183-189.

24. Michalowski, R. L., and You, L. (2000). Displacement of reinforced slopes subjected to seismic loads. Journal of Geotechnical and Geoenvironmental Engineering, 126(8), 685–694.
25. Nadukuru, S. S., and Michalowski, R. L. (2013). Three-dimensional displacement analysis of slopes subjected to seismic loads. Canadian Geotechnical Journal, 50(6): 650-661.
26. Newmark, N. W., (1965). Effects of Earthquakes on Dams and Embankments. The Fifth Rankine Lecture of the British Geotechnical Society, Geotechnique, 15(2): 137-160.
27. Poulos, H.G., (1995). Design of reinforcing piles to increase slope stability. Canadian Geotechnical Journal, 32(5): 808–818.
28. Prevost, J.H. 1981. DYNA-FLOW: a nonlinear transient finite element analysis program. Princeton University, Department of Civil Engineering, School of Engineering and Applied Science.
29. Prevost, J.H. 1985. Wave propagation in fluid-saturated porous media: an efficient finite element procedure. International Journal of Soil Dynamics and Earthquake Engineering, 4(4): 183-202.
30. Sarma, S.K. 1975. Seismic stability of earth dams and embankments. Geotechnique, 25(4): 743-761.
31. Seed, H. B., Lee, K. L., and Idriss, I. M., (1969) "Analysis of the Sheffield Dam Failure." Journal of the Soil Mechanics and Foundations Division, ASCE, 95(6): 1453-1490.
32. Seed, H.B., Lee, K., Idriss, I.M., and Makdisi, F. 1975. The slides in the San Fernando dams during the earthquake of February 9, 1971. Journal of Geotechnical and Geoenvironmental Engineering, 101(ASCE# 11449 Proceeding).
33. Seed, H. B., (1979) "Considerations in the Earthquake-Resistant Design of Earth and Rockfill Dams." Geotechnique, 29(3): 215-263.
34. Serff, N. 1976. Earthquake induced deformations of earth dams. College of Engineering, University of California.

35. Siegel, R.A., Kovacs, W.D., and Lovell, C.W. (1981). “Random surface generation in stability analysis.” ASCE, journal of Geotechnical Engineering, 107: 996-1002.

CHAPTER 6

CONCLUSIONS AND FUTURE WORK

6.1 SUMMARY AND CONCLUSIONS

Slope failures and landslides occur extensively in all parts of the word and frequently result in a tremendous toll of death and destruction of properties. It is therefore of prime importance to devise the means to enhance the stability of the slopes. The term landslide refers to a sudden rupture of a mass of rock or soil and its movement downslope by the force of gravity. Stabilizing piles, as one of the most widely used countermeasure in reinforcement engineering of slopes, has been proved to be an efficient solution to landslides. In the planning and design of stabilizing piles, it is necessary to analyze the soil-pile pressure acting on the piles. In addition, since the earthquake-induced landslides occur frequently in recent years, it is important to analyze the movement behaviors of a potential landslide under seismic loadings. Therefore, the current study focuses on analysis of (1) soil-pile pressure acting on the piles and (2) landslide movement behaviors.

For the soil-pile pressure analysis, the author modified the analytical model (Ito and Matsui (1975)) by considering soil arching effects along the depth of the moveable soil between two piles. In addition, many researchers analyze the behavior of the stabilizing piles in slopes without considering the effects of slope angle, while the natural slopes always incline with different angles. Therefore, the effects of the slope angle on the distribution of the lateral force acting on the piles are analyzed as well.

For the landslide movement analysis, the three dimensional (3D) failure mechanisms are considered. In addition, the lateral forces provided by the piles are evaluated by the formulation proposed in **Chapter 3**. Based on the kinematic theory within the frame of the pseudo-static approach, a 3D model is proposed for evaluating

the critical state and the subsequent displacement response. Furthermore, the Newmark's analytical procedure (1965) is employed to estimate the cumulative displacement induced by given earthquake loads.

Detailed contributions in regard to these two mentioned aspects are listed below:

(1) A larger number of analysis examples show that the influence of soil arching effects between two neighboring piles is significant on the distribution of lateral force acting on piles. The lateral force predicted by Ito and Matsui (1975) can be modified if the soil arching effects are considered.

(2) The soil arching theory proposed by Paik and Salgado (2003) is extended for c-φ soil. The trajectory of soil arching in c-φ soil is assumed to be an arc of a circle. The soil arching zone is determined in the c-φ soil, and subsequently, the active soil stress between two neighboring piles is analyzed.

(3) Combining the soil arching effects and the 'squeezing effect' between two neighboring piles, two new formulae are proposed to estimate the ultimate lateral force acting on piles due to the soli movement for cohesionless soil and c-φ soil respectively. Furthermore, it should be noted that the overload pressure exerted on the ground surface in cohesionless soil is also taken into account when the soil arching effects are analyzed.

(4) Comparing to the field observed data, it illustrates that the prediction of the proposed model shows a greater agreement than the results of Ito and Matsui's method. Especially, the maximum force and the corresponding position calculated by the proposed method are in line with the field measurements. In addition, a result by numerical simulation conducted by other researcher is introduced to validate the proposed model.

(5) The parametric study shows the lateral force increase with the growth of the height of the unstable soil layer H, the internal friction angle φ, the cohesion c, and the pile diameter D_1-D_2.

(6) Considering the inclination of the slope, a new method is proposed to estimate the effects of slope on the distribution of the lateral force acting on piles. The numerical results and laboratory experimental results conducted by others are introduced to validate the proposed model. It is shown that Ito and Matsui's approach provides a linear solution for estimating the soil-pile pressure, while a nonlinear solution is obtained from the proposed model, which shows better agreement with the simulation results.

(7) The parametrical study of the effect of slope angle implies that if the magnitude of the soil-pile pressure on a pile is the only factor considered, ignoring the change of the point application of the force with slope angle, it is reasonable to use a horizontal soil model ($\beta = 0^{o}$) as a simplified way to estimate the response of stabilizing piles in slopes ($\beta \neq 0^{o}$).

(8) It is also shown that in the inclined slope model, both the slope angle and internal friction angle affect the distribution of the soil-pile pressure per unit length of the pile; the shape of the distribution of the soil-pile pressure is mainly affected by the slope angle, whereas the internal friction angle has a greater effect on the magnitude of the soil-pile pressure on the pile than the slope angle. Additionally, the height of the resultant lateral force varies with the slope angle and the internal friction angle in the proposed model, whereas it remains constant in Ito and Matsui's approach.

(9) Three-dimensional (3D) limit analysis of seismic stability of slopes reinforced with one row of piles is presented. A 3D rotational mechanism for earth slope is adopted. The lateral forces provided by the piles are evaluated by proposed formula in **Chapter 3**. Expressions for calculating the yield acceleration coefficient are derived. A random iteration method is employed to find the critical acceleration coefficient for the 3D slopes with or without reinforcement. Based on the kinematic theory within the frame of the pseudo-static approach, a 3D model is proposed for evaluating the

critical state and the subsequent displacement response. Furthermore, the Newmark's analytical procedure is employed to estimate the cumulative displacement induced by given earthquake loads.

(10) Based on the limit analysis, the following two phase of the work are presented: (1) the determination of the yield acceleration and its corresponding failure mechanism (especially the width of the 'plane insert' is determined) in 3D mechanism; (2) the estimation of the seismic displacement of the 3D reinforced slope. A simple example is given, and the findings are: the yield accelerations of 2D mechanism (B/H = 10) are less than that in 3D mechanism with the same soil properties; the displacements in 2D mechanism are much large than that in 3D conditions; it is possible to reduce the seismic displacement of the soil slopes using stabilizing piles both in 2D and 3D conditions.

6.2 FUTURE STUDIES

(1) More investigations and shaking table tests should be carried out to validate the effects of soil arching on the lateral force distribution acting on piles. Furthermore, the prediction using the proposed method shows limited accuracy. Thus, to improve the prediction results, the model needs further modification in the future by considering the soil movement and the corresponding pile deflection.

(2) 3D limit analysis method for slope displacement analysis based-on the rotational failure mechanism is presented. However, both natural and constructed slopes exhibit a complex configuration, which means that the tension failure has been observed in many earthquake-induced landsides, top surface of potential landslides and shaking table tests. Therefore, 3D limit analysis method for seismic slope stability based-on tension-shear failure mechanism should be presented. And other external forces (e.g. surcharge, pore water press, anchor force and so on) should be considered.

(3) The seismic permanent displacement of slope should be further studied

using a complex model rather than a simple single sliding block. In addition, rigorous elastic-plastic model should be presented to take the more realistic feature of sliding mass rather than rigid-plastic model.

(4) The toe-failure mechanism a lone is considered in this thesis. However, in general, the slope collapse can be divided into three types: toe failure, face failure and base failure. The effects of the reinforcement of piles in face failure and base failure mechanisms should be studied in further.

REFERENCES

1. Ito, T., and Matsui, T., (1975). Methods to estimate lateral force acting on stabilizing piles. Soils and Foundations, 15(4): 43–59.
2. Newmark, N. W., (1965). Effects of Earthquakes on Dams and Embankments. The Fifth Rankine Lecture of the British Geotechnical Society, Geotechnique, 15(2): 137-160.
3. Paik K. H., and Salgado R. (2003). Estimation of active earth pressure against rigid retaining walls considering arching effects, Geotechnique, 53(7): 643-653.

APPENDIX A

The squeezing effects between two neighboring piles (Derivation of Eqs. (3.24) and (3.25).)

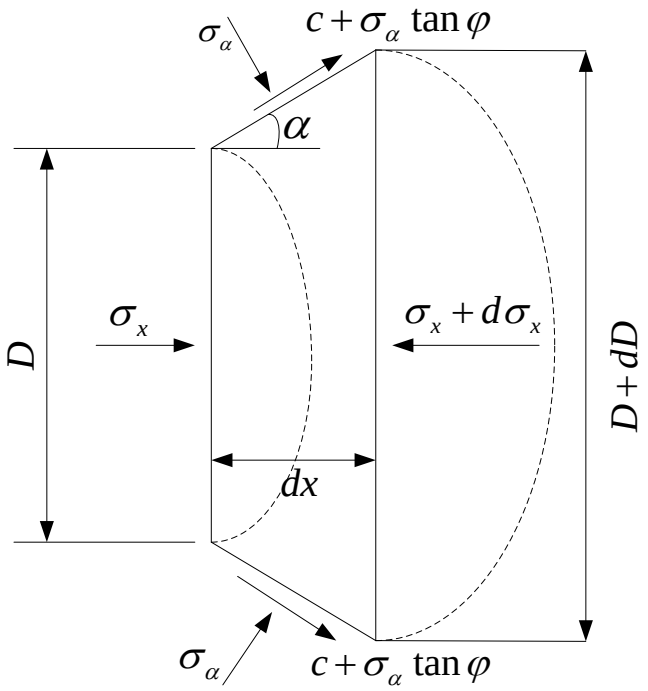

Figure A1 Differential element (EBB′E′) between two neighboring piles (Ito and Matsui (1975)).

The squeezing effects have been proved by Ito and Matsui (1975). It is summarized as follows.

Firstly, all the assumptions they made are adopted in this paper. In the zone EBB′E′ (**Figure 3.4**), the equilibrium of the forces in *x* direction on a differential element is considered (as shown in **Figure A1**):

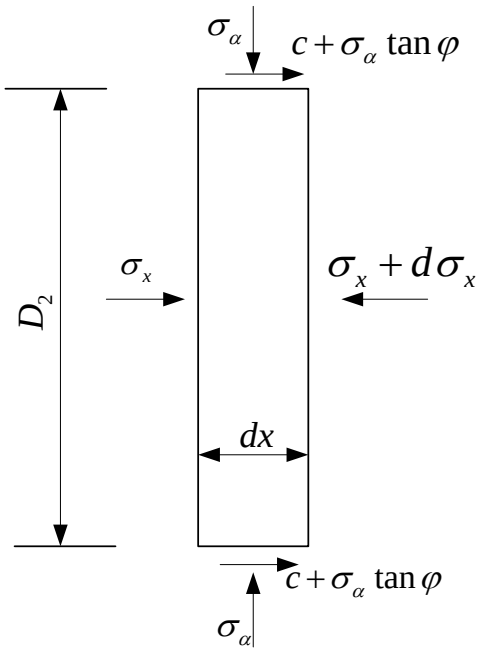

Figure A2 Differential element (AEE′A′) between two neighboring piles (Ito and Matsui (1975)).

$$2dx[\sigma_\alpha \tan(\frac{\pi}{4}+\frac{\varphi}{2})+\sigma_\alpha \tan\varphi + c] - Dd\sigma_x - \sigma_x dD = 0 \tag{A-1}$$

The normal stress σ_α on the surface EBB′E′ (**Figure 3.4**) is assumed to equal to the principal stress σ_x. The Mohr-Coulomb's yield criterion is expressed as:

$$\sigma_\alpha = \sigma_x N_1 + 2cN_1^{1/2} \tag{A-2}$$

in which $N_1 = \tan^2(\pi/4+\varphi/2)$. The geometrical condition gives:

$$dx = \frac{d(D/2)}{\tan(\pi/4+\varphi/2)} \tag{A-3}$$

Substituting Eq. (A-2) and (A-3) into Eq. (A-1), and then making integration,

$$\sigma_x = \frac{(C_1 D)^{(N_1^{1/2}\tan\varphi + N_1 - 1)} - c(2\tan\varphi + 2N_1^{1/2} + N_1^{-1/2})}{N_1^{1/2}\tan\varphi + N_1 - 1} \tag{A-4}$$

where, C_1 is an integration constant.

Then, in the zone AEE′A′ (**Figure 3.4**), the equilibrium of the forces on a small soil element in *x* direction is also considered, as shown in **Figure A2**.

$$D_2 d\sigma_x = 2(\sigma_\alpha \tan\varphi + c)dx \tag{A-5}$$

Substituting Eq. (A-2) into Eq. (A-5), and integrating it,

$$\sigma_x = \frac{C_2 \exp(\frac{2N_1 \tan\varphi}{D_2} x) - c(2N_1^{1/2} \tan\varphi + 1)}{N_1 \tan\varphi} \tag{A-6}$$

where, C_2 is an integration constant.

The solution for lateral force acting on stabilizing pile in cohesionless ground

For cohesionless soil, the active earth pressure acts on the plane AA′ is obtained by Eq. (3.23), where $c = 0$, thus the equation can be expressed as

$$[\sigma_x]_{x=0} = \sigma_h = \frac{\gamma H K_{an}}{1 - K_{an} \tan\varphi \tan\beta}[(1 - \frac{z}{H})^{K_{an} \tan\varphi \tan\beta} - (1 - \frac{z}{H})] + K_{an} q (1 - \frac{z}{H})^{K_{an} \tan\varphi \tan\beta} \tag{A-7}$$

in which, z is an arbitrary depth below the ground surface, γ the unit weight of the soil, q the vertical pressure exerted on the surface of the ground. The Eq. (A-7) is considered as the boundary condition of Eq. (A-6), then,

$$C_2 = \sigma_h N_1 \tan\varphi \tag{A-8}$$

Substituting Eq. (A-8) into Eq. (A-6) yields

$$[\sigma_x]_{x=\frac{D_1 - D_2}{2}\tan(\frac{\pi}{8}+\frac{\varphi}{4})} = (\sigma_h N_1 \tan\varphi) \exp[\frac{D_1 - D_2}{D_2} \cdot N_1 \tan\varphi \tan(\frac{\pi}{8} + \frac{\varphi}{4})] \tag{A-9}$$

The constant C_1 in Eq. (A-4) is obtained by considering the Eq. (A-9) as the boundary condition. Then,

$$(C_1 D_2)^{(N_1^{1/2} \tan\varphi + N_1 - 1)} = \frac{(N_1^{1/2} \tan\varphi + N_1 - 1)}{N_1 \tan\varphi}[\sigma_h N_1 \tan\varphi \cdot \exp(\frac{D_1 - D_2}{D_2} N_1 \tan\varphi \tan(\frac{\pi}{8} + \frac{\varphi}{4}))]$$

(A-10)

The Eq. (A-4) and Eq. (A-10) are used to obtain the solution of lateral force $P_{BB'}$ acting on the plane BB′ per unit thickness of layer in x direction, which is shown as follow:

$$p_{BB'} = D_1\left(\frac{D_1}{D_2}\right)^{(N_1^{1/2}\tan\varphi+N_1-1)}\left[\sigma_h \cdot \exp\left(\frac{D_1-D_2}{D_2}N_1\tan\varphi\tan\left(\frac{\pi}{8}+\frac{\varphi}{4}\right)\right)\right] \tag{A-11}$$

Finally, subtracting the active lateral force acting on the plane AA' from $P_{BB'}$, the lateral force acting on a pile per unit thickness of layer in x direction is obtained.

$$\begin{aligned} p &= p_{BB'} - D_2[\sigma_x]_{x=0} \\ &= \left\{\frac{\gamma H K_{an}}{1-K_{an}\tan\varphi\tan\beta}\times\left[\left(1-\frac{z}{H}\right)^{K_{an}\tan\varphi\tan\beta}-\left(1-\frac{z}{H}\right)\right]+K_{an}q\left(1-\frac{z}{H}\right)^{K_{an}\tan\varphi\tan\beta}\right\} \\ &\quad\times\left\{D_1\left(\frac{D_1}{D_2}\right)^{N_1^{1/2}\tan\varphi+N_1-1}\times\exp\left[\frac{D_1-D_2}{D_2}N_1\tan\varphi\tan\left(\frac{\pi}{8}+\frac{\varphi}{4}\right)\right]-D_2\right\} \end{aligned} \tag{A-12}$$

Eq. (A-12) is the solution for lateral force acting on a pile in the cohesionless ground.

Similarly, in the c-φ soil ground, the solution is obtained,

$$\begin{aligned} p &= cD_1\left(\frac{D_1}{D_2}\right)^{N_1^{1/2}\tan\varphi+N_1-1}\left\{\frac{(2N_1^{1/2}\tan\varphi+1)}{N_1\tan\varphi}\times\left[\exp\left(\frac{D_1-D_2}{D_2}N_1\tan\varphi\tan\left(\frac{\pi}{8}+\frac{\varphi}{4}\right)\right)-1\right]\right. \\ &\quad\left.+\frac{2\tan\varphi+2N_1^{1/2}+N_1^{-1/2}}{N_1^{1/2}\tan\varphi+N_1-1}\right\}-cD_1\frac{2\tan\varphi+2N_1^{1/2}+N_1^{-1/2}}{N_1^{1/2}\tan\varphi+N_1-1} \\ &\quad+\sigma_h\times\left[D_1\left(\frac{D_1}{D_2}\right)^{N_1^{1/2}\tan\varphi+N_1-1}\times\exp\left(\frac{D_1-D_2}{D_2}N_1\tan\varphi\tan\left(\frac{\pi}{8}+\frac{\varphi}{4}\right)\right)-D_2\right] \end{aligned} \tag{A-13}$$

APPENDIX B

Total lateral force and the point application of the force

The total lateral force p_t on a pile can be obtained by integrating Eq. (4.28) with respect to z:

$$p_t = \int_0^H p\,dz \tag{B-1}$$

Substitution of Eq. (4.28) into the above equation yields

$$\begin{aligned} p_t = & \frac{\gamma H^2 K_{an} \cos\beta}{2[(K_{an}\tan\varphi - K_{an}\tan\beta + m)\dfrac{\sin\theta}{\cos\theta_1} + 1]} \\ & \times\{D_1(\frac{D_1}{D_2})^{N^{1/2}\tan\varphi + N - 1} \times \exp[\frac{D_1 - D_2}{D_2} N\tan\varphi\tan(\frac{\pi}{8} + \frac{\varphi}{4})] - D_2\} \end{aligned} \tag{B-2}$$

The height of the point application of the force is obtained by dividing the moment of the soil-pile pressure about the failure surface by the total lateral force on a pile. The moment M of the soil-pile pressure about the failure surface is obtained as follow:

$$M = \int_0^H p(H - z)dz \tag{B-3}$$

Dividing Eq. (A-21) by Eq. (A-20) yields the height of the point application of the force, h_p:

$$\begin{aligned} h_p &= \frac{\displaystyle\int_0^H p(H - z)dz}{p_t} \\ &= \frac{2[(K_{an}\tan\varphi - K_{an}\tan\beta + m)\dfrac{\sin\theta}{\cos\theta_1} + 1]}{3[(K_{an}\tan\varphi - K_{an}\tan\beta + m)\dfrac{\sin\theta}{\cos\theta_1} + 2]} \end{aligned} \tag{B-4}$$

APPENDIX C

$$W_{\gamma}^{3D} = 2\omega\gamma[\int_{\theta_0}^{\theta_B}\int_{0}^{x^*}\int_{a}^{y^*}(r_m + y)^2\cos\theta dydxd\theta + \int_{\theta_B}^{\theta_H}\int_{0}^{x^*}\int_{d}^{y^*}(r_m + y)^2\cos\theta dydxd\theta] \tag{C-1}$$

The integration limits along x are $x^* = \sqrt{R^2 - a^2}$ and $x^* = \sqrt{R^2 - d^2}$ in the first and second integral respectively, with R, r_m, a and d all being function s of θ, shown as following

$$r_m = \frac{r + r'}{2},\ R = \frac{r - r'}{2} \tag{C-2}$$

$$d = \frac{\sin(\beta + \theta_h)}{\sin(\beta + \theta)} r_0 e^{(\theta_h - \theta_0)\tan\varphi} - r_m,\ a = \frac{\sin\theta_0}{\sin\theta} r_0 - r_m \tag{C-3}$$

$$D^{3D} = -2\omega r_0^2[\sin^2\theta_0\int_{\theta_0}^{\theta_B}\frac{\cos\theta}{\sin^3\theta}\sqrt{R^2 - a^2}d\theta + e^{2(\theta_h - \theta_0)\tan\varphi} \times \sin^2(\theta_h + \beta)\times\int_{\theta_B}^{\theta_h}\frac{\cos(\theta + \beta)}{\sin^3(\theta + \beta)}\sqrt{R^2 - d^2}d\theta] \tag{C-4}$$

$$f_1^s = \frac{(3\tan\varphi\sin\theta_h - \cos\theta_h)\exp[3(\theta_h - \theta_0)\tan\varphi] - 3\tan\varphi\sin\theta_0 + \cos\theta_0}{3(1 + 9\tan^2\varphi)} \tag{C-5}$$

$$f_2^s = \frac{L}{3r_0}\sin^2\theta_0 \tag{C-6}$$

$$f_3^s = \frac{\exp[(\theta_h - \theta_0)\tan\varphi]}{6}(\frac{H}{r_0})\frac{\sin(\theta_h + \beta)}{\sin\beta}\times\{2\sin\theta_h\exp[(\theta_h - \theta_0)\tan\varphi] - \frac{H}{r_0}\} \tag{C-7}$$

$$f_4^s = \int_{\theta_0}^{\theta_B}\int_{0}^{x^*}\int_{a}^{y^*}(r_m + y)^2\sin\theta dydxd\theta + \int_{\theta_B}^{\theta_H}\int_{0}^{x^*}\int_{d}^{y^*}(r_m + y)^2\sin\theta dydxd\theta \tag{C-8}$$

The integration limits x and the variable parameters R, r_m, a, d are the same with Eq. (A1).

$$G = G^{2D} + G^{3D} \tag{C-9}$$

in which G^{2D} is the weight of the 2D sliding block bounded by the log-spiral failure and the insert plane with width b; G^{3D} is the weight of the 3D sliding block (CDEFG, referring to Fig.2 (a)).

$$G^{3D} = 2\gamma[\int_{\theta_0}^{\theta_B}\int_0^{x^*}\int_a^{y*}(r_m + y)^2\,dydxd\theta + \int_{\theta_B}^{\theta_H}\int_0^{x^*}\int_d^{y*}(r_m + y)^2\,dydxd\theta] \tag{C-10}$$

$$l = \sqrt{(\frac{W_r^{3D}}{\omega} + \frac{W_r^{2D}}{\omega})^2 + (\gamma r_0^3 b(f_1^s - f_2^s - f_3^s) + 2\gamma f_4^s)^2} \tag{C-11}$$

In this Appendix, only the equations relate to the 3D portion of the composite mechanism are presented. As to the equations needed for the calculation of the 2D portion, including the work rate of the soil weight and the dissipation, can be found in literatures (e.g. Chen 1975; Chen and Liu 1990).